A STUDY OF THE RELIABILITY OF PLATED WIRE COMPUTER COMPONENTS

by

O. S. Lutes
R. B. Fryer
J. O. Holmen
J. R. Kench

FINAL TECHNICAL REPORT

December 1, 1969

NATIONAL AERONAUTICS AND SPACE ADMINISTRATION
ELECTRONICS RESEARCH CENTER
CAMBRIDGE, MASSACHUSETTS 02139

Contract No. NAS 12-2003

Honeywell Inc.
Corporate Research Center
Hopkins, Minnesota

N70-30039

A STUDY OF THE RELIABILITY OF

PLATED WIRE COMPUTER COMPONENTS

by

O. S. Lutes
R. B. Fryer
J. O. Holmen
J. R. Kench

FINAL TECHNICAL REPORT

December 1, 1969

NATIONAL AERONAUTICS AND SPACE ADMINISTRATION
ELECTRONICS RESEARCH CENTER
CAMBRIDGE, MASSACHUSETTS 02139

Contract No. NAS 12-2003

Honeywell Inc.
Corporate Research Center
Hopkins, Minnesota

120

FOREWORD

This report was prepared by the Honeywell Corporate Research Center, Hopkins, Minnesota, under NASA Contract No. NAS 12-2003. The work was administered under the direction of the NASA Electronics Research Center, Cambridge, Massachusetts, Neil Patt, Technical Monitor.

The report covers research work conducted from July 1, 1968 through September 30, 1969. The work was performed in the Magnetics Department, J.A. Sartell, Department Head. O.S. Lutes was Principal Investigator.

Preceding page blank

TABLE OF CONTENTS

TABLE OF CONTENTS (Continued)

LIST OF ILLUSTRATIONS

LIST OF ILLUSTRATIONS (Continued)

LIST OF ILLUSTRATIONS (Continued)

LIST OF TABLES

I. INTRODUCTION

This report describes research on the reliability of plated wire computer components under various conditions of environment and operation. The objective of the research was to establish methods of evaluation and directions for improving the aging characteristics. In the case of evaluation the emphasis was on observing the change of memory operating characteristics, chiefly the degradation of electrical output under simulated conditions of write, read, and adjacent bit disturbance. To establish directions for improvement required a broader approach. This consisted first of a thorough characterization of the physical and magnetic properties of the plated wire element, using a wide variety of experimental techniques. This was followed by aging studies of two kinds: (a) observation of aging rates of such properties under various conditions of environment, temperature and magnetic field, and (b) study of the change in aging rates resulting from systematic variation of such properties in the unaged wire.

The remainder of this report is organized into five main sections. In Section II, a review is given of the electrodeposition process. Section III contains the methods and results of the physical and magnetic characterization of the plated wire element. Section IV is the main location of experimental results and interpretation of the aging studies. It is conveniently divided according to the aging properties in the absence of or in the presence of magnetic fields. These two conditions are referred to as shielded and field aging, respectively. Section V describes the relation between aging failure modes and worst-case pulse programs which simulate operating conditions of the memory element. Section VI contains an overall summary and discussion. Three appendices are included. The first two are elaborations of statements in the body of the report. The third appendix, on new technology, is a statement of the practical implications of the research results.

II. ELECTRODEPOSITION OF CYLINDRICAL FILMS

The process described in this section can be utilized to continuously deposit magnetic material on Be-Cu substrate wire. A wide range of magnetic characteristics can be obtained.

The 5 mil Be-Cu substrate wire is first cleaned and electro-polished, and then 0.0001 to 0.002 inch of material is removed from the Be-Cu surface. After a thorough water rinse, the wire is pushed through the rest of the plater. This is done to minimize skew during plating. The cleaned Be-Cu substrate is plated with 1 to 2 microns of copper to yield a uniform, fine grained surface. The wire is again rinsed, and plated with 1 micron of near zero magnetostrictive Permalloy (80 Ni-20 Fe) in the presence of a 15 to 20 Oe. circumferential orienting field. After a final water rinse the wire passes through an annealing station where the magnetic properties are further developed and stabilized.

The electro-polish solution is a phosphoric acid type, the Cu plating bath is a $K_4P_2O_7$, $Cu_2P_2O_7$ solution with no additives and the permalloy plating bath is of the simple sulfate type. Normal co-deposition of metals from baths containing simple metal ions is a diffusion controlled process.(1) The more noble metal deposits preferentially and the percentage of this metal will be increased by plating conditions such as an increase in bath temperature, increased electrolyte agitation, decrease in current density, or other factors which will increase the percentage of ions in the cathode diffusion area. Co-deposition characterized by the less noble metal deposition preferentially is referred to as anomalous co-deposition.(1) The electrodeposition of iron-nickel alloys from non-complexing solutions is a characteristic example of anomalous co-deposition.(2) Since the Ni-Fe plating bath used is of a simple sulfate type, the less noble metal, iron, deposits preferentially. Therefore, to obtain the desired zero magnetostrictive material at approximately 80-20 Ni-Fe, the Ni^{++} to Fe^{++} ratio must be relatively large. In the present system this ratio is 80:1. In order to obtain the range of composition used in this study, the Ni^{++} to Fe^{++} ratio was varied from 50:1 to 180:1. The magnetostriction coefficient, η_o is obtained by using Long's method[3] of measuring the torsional strain sensitivity, $H_{\ell/\gamma}$. $\left(\eta_o \equiv -3.1 H_{\ell/\gamma}\right)$. A change in η_o of 1000 Oe corresponds to a composition change of approximately 0.12%. We note that the sign convention used by us for η_o makes it positive for positive magnetostrictive (Fe-rich) material. This is opposite to the convention of reference (3).

A number of plating parameters can be varied to obtain relatively close control of the composition of the depositing alloy. Due to anomalous co-deposition, the amount of iron in the deposit can be increased by increasing the bath temperature, increasing the electrolyte flow rate or by decreasing the plating current density. Control of the electrolyte flow rate was used to provide relatively fine control of composition, while changing the Ni^{++} to Fe^{++} ratio was used to produce large compositional changes. The flow rate can be controlled to within 5 ml/min. This control is sufficient to yield a magnetic material that is within compositional variation tolerance of ±0.1%. Figure 1 is a plot of the flow rate vs η_o. The positive values of η_o are defined as being iron-rich. It can be seen that an increase in flow rate increases the percentage of iron in the deposit. Since iron is the more readily deposited metal in this system, the decreased depletion layer thickness brought about by increased flow rate (agitation) should enhance iron deposition.[4][5]

Copper plating parameters which can influence the surface texture of the substrate are the bath temperature, electrolyte flow rate and plating current density. The surface roughness of the film can be correlated with surface area by a radio-tracer technique developed at Honeywell.[6] This method gives a means of determining the relative roughness of copper deposited under different plating conditions.

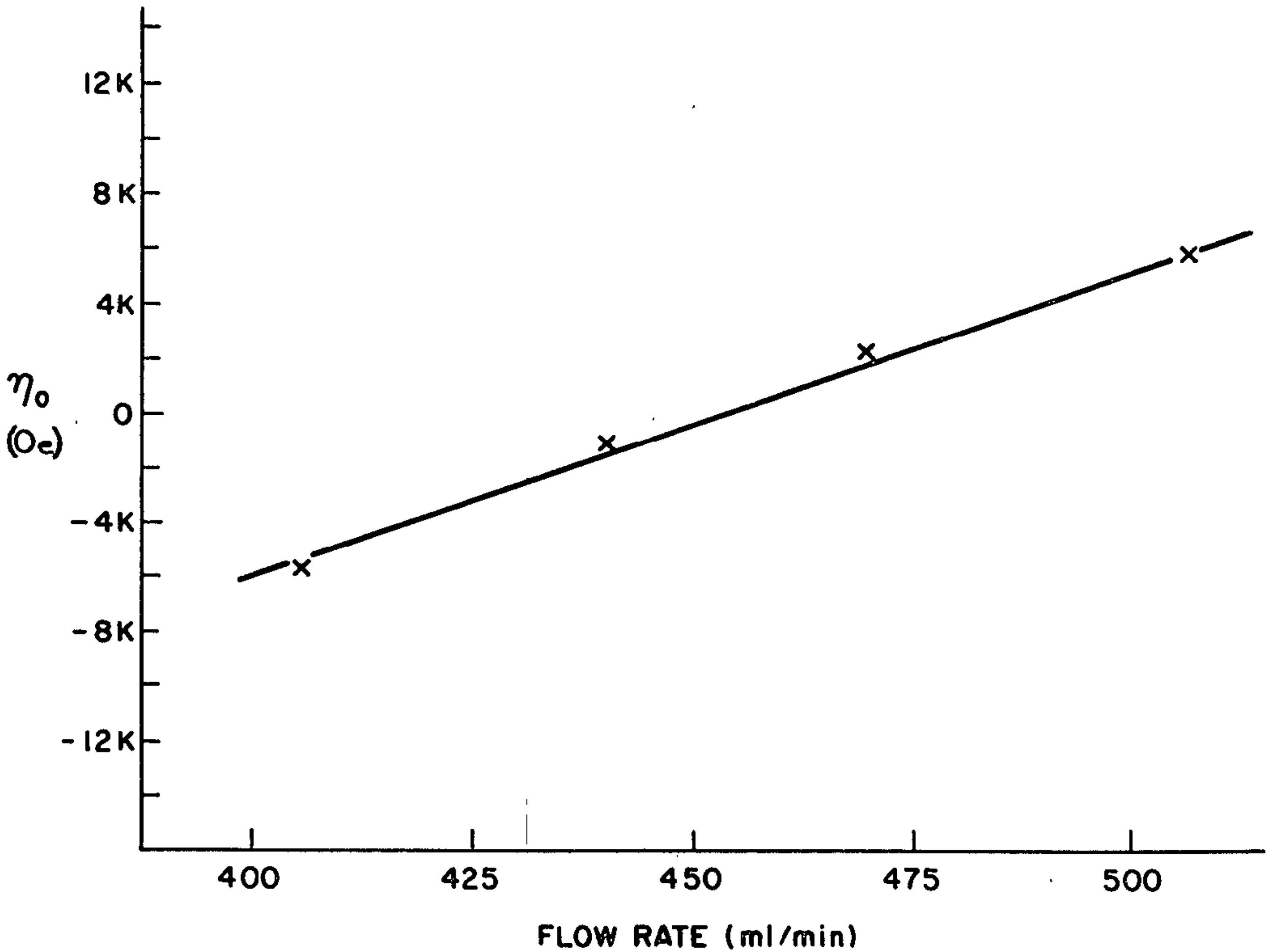

Figure 1. Flow Rate Dependence of Magnetostriction. Plated Wire Deposition Process

The permalloy thickness can be varied by using one or more plating cells, wire speed variations, and by reducing the current density. The films are annealed on-line in the presence of a 12 to 15 Oe. circumferential orienting field. The films are heated to temperatures up to 425°C for durations as long as 90 seconds. Nitrogen gas is utilized for the annealing atmosphere.

Both copper and gold have been deposited on the Be-Cu as a substrate for the Ni-Fe plate. A copper pyrophosphate bath was used. The bath contained no addition agents. The plating variables were maintained at levels which are reported to yield a ductile copper deposit.[7] The gold was deposited by the "Jel-Rex Autronex" process which is commercially available. The bath is an acid type which is designed to give a hard, bright deposit.

The effects of saccharin additions to the plating have been studied. Samples of various types of wire produced with this additive have been plated on copper and gold substrates. The addition of saccharin to the plating bath markedly affects the magnetic properties. α_{90}, H_c and H_k are significantly reduced and wire stability is decreased. As saccharin is added to the bath, NDRO properties deteriorate and the wire can be used only in the DRO mode of operation. This occurs with addition of <100 mg/1 of saccharin to the plating bath.

Saccharin has been employed as a stress reducer in nickel plating baths for some time.[8][9] Other chemicals such as the aromatic di-sulfonic acids have been used as brighteners and stress relieving agents, individually and in conjunction with saccharin. Workers have studied the effect of these types of addition agents on the microstructure and hardness of nickel deposits which have been annealed over relatively wide temperature ranges.[10] Fisher studied the effects of saccharin on the residual stress and magnetic characteristics of electrodeposited nickel and cobalt.[11] The effects of saccharin on the structure and magnetic properties of iron-nickel films have been studied by Smith, et al.[12] They found that H_c decreased with the addition of saccharin to the plating bath and films deposited from saccharin-free baths were much rougher than those deposited from baths containing saccharin. They found that saccharin markedly reduces the amount of total gas in the film and the crystal size of the deposited material is relatively independent of pH over the range of 2.1 to 3.1 in baths containing saccharin. At the pH level where HCRC films were deposited, Smith, et al, observed a crystal size of 720 Å with saccharin and approximately 1500 Å without saccharin. The marked changes in properties brought about by the addition of saccharin can be explained, at least to some significant degree, by the structural changes effected by saccharin.

The magnetic characteristics of the plated wire can be varied over relatively wide ranges by modifying the plating process parameters. A wide range in coercivity (H_c) is possible. H_c can be controlled by varying such factors as bath temperature, substrate roughness and annealing cycles. The surface roughness is measured utilizing a radio-tracer technique developed at HCRC and a direct correlation between roughness and H_c is observed.

The anisotropy field (H_k) has been found to be a very important factor in developing NDRO properties. H_k can be controlled to yield a relatively wide range of magnetic storage properties by varying annealing cycles and by modifying the Ni-Fe electrolyte.

Normally the skew is held to less than 0.5 degree. The skew can be reduced to a negligible level by application of an axial field generated by a pair of Helmholz coils on the plating line. Any skew present appears to be constant and does not vary significantly in magnitude or direction over relatively long periods of time, thus the skew can be effectively cancelled. This technique does not appear feasible if the wire is pulled through the plating cells since twisting of the wire causes skew to vary.

The dispersion is usually kept below 2 degrees. The substrate surface texture, orienting field and annealing cycle all can affect the development of easy axis dispersion.

The NDRO operating window (that range of digit and word currents where the wire functions in the NDRO mode for a specified test pattern) can be controlled or influenced by a wide range of plating parameters and processes. Window shift in the digit and word directions can be accomplished by variations and control of such parameters as the surface texture, bath temperature, annealing cycle, bath constituents, initial surface and substrate surface properties, bath pH, etc. The tendency of wire to age or deteriorate with time can be minimized by a number of process and control adjustments. Two of the most important factors which affect stability in plated wire are annealing temperature and duration of anneal. Other factors which minimize aging effects are control of the substrate surface itself and control of the type of undercoat deposited on the beryllium copper wire. The thickness of the magnetic deposit as well as the actual plating parameters which bring about the desired magnetic properties also are important in improving the stability of plated wire.

III. PHYSICAL AND MAGNETIC PROPERTIES OF PLATED WIRE

A. PHYSICAL PROPERTIES

1. Introduction—The structure of a plated wire must necessarily be considered at different levels. There is first the macroscopic structure involving such gross aspects as plating thickness, large-scale residual stresses, average composition and preferred orientation. Secondly, there are microstructural features such as grain size distribution, small scale composition fluctuations, phase structure and crystalline defects such as faults or twins.

In this section of the report we present the results of examination of unaged plated wires by metallography, X-ray diffraction, electron-beam microprobe, transmission electron microscopy and electron diffraction techniques. In this way it is possible to build up a coherent picture of a plated wire starting from its gross features and working down to detail on a microstructural level.

2. Metallographic Examination—A cross-sectional view of a typical plated wire is shown in Figure 2. Three components of the wire may be distinguished:

(a) The beryllium copper alloy core, of about 0.005 inch diameter.

(b) A copper plating of irregular thickness, varying from 1μ to 5μ around the circumference.

(c) A permalloy plating which is of constant thickness, about 1μ and follows the contour of the copper deposit.

It may further be noted that the copper-beryllium wire etches very irregularly but shows no grain structure, while the copper plating appears to consist of columnar grains extending completely through its thickness. The permalloy plating shows no structure at all at this magnification.

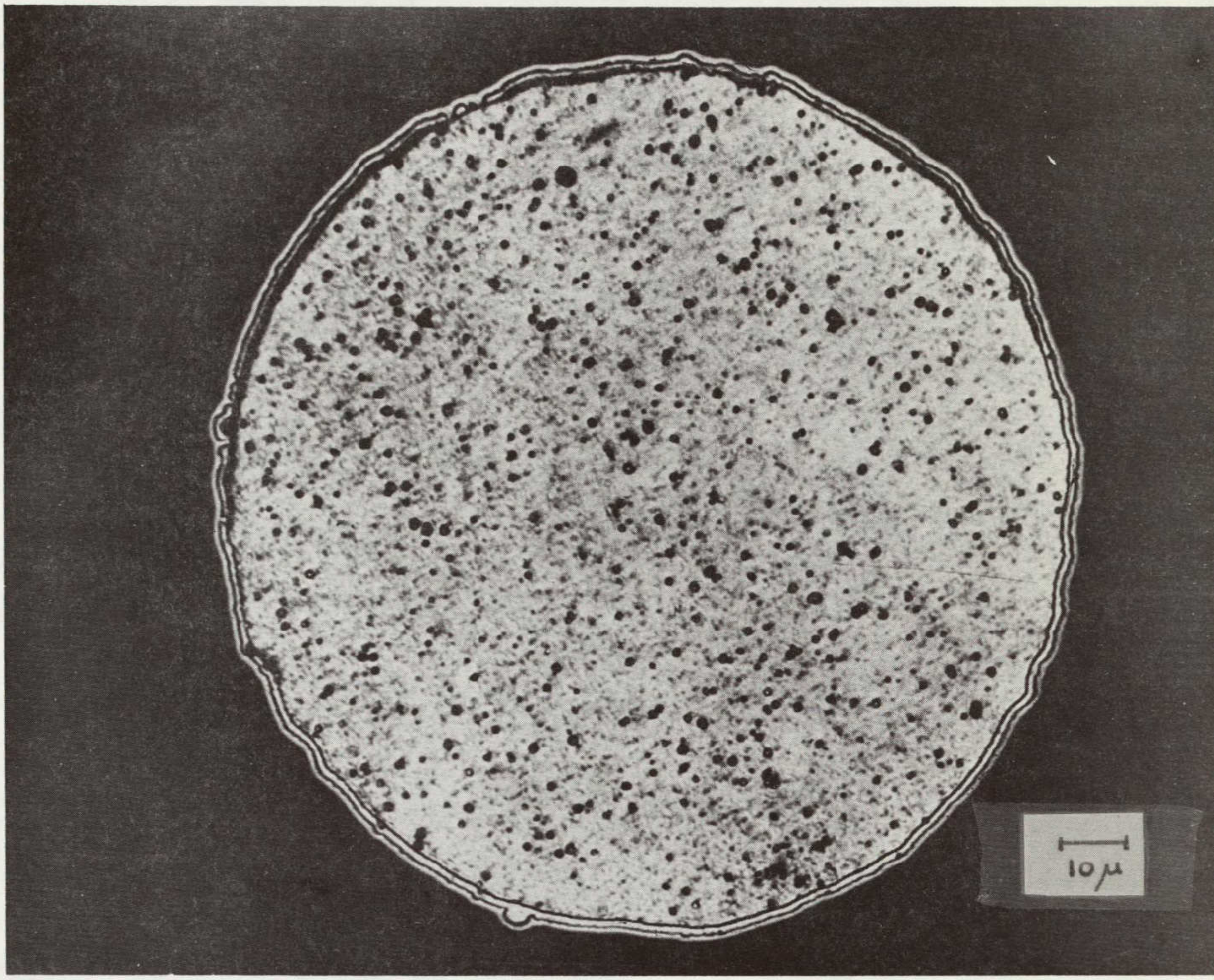

Figure 2. Cross-sectional View of a Plated Wire X1200

A scanning electron micrograph of the surface of a typical wire is shown in Figure 3. The surface, it may be noted, is extremely irregular, with a random distribution of hemispherical blobs of a few microns diameter. In addition, the surface appears to be wavy on a sub-micron scale. Taken together, these micrographs suggest that during copper plating conditions are such that irregular outgrowths of copper occur randomly in an otherwise fairly smooth columnar structure. Permalloy plating, by contrast, is evidently performed under such conditions as favor a smooth, regular, fine-grained deposit.

3. <u>X-ray Diffraction Investigations</u>—Wire samples of various compositions and with both copper and gold plated substrates were examined by X-ray diffraction techniques and the alloy phases present were determined by lattice parameter measurements. Results are shown in Table I, together with parameters measured on unplated copper-beryllium wires in both solution-treated and fully-aged conditions.

Several interesting features emerge from the results tabulated, throwing further light upon each component of the wires.

(a) The copper-beryllium wire invariably contains a precipitate of Cu-Be compound of lattice parameter 2.70 Å, suggesting that it is difficult to prepare the alloy in the homogeneous single-phase condition. However, it is possible crudely to judge the extent of transformation from the lattice parameter of the solid solution phase. The parameter of the solution-treated wire is about 3.583 Å increasing to 3.606 Å in the over-aged sample.

Every one of the plated wires shows an intermediate solid solution parameter of 3.596 Å and it is clear that the wire stock used to prepare plated wires is in a partly aged condition.

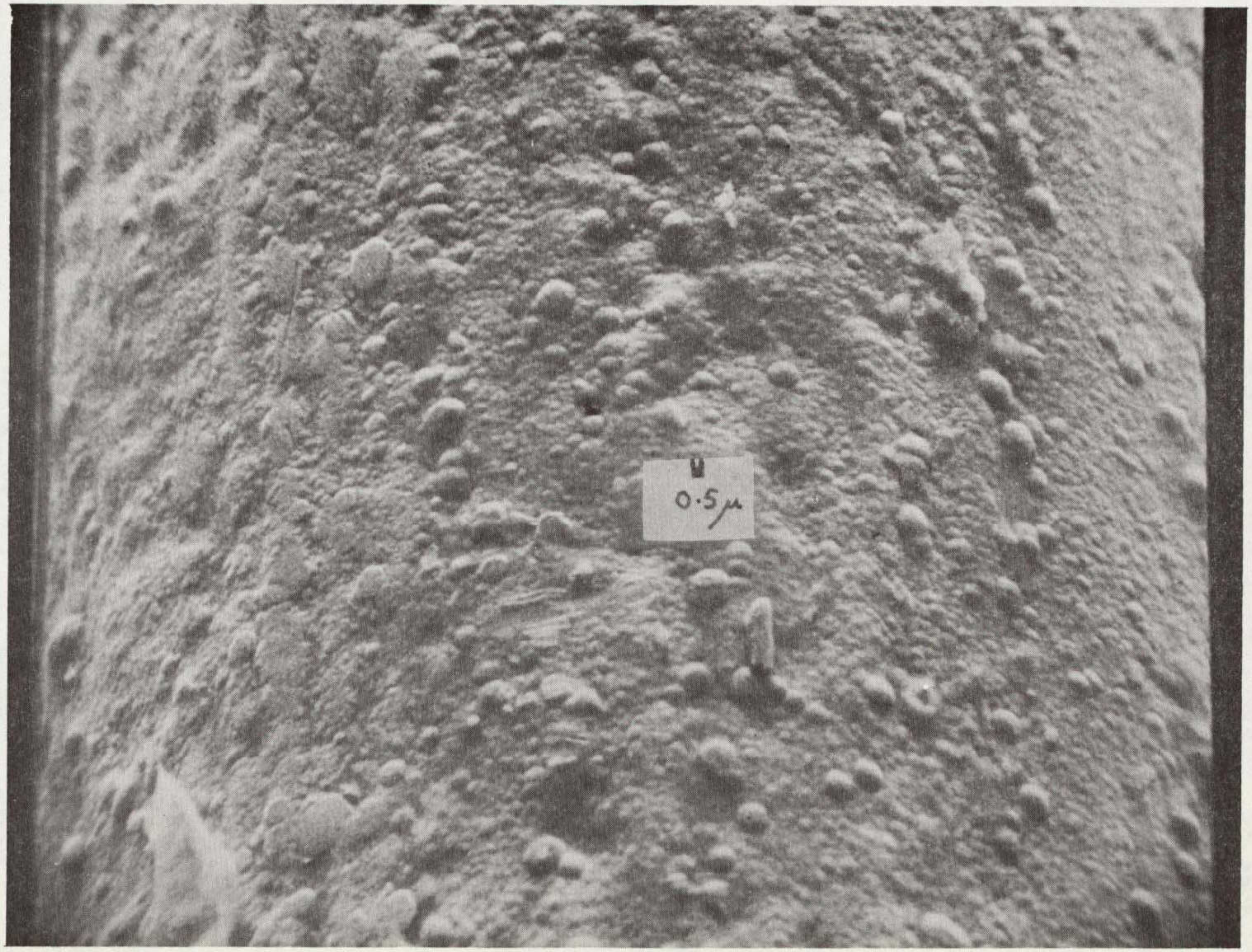

Figure 3. Scanning Electron Micrograph of the Surface of a Plated Wire

TABLE I. LATTICE PARAMETERS OF PHASES PRESENT

SUBSTRATE	NOMINAL PERMALLOY COMPOSITION	γ F.C.C.	CU F.C.C.	CU-BE SOLID SOLUTION F.C.C.	CU-BE COMPOUND 'ORDERED B.C.C.'(Å)
COPPER	IRON RICH NI 76 - 24 FE	N. D.	3.614	3.596	2.70
	ZEROSTRICTIVE NI 82 - FE 18	N. D.	3.616	3.596	2.70
	NICKEL RICH NI 88 - FE 12	N. D.	3.614	3.596	2.70
	PURE NICKEL	3.51	3.614	3.596	2.70
			AU F.C.C.		
GOLD	ZEROSTRICTIVE NI 82 - FE 18	3.54	4.072	3.595	2.70
COPPER BERYLLIUM WIRE	NONE	SOLUTION TREATED	-	3.583	2.70
		AGED AT 430 °C	-	3.606	2.70

(b) Substrate platings, whether copper or gold, yielded good diffraction patterns with fairly sharp high-angle lines permitting a reasonably accurate determination of their parameter. This fact suggests that substrate platings are neither very fine-grained nor very highly stressed, since otherwise accurate parameter determinations would be difficult.

(c) Accurate lattice parameters of permalloy platings on copper substrates could not be made because no high-angle permalloy lines were visible on the films. As discussed above, this fact suggests either that permalloy platings are extremely fine-grained or that they contain large internal stresses.

A final observation made from the films is that the copper-beryllium wires exhibit a considerable degree of preferred orientation, judging from the anisotropy of the copper-beryllium solid solution lines. No plating, whether substrate, permalloy, or nickel showed any evidence of preferred orientation.

4. Stress Measurements–In view of the X-ray diffraction results, attempts were made to estimate the stresses residing in permalloy platings. A spirometer (contractometer) was used [(9)] which consists of a spiral metal strip, one end of which is free to rotate relative to the other. The amount of rotation is a measure of the stress induced in the spiral either by direct loading or by electroplating a permalloy layer onto it. The direct loading deflections enable the rotation, or twist, of the spiral to be calibrated in terms of known stresses, so when an unloaded spiral is electroplated with permalloy, the plating stresses may be directly inferred from the observed twisting.

Experiments showed that permalloy platings contain residual tensile stresses of about 70, 000 psi. These measurements are discussed elsewhere in connection with observed strain-dependent aging phenomena.

5. Grain Size Measurements–Since metallographic and X-ray diffraction investigations both suggested that permalloy platings exhibit very fine grain sizes, it was necessary to use transmission electron microscopy techniques in order to make any measurements of grain-size distributions in plated wires. In order to prepare samples which could be examined, transmission electropolishing techniques were used to thin the permalloy platings which were then removed from the wires by dissolving the Cu-Be and copper substrate in ammoniacal solution. A typical electron micrograph is shown in Figure 4 from which it may be seen that the grain-structure is rather heterogeneous and that many grains show evidence of faulting. There appear to be at least two different types of fault:

(a) sharp, parallel, faults thought to be twins

(b) irregular shaped faults.

In the case of the pure nickel plating shown in Figure 5 the grains are seen to be much more regular than in the permalloy case, and practically all the faults are sharp, parallel, twins.

Grain-size distributions were estimated by measuring about one hundred grains in six or seven foils made from each sample. They are only to be regarded as semi-quantitative, since subjective decisions were inevitably involved in the choice of grains to measure.

Figure 6 shows plotted histograms of observed grain-sizes versus frequency for samples of iron-rich, zerostrictive, and nickel-rich wires. Two types of zerostrictive wires were examined; those prepared by normal plating techniques, and those prepared with a saccharin additive in the plating bath.

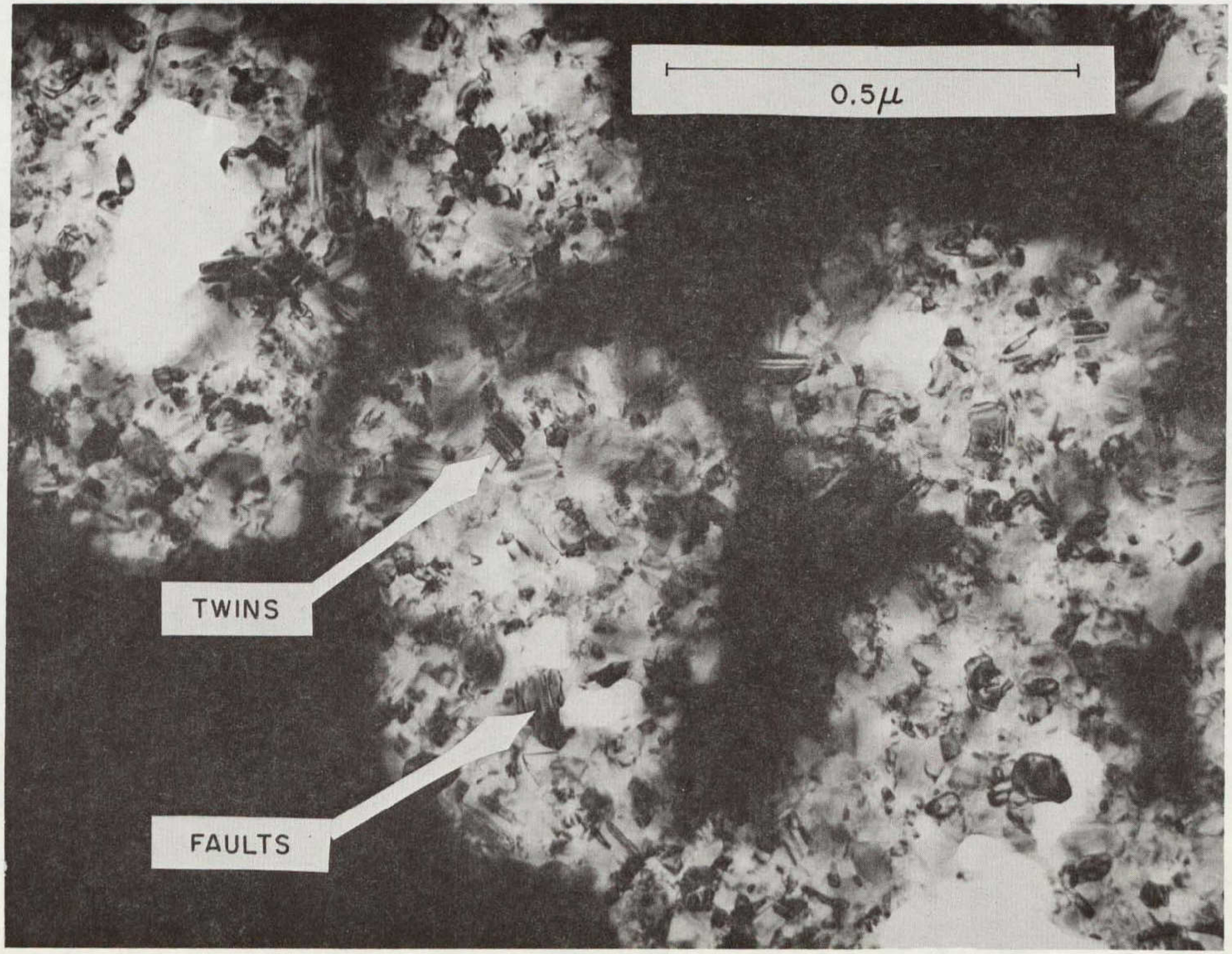

Figure 4. Transmission Electron Micrograph of Zerostrictive Alloy Plating

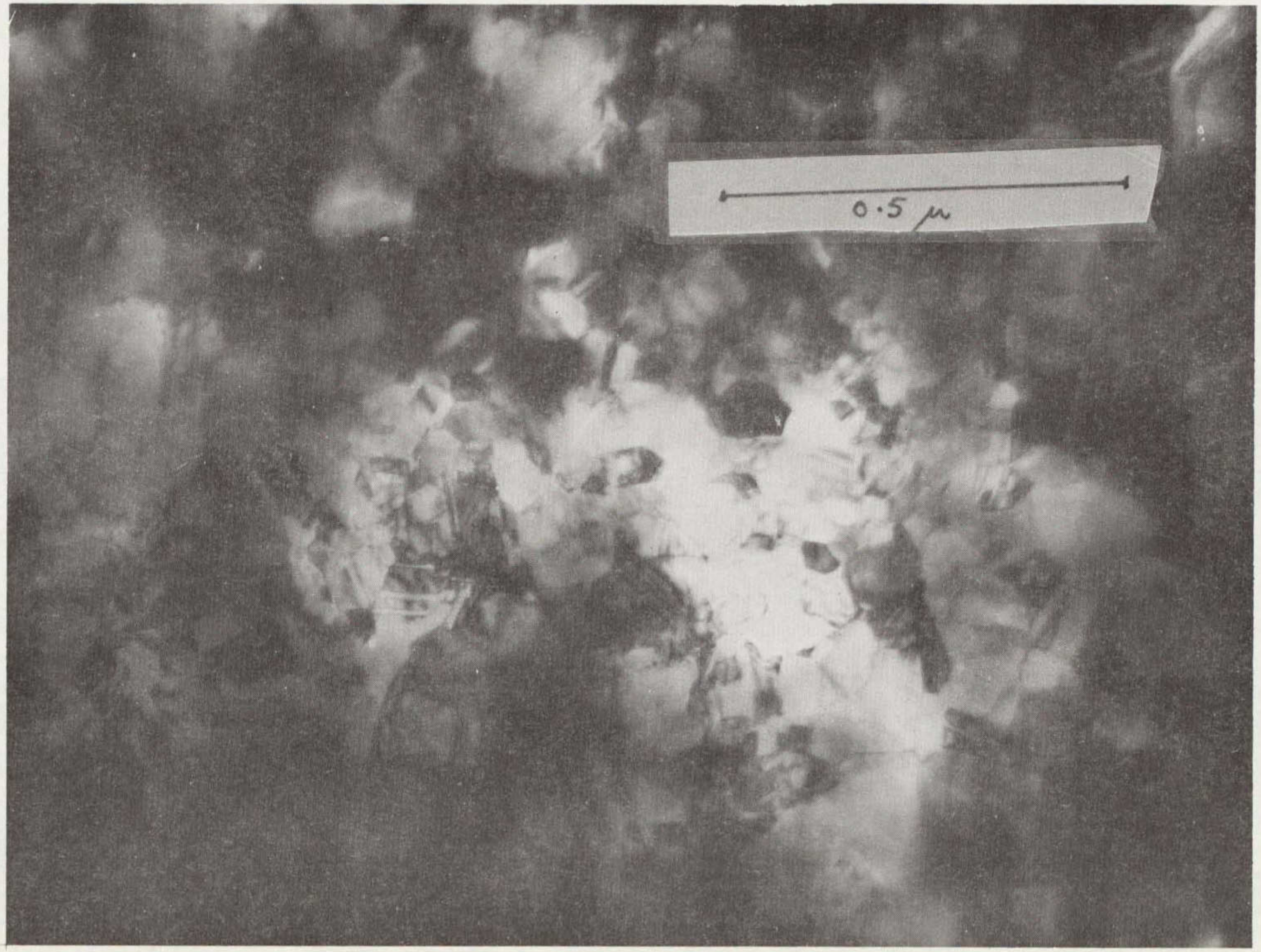

Figure 5. Transmission Electron Micrograph of Pure Nickel Plating

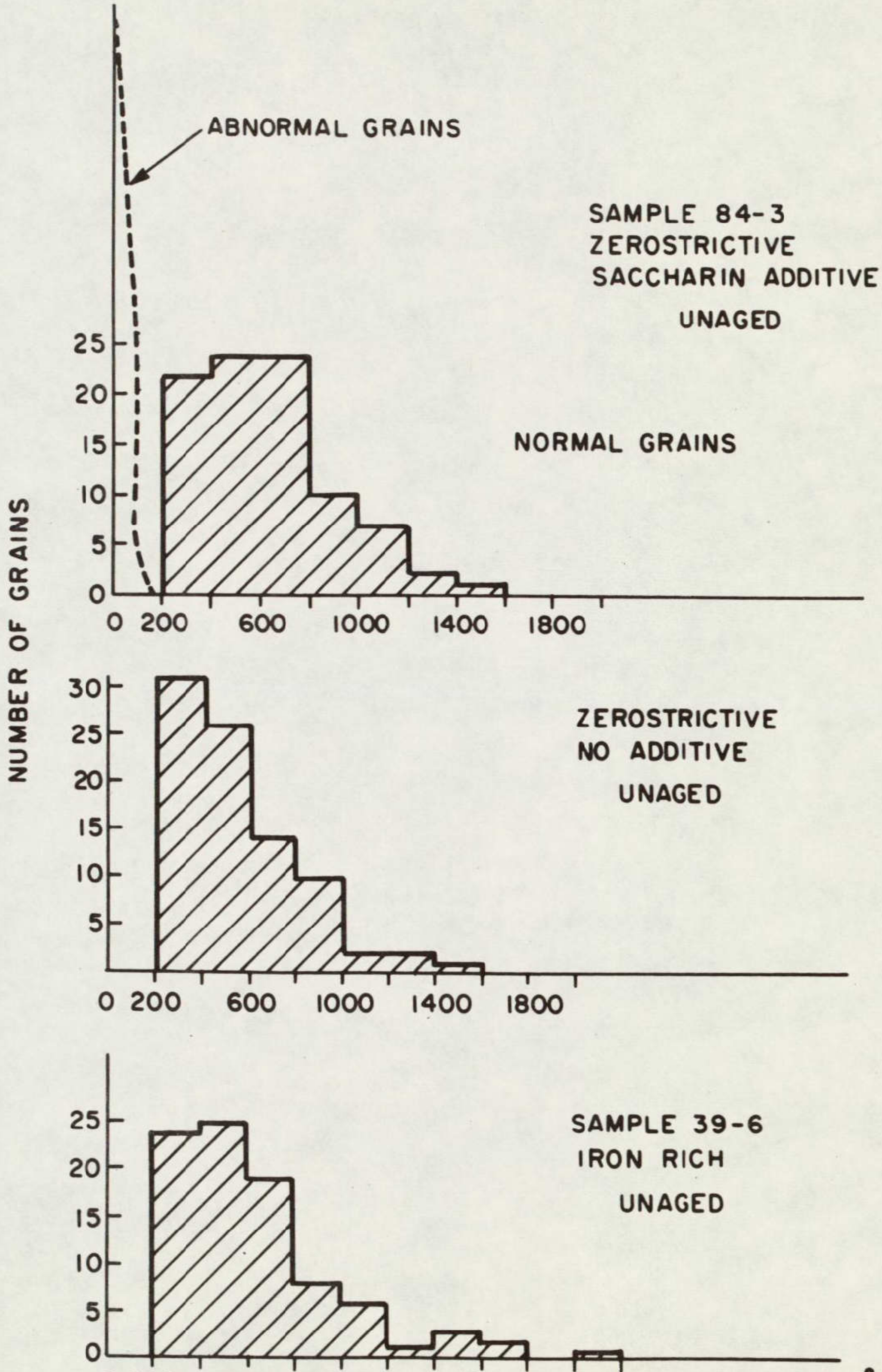

Figure 6. Grain-size Distributions Observed in Various Permalloy Platings

The 'normal' platings all exhibited a skewed distribution of grain size, with modal values in the 200 to 600 Å range, but with occasional grains as large as 1600 to 2800 Å. By contrast, the plating made with saccharin additive appeared to have two quite different grain-size populations, as may be seen from Figure 6.

One population yielded a skewed grain-size distribution with a modal value around 600 Å, but the second population consisted of extremely fine grains, less than 200 Å diameter. Both distributions are shown in Figure 6.

One further point is worth noting. Out of some 700 transmission micrographs made, none yielded a transparent area much larger than 0.5μ across. This fact may perhaps reflect the observed irregularity of the surfaces of these wires. It was previously noted that a wire exhibits a wavy appearance at its surface, on a sub-micron scale, and it may well be that this irregular topography affects the electropolishing behavior of the materials.

6. Phase Structure of Platings—Electron diffraction patterns were recorded for all the samples examined in transmission, and from these patterns it is possible to determine the phases present in the platings. It should be clearly understood that electron diffraction patterns do not allow accurate lattice parameters to be measured for the simple reason that the beam divergence inevitable in the instrument causes a "spread" of apparent Bragg angle of about 10 minutes of arc in the worst case. While this spread would be negligible in the X-ray case, where parameters are determined from lines corresponding to Bragg angles $\sim 90°$, in electron diffraction Bragg angles are close to $1°$, and hence a spread of 12% in the apparent parameter can be expected.

Even with this restriction, however, the patterns are still useful in providing qualitative analysis of phases present, providing the spread of the strong lines does not obscure all the weaker lines which may be present.

Examination of a few hundred patterns revealed three distinct types, shown in Figure 7.

(a) The first pattern is due to pure nickel, and shows the normal F. C. C. lines expected, together with two very diffuse broad rings. Approximate parameters are plotted in Figure 8 and it seems clear that the nickel pattern includes extra diffuse reflections due to double-diffraction effects at twin boundaries.

(b) The second type of pattern was only consistently observed in permalloy platings which had not been subject to annealing. In this case, three weak spotty rings extra to the F. C. C. pattern were observed at d spacings of around 1.45 Å, 1.35 Å and 1.13 Å.

It is considered very unlikely that these extra rings are due to contamination, so they indicate the presence of a phase different from the γF. C. C. one based on nickel. The fact that the rings are spotty suggests that the new phase is present as discrete particles and seems to rule out the possiblity that the lines might be artifacts due to planar features such as twin boundaries or stacking faults in the F. C. C. crystals.

(c) The third type of pattern was typical of permalloy platings which had been subjected to a flash anneal at ~375°C for a few seconds subsequent to plating. Though otherwise similar to the unannealed plating, these patterns consistently showed only <u>two</u> extra spotty rings, at approximate d spacings of 1.45 Å and 1.13 Å. Apparently, therefore, annealed platings contain a phase related to that observed in unannealed platings, yet missing a diffraction line.

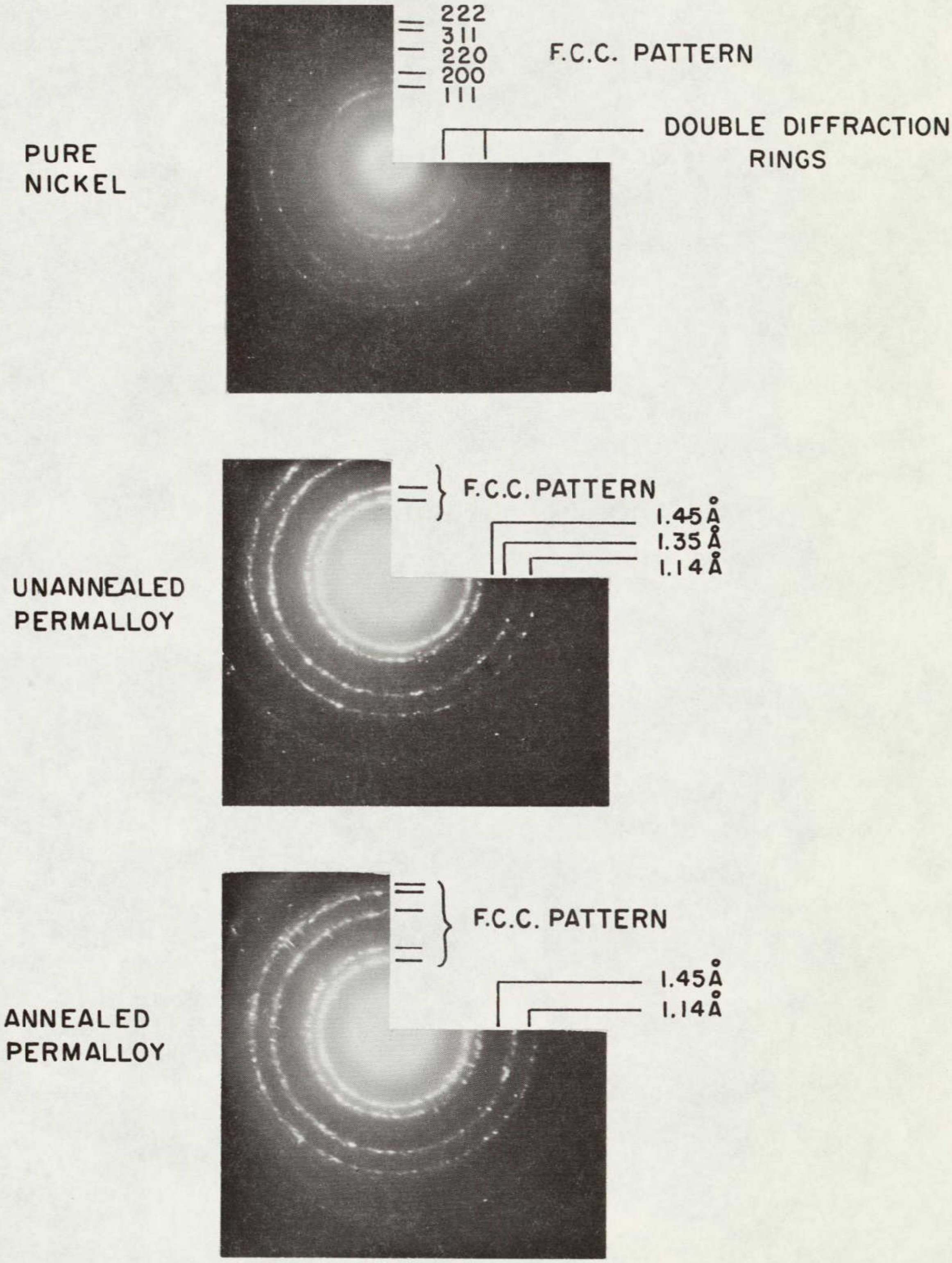

Figure 7. Electron Diffraction Patterns Observed in Platings

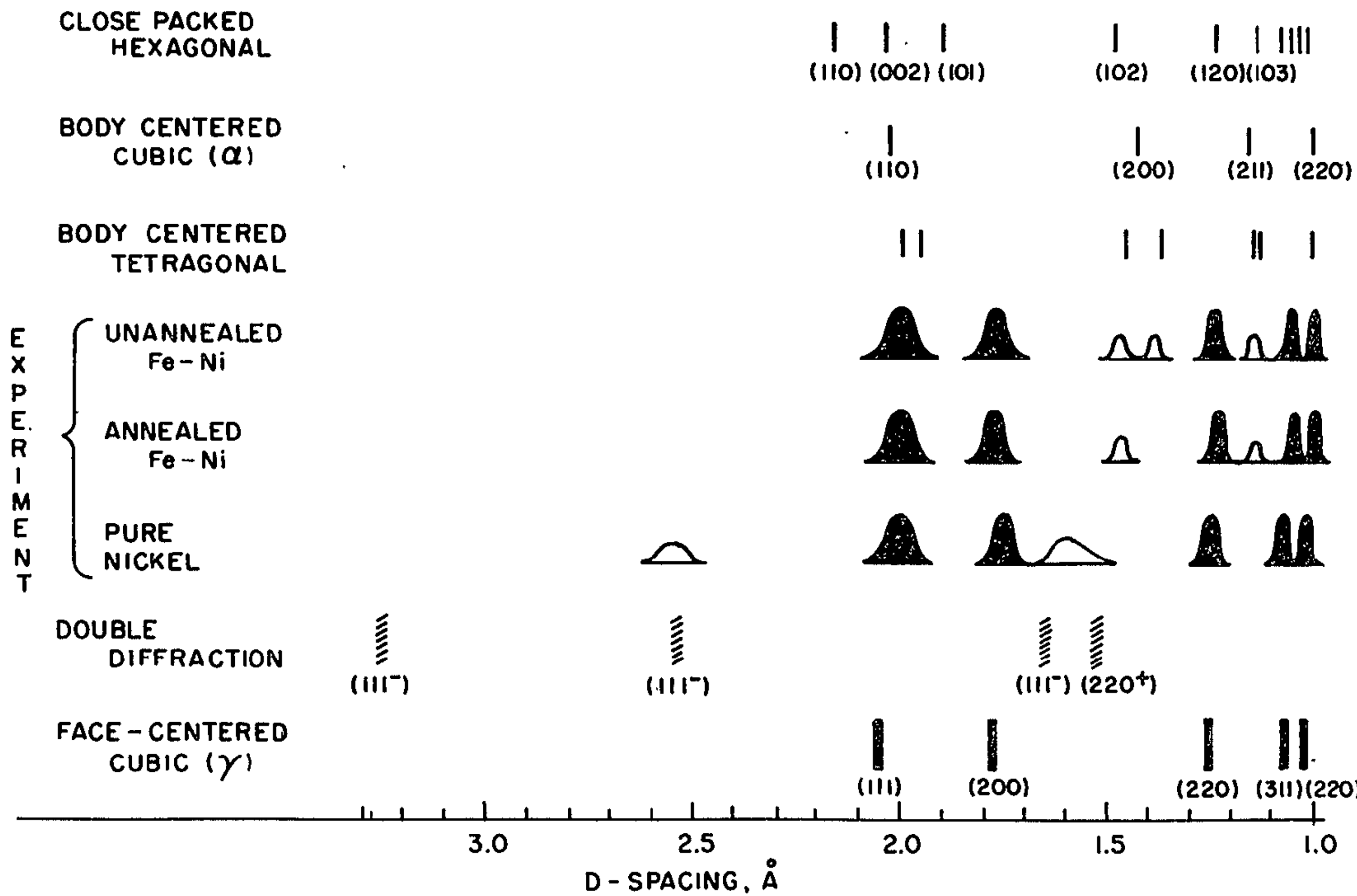

Figure 8. Approximate Lattice Parameters (D-spacing) of X-ray Diffraction Lines Observed in Platings

Now the interpretation of these results seems to demand a phase present in permalloy which is not present in pure nickel, and that the phase itself transforms on annealing. Three major candidates present themselves for consideration:

(a) The ordered γ' F. C. C. phase.

(b) A metastable C. P. H. phase based on γ nickel.

(c) The martensite α phase derived from γ by a shear transformation.

The ordered γ' phase seems unlikely because:

(a) The difference in scattering power of iron and nickel atoms is extremely small, and ordering lines are normally invisible.

(b) There seems no reason why one ordering line should disappear on annealing at 375°C - indeed the ordering should be even more marked under those conditions.

(c) The extra lines were consistently observed in permalloys of composition 88 Ni-12 Fe. This particular alloy has never been observed to show ordering.

The metastable C. P. H. phase has been sporadically reported in the literature, but its existence has never been universally agreed. In the present case two further objections are clear:

(a) The phase is not observed in pure nickel, though there seems no reason why it should be less stable in the pure element than in the alloy containing only 12% iron.

(b) Even though the C. P. H. phase might account for the appearance of lines at 1.45 Å and 1.14 Å in annealed samples, it is clearly incapable of explaining the presence of a line at 1.35 Å in the unannealed case.

The remaining possibility is that the lines are due to the appearance of the martensite structure within the F. C. C. grains. This seems to be the most acceptable explanation of the extra lines for the following reasons:

(a) Martensite would only be expected in alloys containing iron, and this provides a natural explanation of the absence of the extra lines from pure nickel samples.

(b) Martensites, though based on the B. C. C. α-iron structure, are frequently observed to be slightly tetragonal if containing interstitial solutes. The lines at 1.45 Å and 1.35 Å in the unannealed samples could therefore correspond to the (200) and (002) planes in the body-centered tetragonal structure. As will be shown later in this report, as-plated wires contain significant quantities of dissolved hydrogen in interstitial solution, and interstitial solutes are known to induce tetragonality in martensites.

(c) Annealing, as will be shown later in this report, results in the evolution of most of the hydrogen dissolved in permalloy platings, and it is therefore reasonable to suppose that the martensite in annealed foils may have relaxed to a body-centered cubic structure.

The line at 1.45 Å would then correspond to the (200) reflection, while the (002) line would be expected to merge with the (200).

(d) The α-iron B. C. C. phase is the only phase (other than γ F. C. C.) know to be stable in the iron-nickel system, and as will be shown in a later section of this report, the lines at 1.45 Å and 1.14 Å are present in wires aged 600 hours at 230°C.

(e) The presence of martensite in the permalloys would possibly account for the irregular faults seen in addition to sharp twins, and for the high level of internal stress already mentioned.

If the above interpretation of the electron diffraction results are accepted, then it must follow that the alloy composition fluctuates as much as 60% on the scale of 1000 Å or less. This is so because a great deal of work on iron nickel martensites has shown that the $\gamma \rightarrow \alpha$ transformation only occurs at room temperature in alloys containing less than about 20% nickel. The irregular faults are seen from Figure 4 to be comparable in dimension to the grain size, <1000 Å.

7. <u>Microprobe Investigations</u>–Electron-beam microprobe studies were carried out to obtain direct estimates of permalloy compositions and thus to supplement the estimates of alloy composition based on macroscopic magnetostriction measurements.

In discussing the microprobe results it is important to bear in mind their scale. Magnetostriction tests are performed on 2 inch lengths of wire, and give an estimate only of the composition of the permalloy plating averaged over a volume of some 2.10^7 cubic microns.

In the microprobe, the volume of material irradiated by the electron beam was typically only 20 cubic microns, thus yielding an estimate of composition of a sample one-million times smaller than that used in magnetostriction tests.

Even on this scale, however, the microprobe would be quite incapable of showing up composition fluctuations on a 1000 Å scale, since the volumes of material would then be of the order 10^{-3} cubic microns, a factor ten thousand smaller than the instrument can interrogate.

Clearly one might expect the microprobe results to be somewhere intermediate between the uniform composition suggested by magnetostriction and the ±30% composition variations predicted by the electron diffraction patterns.

Figures 9 and 10 show that the results are as expected. Composition variations of the order ±2% in alloy content were observed in all wires. The most interesting feature of the results is that the variations are not random, but occur in almost a sinusoidal fashion around the circumference of the wires, while being relatively uniform along the wire axis at any given azimuth. The circumferential variation has been reported previously.[13]

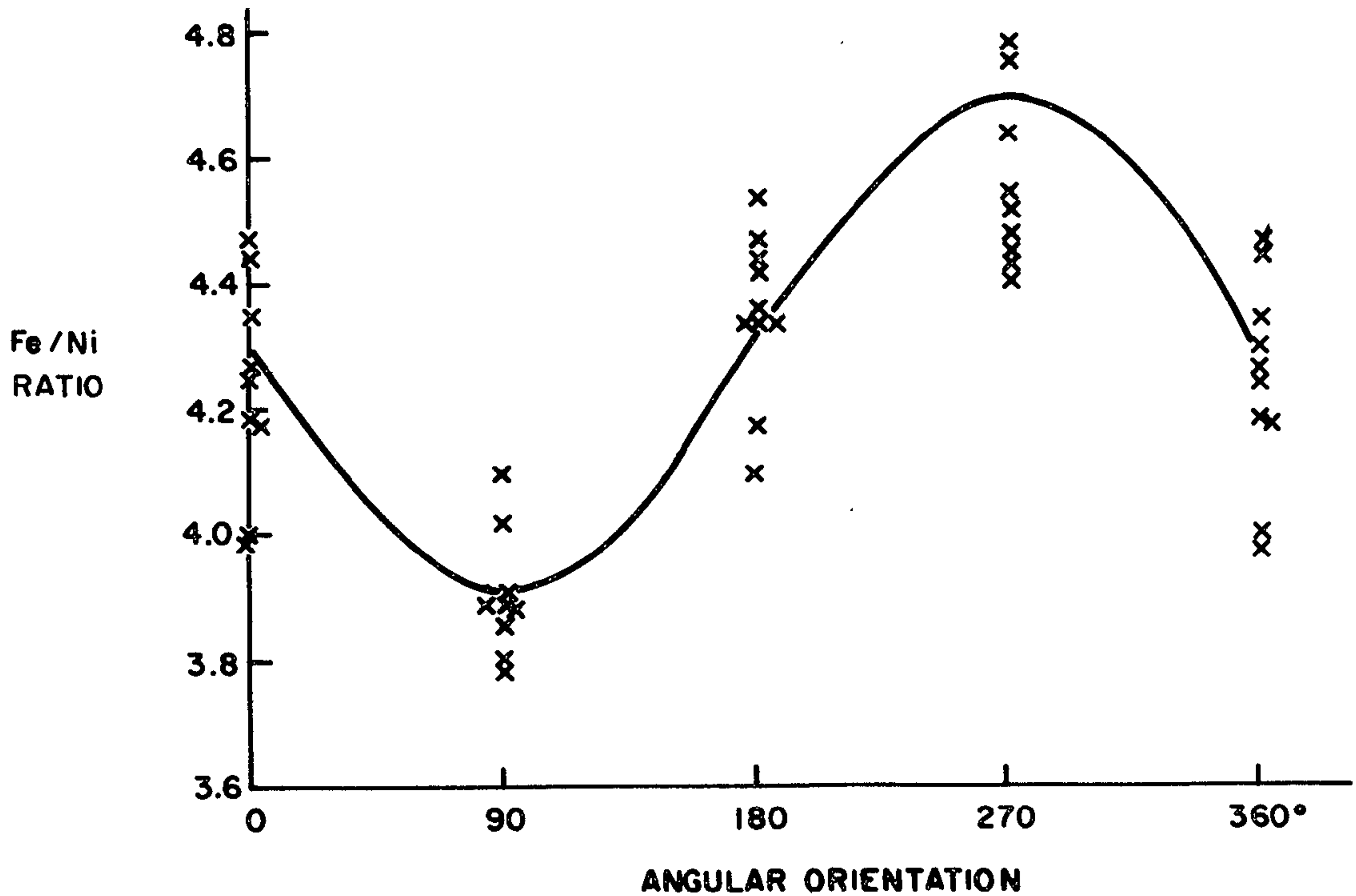

Figure 9. Observed X-ray Intensity Ratios in a Zerostrictive Alloy Plated on Copper

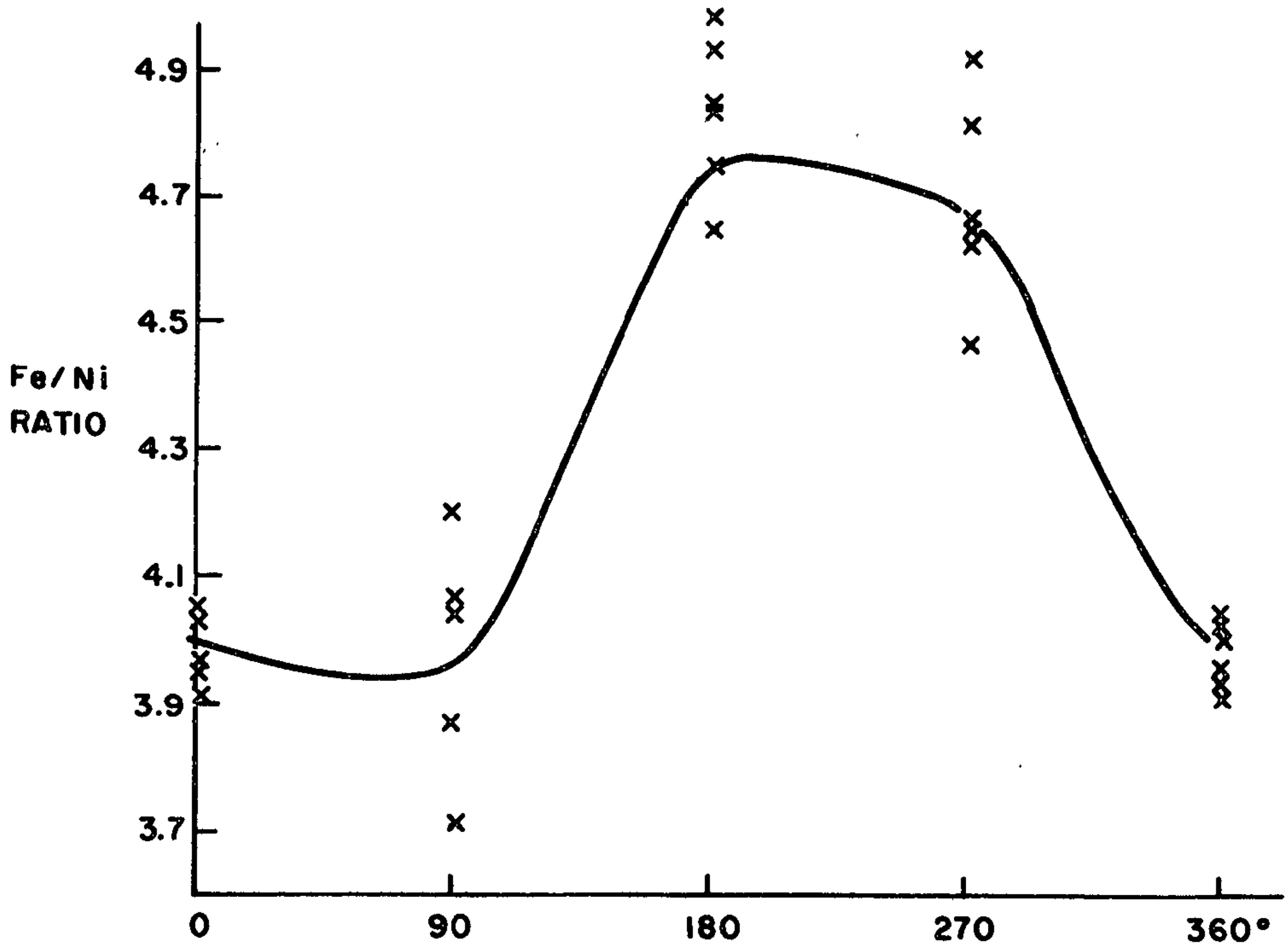

Figure 10. Observed X-ray Intensity Ratios in a Zerostrictive Alloy Plated on Gold

No significant differences were noted between platings prepared with, and without, saccharin additives in the bath, nor did there appear to be any difference between nominally identical permalloy platings laid down on gold or copper substrates. This composition variation is undoubtedly connected with the unidirectional flow of electrolyte into the plating cell.

In an effort to check the possibility of composition variations through the thickness of the platings, samples were examined which had either been etched (thereby losing surface material) or been plated at higher speeds so as to be thinner, even though plated under nominally identical conditions otherwise. Results are plotted in Figure 11 from which it may be deduced that the thinner samples tended to be some 3% richer in nickel than standard wires, as though a slight composition gradient extends through the plating as well as around it. The composition scale on the right of the diagram was determined from bulk standards which had been chemically analysed.

8. Summary of Physical Investigations. As a coherent picture has built up, the most striking feature of the plated wires examined has been their heterogeneity. Not only is the surface topography of the wire very irregular, due to the nature of the substrate platings, but the grain sizes in the permalloy platings are far from being single-valued. The grains themselves are inhomogeneous, containing twins and faults ascribed to martensitic transformations; while the alloy composition definitely varies ±2% on the micron scale, and is expected to vary by as much as ±30% at the granular or 1000 Å level. The overall implications of this heterogeneity upon the magnetic behavior of the plated wires during aging will be explored in the following sections of this report.

B. MAGNETIC PROPERTIES

Measurements of low frequency film properties generally follow, in principle, the methods described in the literature[14] for flat films. In the case of the measurement of easy axis dispersion the method of sample

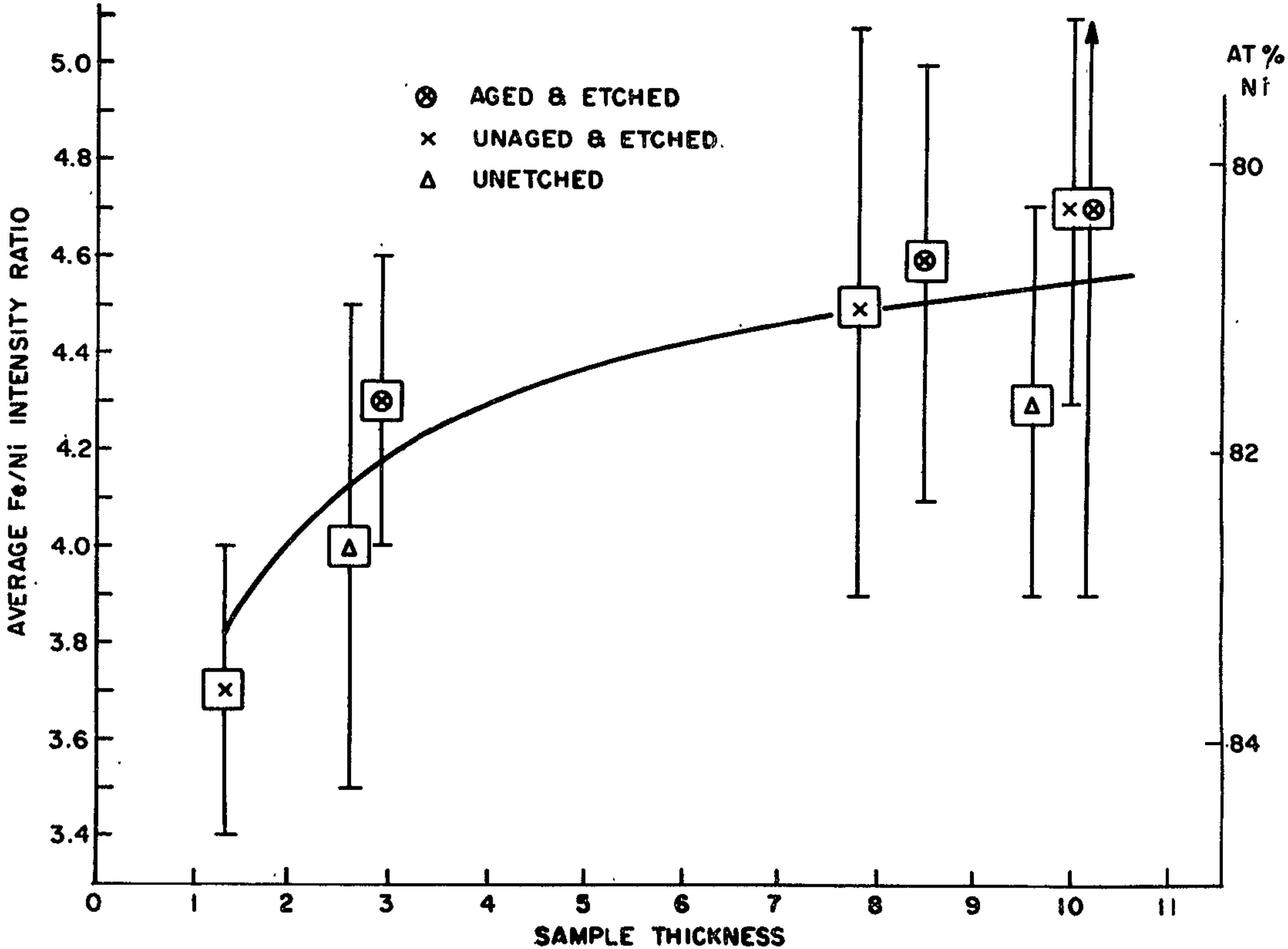

Figure 11. Variation of Average X-ray Intensity Ratios as a Function of Plating Thickness

rotation generally used for flat films[14, 15] is not applicable to plated wire. Instead, the usual plated wire method is that due to Belson.[16] We have supplemented the Belson test with a method which essentially substitutes a rotation of the magnetic field for that of the sample.[17] In addition the accepted torsional method of measuring magnetostriction has been supplemented, for the reasons made clear in Section IV, by a tension sensitivity test described in Appendix I. Background material for the understanding of the properties of magnetic thin films may be found in standard references.[18]

IV. BASIC AGING STUDIES

A. PROCEDURES

Aging conditions fall under two general classes:

(1) Annealing at elevated temperatures in near-zero (<0.1 Oe) magnetic field. This is referred to as shielded aging.

(2) Annealing at elevated temperatures in the presence of axial (hard-direction) magnetic fields of various intensities. This will be called field-aging.

The shielded aging enclosure consisted of a mu-metal box made from 0.035 inch sheet obtained from Allegheny Ludlum Steel Corp. and hydrogen fired according to their specifications. The box was placed in a furnace controllable to ±3°C at temperatures up to 230°C. In the case of field aging, samples were inserted in suitable solenoids contained in the enclosure. Field-mapping in the enclosure and solenoid was accomplished with an axial probe in conjunction with a Bell, Inc. Model 120 Gaussmeter.

In monitoring the course of aging experiments, the samples undergoing aging were periodically removed from the aging environment and the sample properties measured at room temperatures. In most detailed studies, different portions of wire from a single plating process were aged for separate periods, so that samples of a particular aging time could be preserved for metallographic examination. Vacuum aging was carried out by sealing off samples in tubes following overnight evacuation. The residual pressure was less than 10^{-5}mm. Hg.

B. SHIELDED AGING

1. Kinetics Studies – The purpose of aging kinetics studies is to determine time rates of change of magnetic parameters and to predict useful memory lifetime. In a previous publication[19] it was established that the average voltage output, $\bar{V}_1$ of the wire element under NDRO test conditions is a representative

parameter for monitoring aging rates. As a result of these studies, lifetimes and activation energies were determined. It was also found that under field-shielded aging conditions, referred to as "shielded-aging," the memory failure was due to insufficient write and was accompanied by an increase in easy-axis dispersion, α. Since α is a more basic film property than output, i.e. less dependent on memory configuration and method of testing, it was desirable in the present study to use it as the dependent variable in shielded aging studies. The close relationship between output and dispersion is illustrated by Figure 12. This figure shows, for zero magnetostrictive wire, the time dependence of both the electrical output (top) and the easy-axis dispersion (bottom) under shielded aging in air atmosphere at temperatures near 200°C. The output curves are reproduced from the data of Ref. 19, while the dispersion results were obtained under the present study. Both sets of data are normalized to their unaged levels, V_o and α_o. In both sets of data aging times may be arbitrarily defined in terms of changes in the dependent variable. As in Ref. 19 the output time constant is chosen as the time at which $V/V_o = 0.75$. From Figure 12 this level of output degradation is found to correspond approximately to a dispersion ratio of $\alpha/\alpha = 2$. This approximate correspondence is illustrated in Figure 13, which is a semi-log plot of time constants vs. reciprocal absolute temperature. Over limited temperature ranges such plots are expected to obey an equation of the form

$$t_i = A_i \exp (E_i/kT), \qquad \text{IV-1}$$

where t_i is the time constant, E_i the activation energy, k is Boltzmann's constant, T the absolute temperature and A_i a constant.

Eq. IV-1 is derived from the familiar Arrhenius rate equation.[20] The straight line of Figure 13 gives an approximate description of the temperature dependence t_{25}, the time required for 25% output degradation, and t_2, the time for dispersion doubling. Fitting Eq. IV-1 to this straight line, we find:

$$t_{25} \cong t_2 \cong 4.0 \times 10^{-16} \exp (1.7/kt) \qquad \text{IV-2}$$

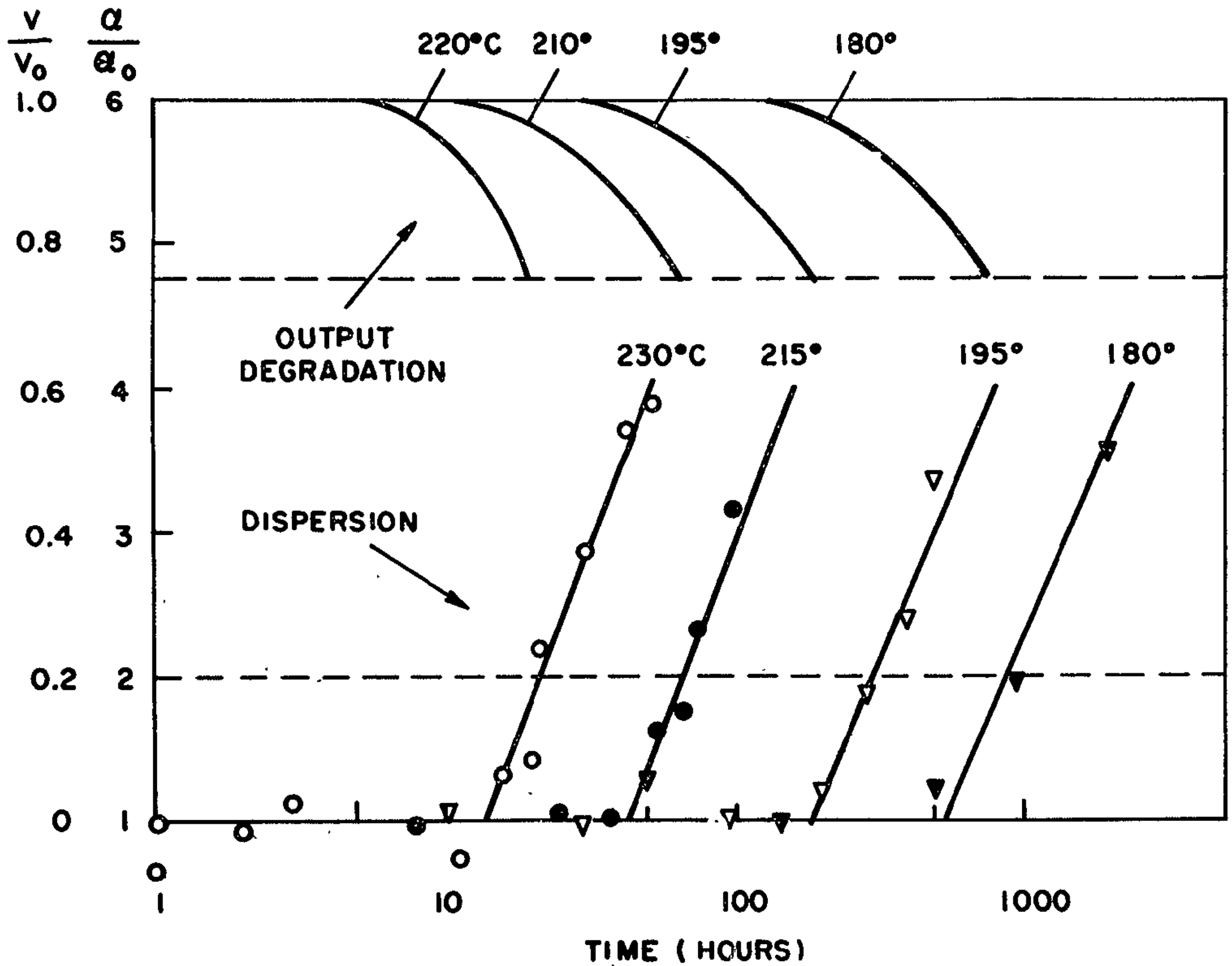

Figure 12. Output Degradation and Dispersion in Shielded Aging (air)

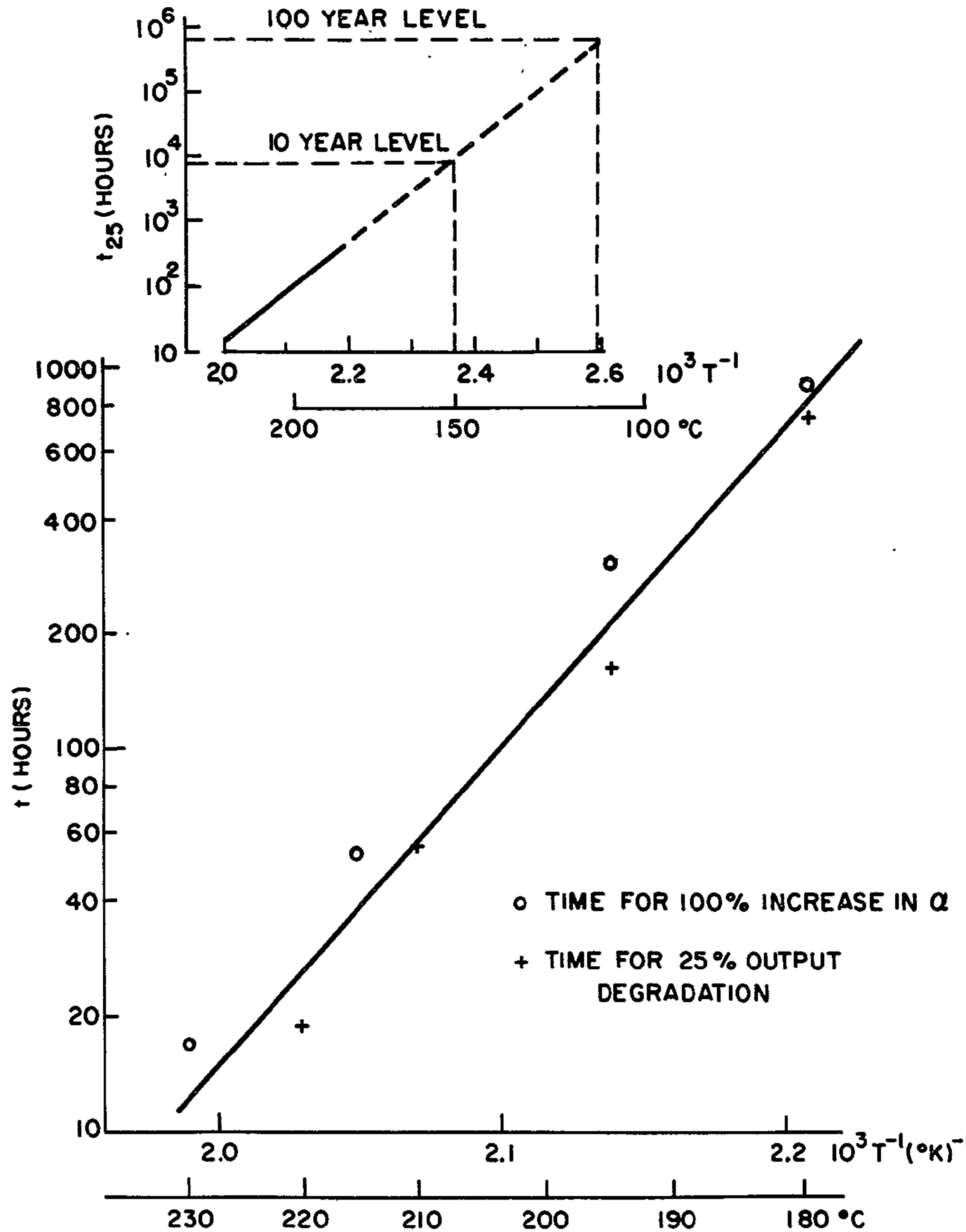

Figure 13. Kinetics of Shielded Aging

where t_{25} and t_2 are in hours and k is in electron volts per OK. The use of Eq. (IV-2) for extrapolating lifetimes is illustrated in the upper part of Figure 13, showing extrapolation of the time constants to the 10 and 100 year levels. These levels correspond to temperatures of about 150°C and 110°C, respectively. These and similar techniques of extrapolation and lifetime predictions have been discussed in previous publications.[19, 21, 22] The present results establish the close connection between shielded memory aging and dispersion increase. Dispersion measurements are used extensively in subsequent sections in various shielded-aging experiments. The relation of field-aging to lifetime evaluation is also discussed in a later section.

2. Microstructure changes—Microstructural changes taking place in wires annealed at elevated temperatures were monitored by X-ray diffraction, electron microscopy and residual stress measurements. Samples examined had been annealed at temperatures from 180°C to 230°C for times ranging from 24 hours to 2000 hours.

In general it was found that X-ray diffraction patterns derived from wires annealed at temperatures below 230°C were similar to those of unaged samples. In particular, the high-angle permalloy lines were absent, except in the case of a 6% Nickel-rich sample aged at the highest temperature (230°C).

Grain-size distributions were measured on zerostrictive Cu-substrate samples which had been aged at temperatures from 180°C to 230°C and the resulting histograms are shown (Figures 14 through 16) with unaged samples for comparison. As mentioned in an earlier section of this report, unaged samples all exhibited a skewed unimodal distribution (except for the sample plated with saccharin additives which appeared to have two distinct grain populations).

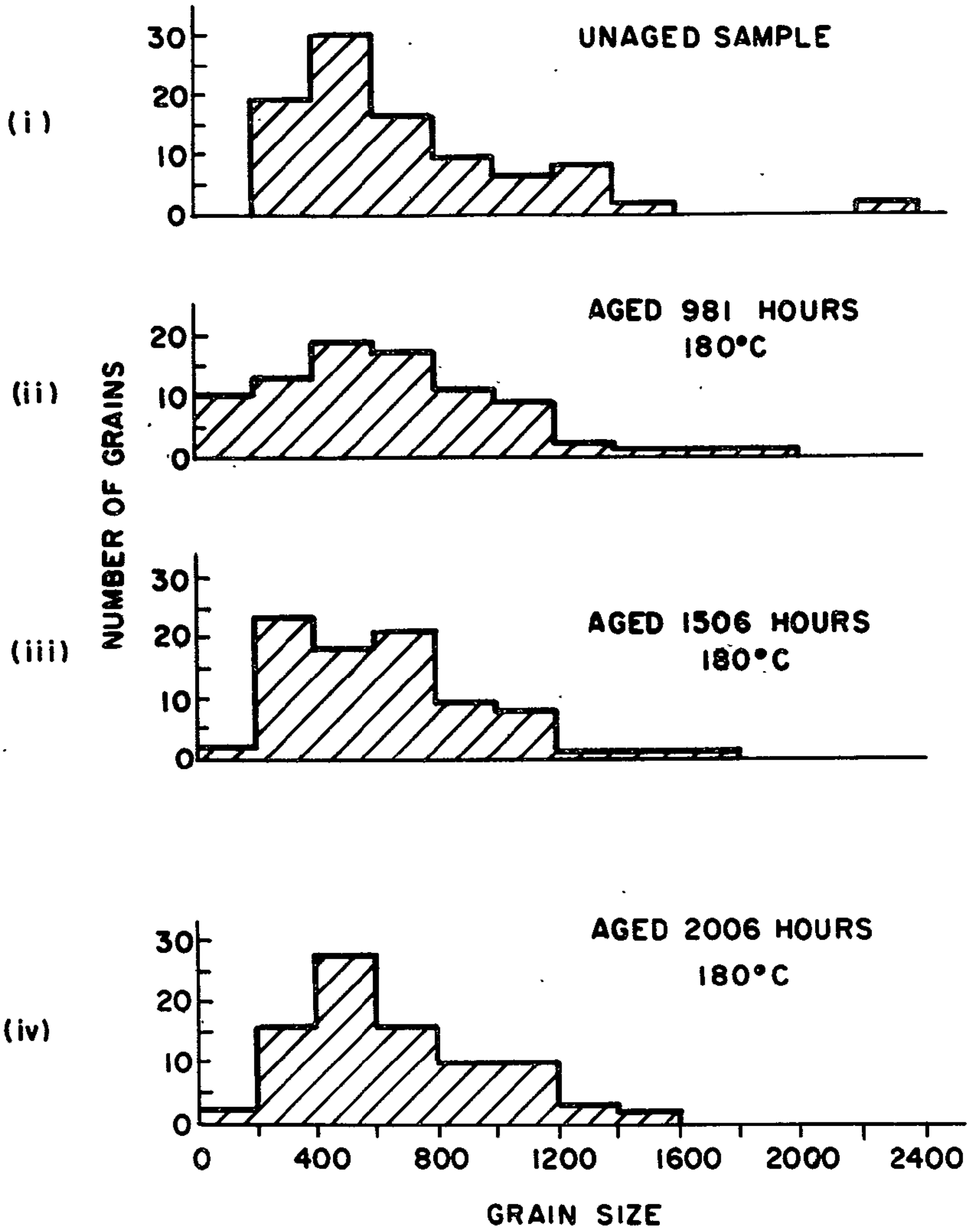

Figure 14. Grain-size Distributions in Samples Aged at 180°C

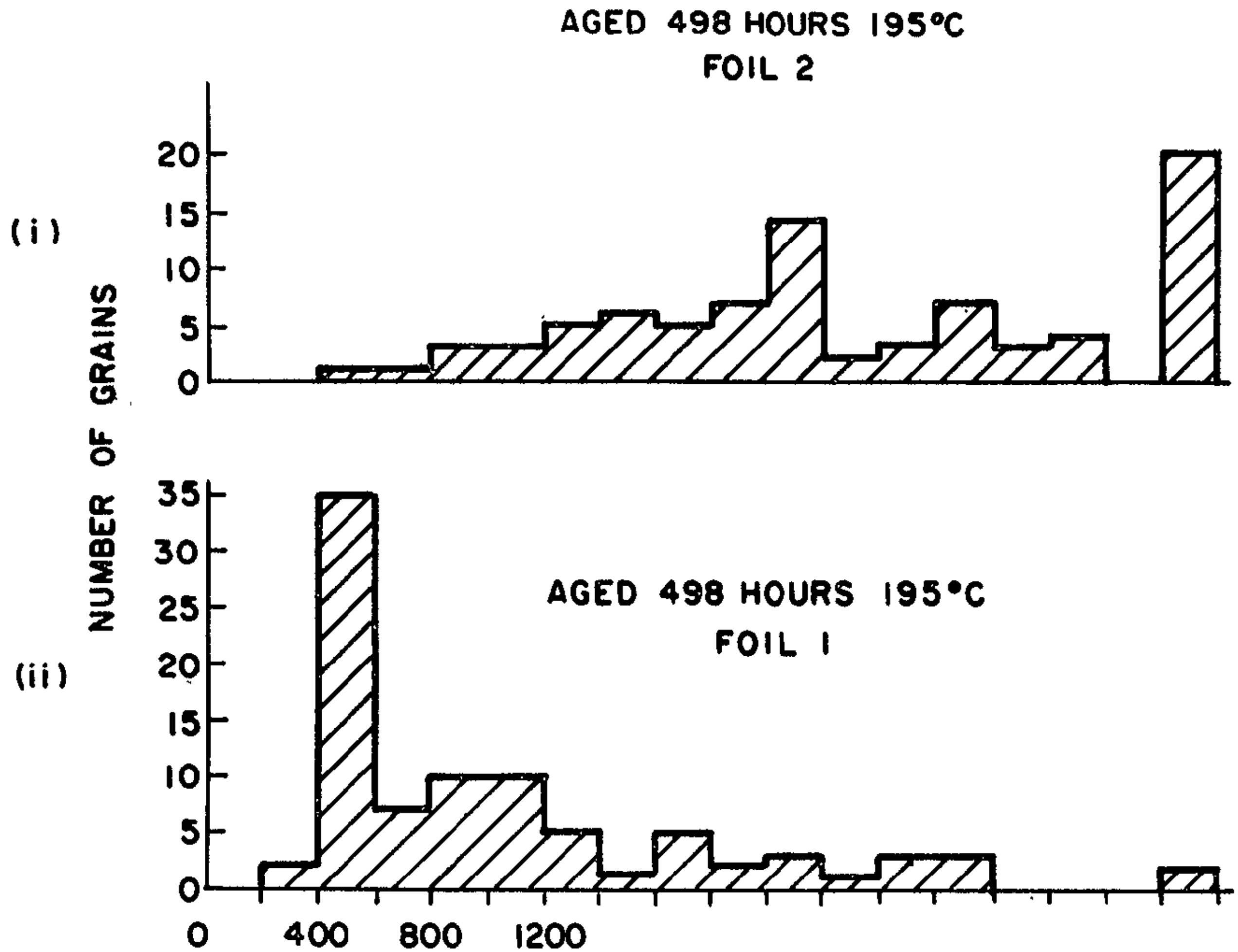

Figure 15. Grain-size Distributions in Samples Aged at 195°C

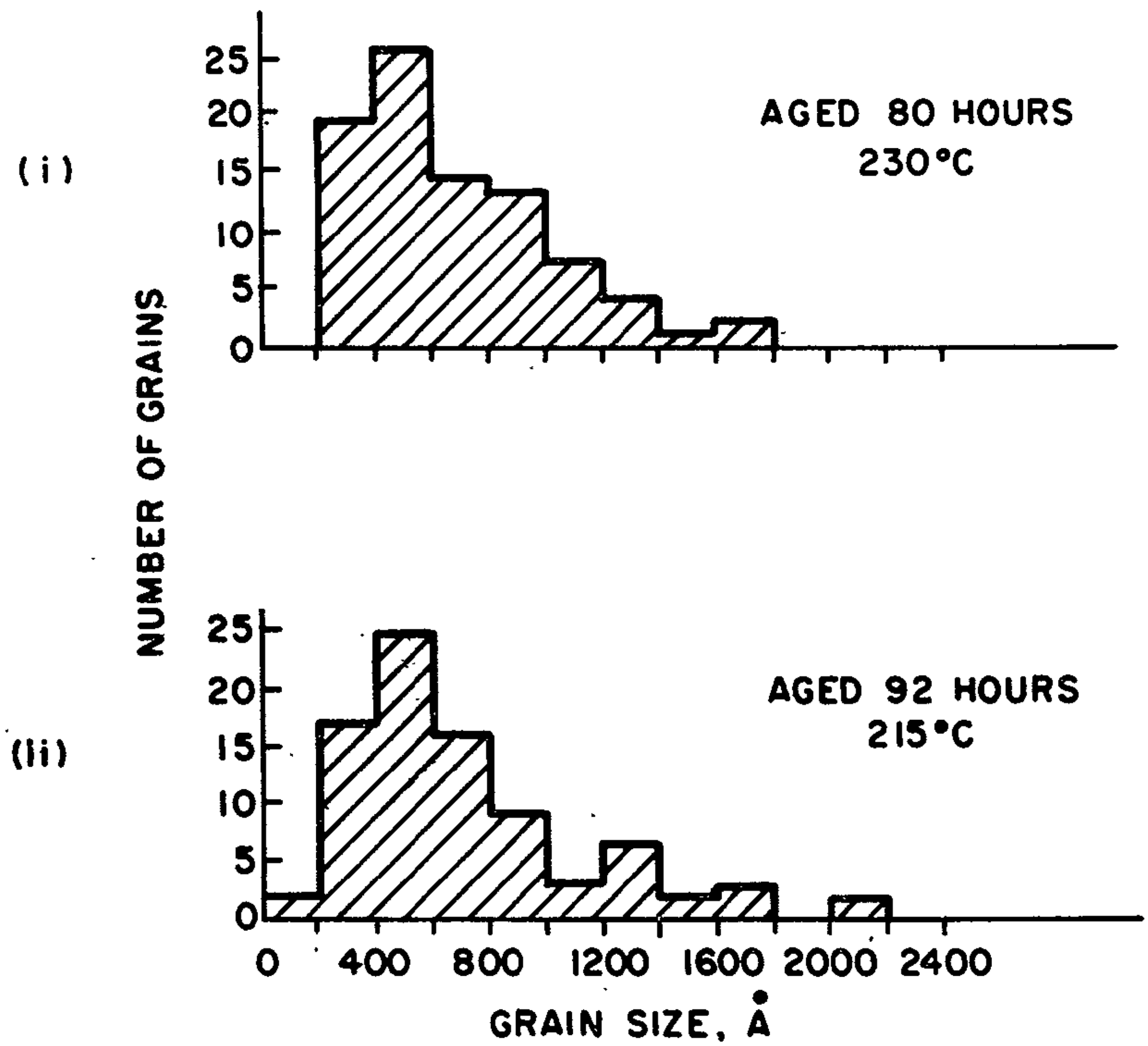

Figure 16. Grain-size Distributions in Samples Aged Above 195°C

Aged samples were found to exhibit any one of three distributions:

(a) Skewed unimodal (Figure 14; i, iv)

(b) Bimodal (Figure 14; iii)

(c) Flat distribution of large grains (Figure 15, i, ii).

These distributions appeared in a random fashion and it was impossible to correlate their appearance with any parameter such as aging time, temperature or alloy composition. There seems only one explanation of these results, that recrystallization may occur in permalloy platings during aging, but that it is a discontinuous, heterogeneous process. This is, of course, characteristic of nucleation and growth processes; depending on the areas examined one might expect to find transformation unstarted, partial or complete.

Electron diffraction patterns derived from aged samples were found to exhibit the following characteristics:

(a) No sample exhibited any measurable degree of preferred orientation.

(b) All specimens yielded diffraction patterns exhibiting weak spotty rings at d spacings of 1.45 Å and 1.14 Å in addition to the F.C.C. γ-nickel pattern.

As was explained in an earlier section of this report, these extra lines were ascribed to a stable α-iron phase derived from the γ by a martensitic process.

3. Substrate Diffusion–In the previous section it was noted that aging had little effect upon the X-ray diffraction patterns of plated wires and that high-angle permalloy lines almost never appeared. These results were considered rather puzzling and it was decided to anneal samples at 450°C for 1 hour in order to fully recrystallize them. Two samples were chosen, both of

zerostrictive composition but deposited on copper or gold substrates respectively. Resulting diffraction patterns are of considerable interest in two respects:

(a) No signs were found of the original substrate materials. Pure copper was not detected in the one case, while in the other the gold was found to be completely converted to the intermetallic compounds Cu_3Au, CuAu, and AuBe.

(b) High-angle permalloy lines were absent from the copper substrate sample but present in the gold substrate case.

It seemed clear from these results that considerable interdiffusion occurred between gold substrates and the copper-beryllium wires, but not between gold and permalloy.

Since copper reflections were lost from the copper/permalloy plating combination it seemed reasonable to conclude that copper interdiffuses with the copper-beryllium wire during high-temperature annealing; furthermore, the absence of high-angle permalloy lines in this sample suggested that copper, unlike gold, might also interdiffuse with permalloy, leading to a chemical inhomogeneity great enough to cause excessive line broadening.

It became of interest, therefore, to see if the postulated interdiffusion of copper and permalloy could be confirmed by electron microprobe analysis and if so, whether or not the process might occur at lower temperatures in the range 180°C to 230°C where magnetic aging studies had been performed. The electron microprobe analytical technique depended upon the fact that the penetration of a 20 KV electron beam in permalloy is about 1.5 μm. Since the permalloy platings of interest were only 1μm thick, it was expected that some electrons would interact with the copper substrate and generate a certain level of copper characteristic X-radiation.

If then, some copper should interdiffuse with the permalloy during annealing, the level of copper X-radiation should increase since the electron beam would interact with a larger number of copper atoms than before.

Thus interdiffusion should be manifested by an increase in copper counts in the X-ray spectrometer.

The samples plated on copper and gold substrates were examined in the as-plated and 450°C annealed condition, and the copper or gold characteristic X-ray intensities measured. Results are shown in Table II in terms of counts per 100 seconds. These results provided a striking confirmation of the interdiffusional effects used to explain the X-ray diffraction patterns. Not only is a large increase of copper radiation observed after annealing a copper substrate wire, but a decrease of gold radiation is apparent after annealing a gold substrate wire. Thus it appears that copper diffuses into permalloy during annealing at 450°C, while gold diffuses away from the permalloy into the copper-beryllium wire under the same conditions.

TABLE II. ELECTRON MICROPROBE RESULTS ON SUBSTRATE DIFFUSION

WIRE SAMPLE	METALLURGICAL CONDITION	X-RAY COUNTS PER 100 SECONDS
Copper Substrate	As plated	28,000
	Annealed 1 hr. 450°C	60,000
Gold Substrate	As plated	7,500
	Annealed 1 hr. 450°C	7,300

In order to see whether or not interdiffusion of copper and permalloy occurred during annealing at temperatures between 180°C and 230°C, several series of nominally zerostrictive wires were examined which had been characterized magnetically after aging tests at 180, 195, 215 and 230°C.

Copper X-radiation intensities are shown in Figure 17 as a function of aging time. It will be noted that the aged samples all exhibited copper intensities greater than those observed in unaged samples; at any given temperature an incubation period exists, being greater the lower the temperature. It is possible to derive activation energies for the diffusion process from these curves. They vary from 29 kcal/mole to 37 kcal per mole (1.25 to 1.61 eV) depending on the degree of interdiffusion considered.

4. The Search for Composition Changes—In view of the observed diffusional effects between permalloy and copper, it became of interest to see if diffusion effects between iron and nickel could be measured in the permalloy itself. Such interdiffusion of elements within the permalloy would be expected to lead to a homogenization of the material on a microscopic scale of 1000 Å or so. As was pointed out in an earlier discussion, however, such effects might be beyond the ability of the electron beam microprobe to detect.

Composition profiles measured around various wires in both unaged and aged conditions are plotted in Figures 18 through 25 from which it will be realized that aging leads to no detectable change in either the average composition, or the amplitude of the composition gradient, of the wires examined.

The only change observed which might possibly be significant is that the scatter of composition at any given azimuth appears to become smaller in samples aged for several hundred hours at the highest aging temperature, 230°C. From a comparison of Figures 24 and 25 it does seem that the scatter is almost halved in the aged samples.

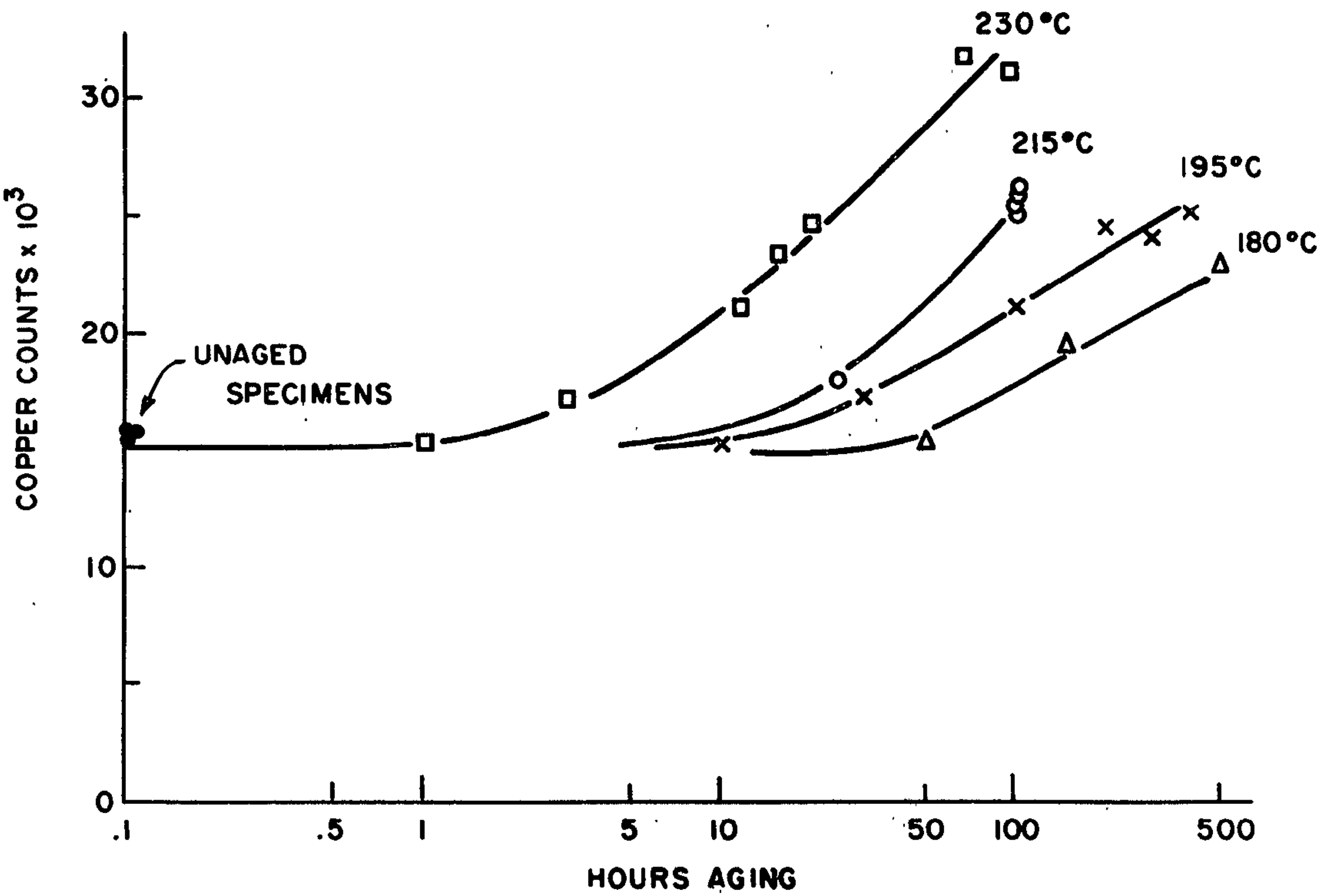

Figure 17. Copper X-ray Counts Observed in Aged Permalloys

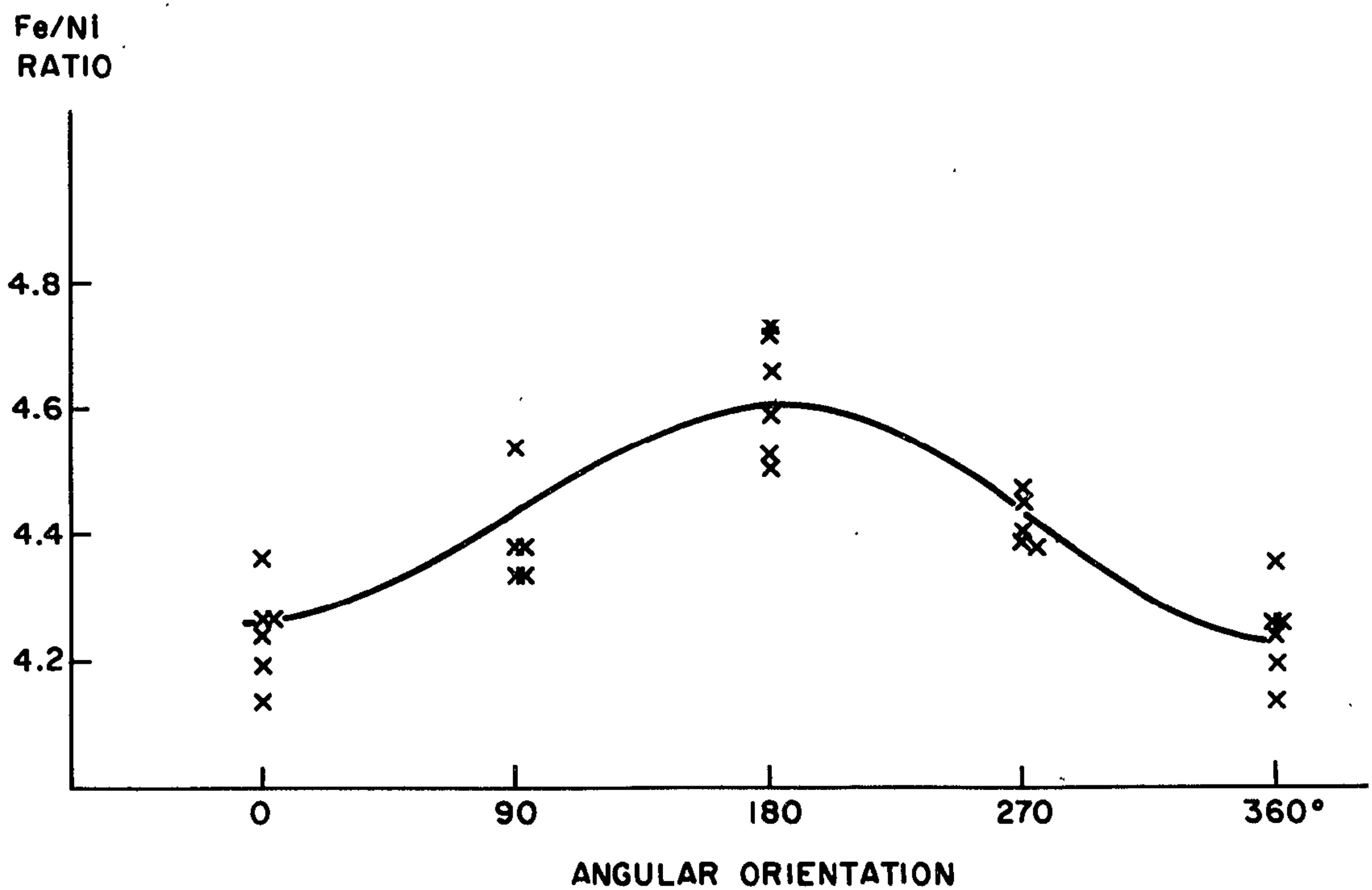

Figure 18. X-ray Intensity Ratios Observed in Zerostrictive Wire, Unaged

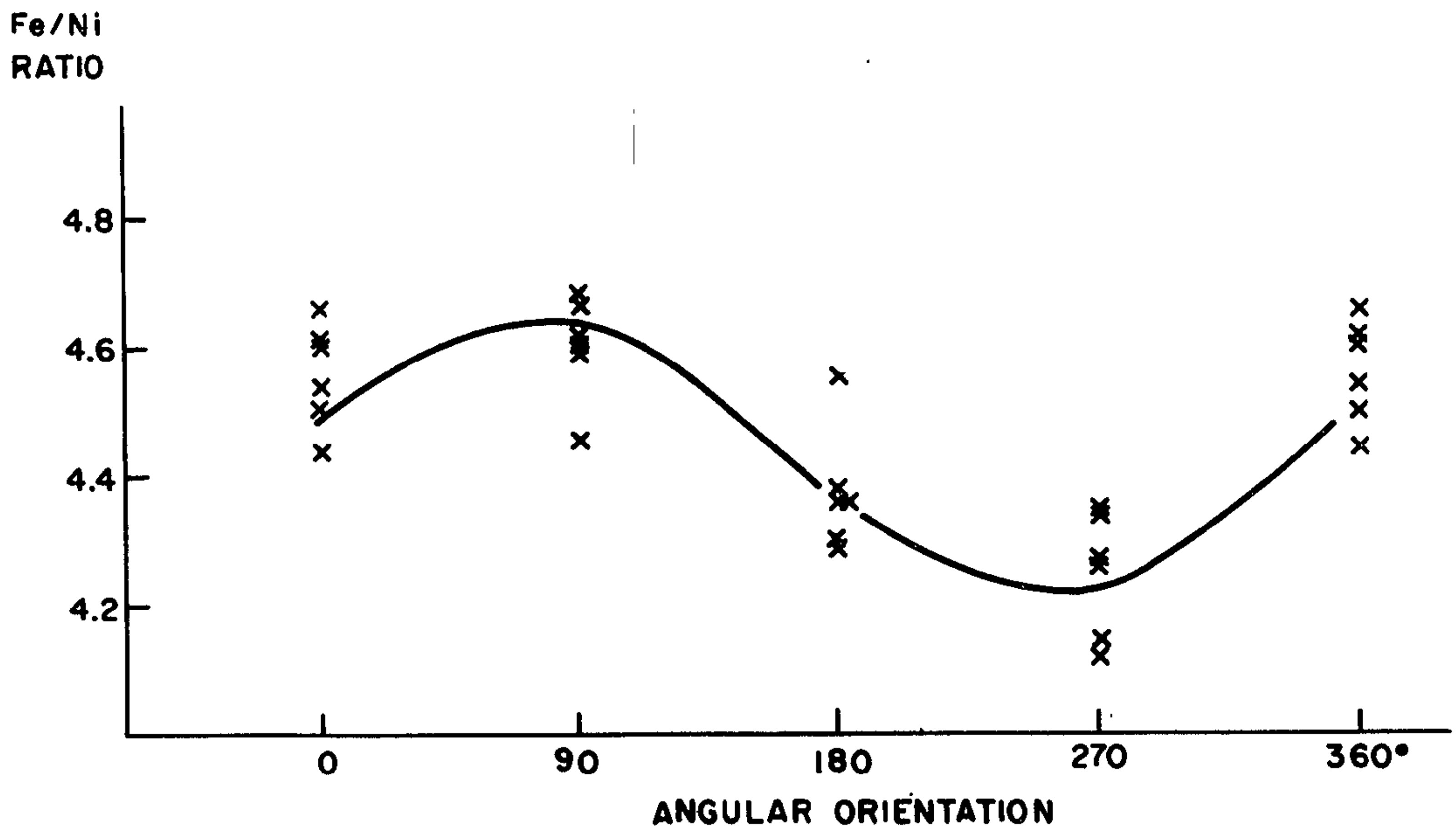

Figure 19. X-ray Intensity Ratios Observed in Zerostrictive, Aged

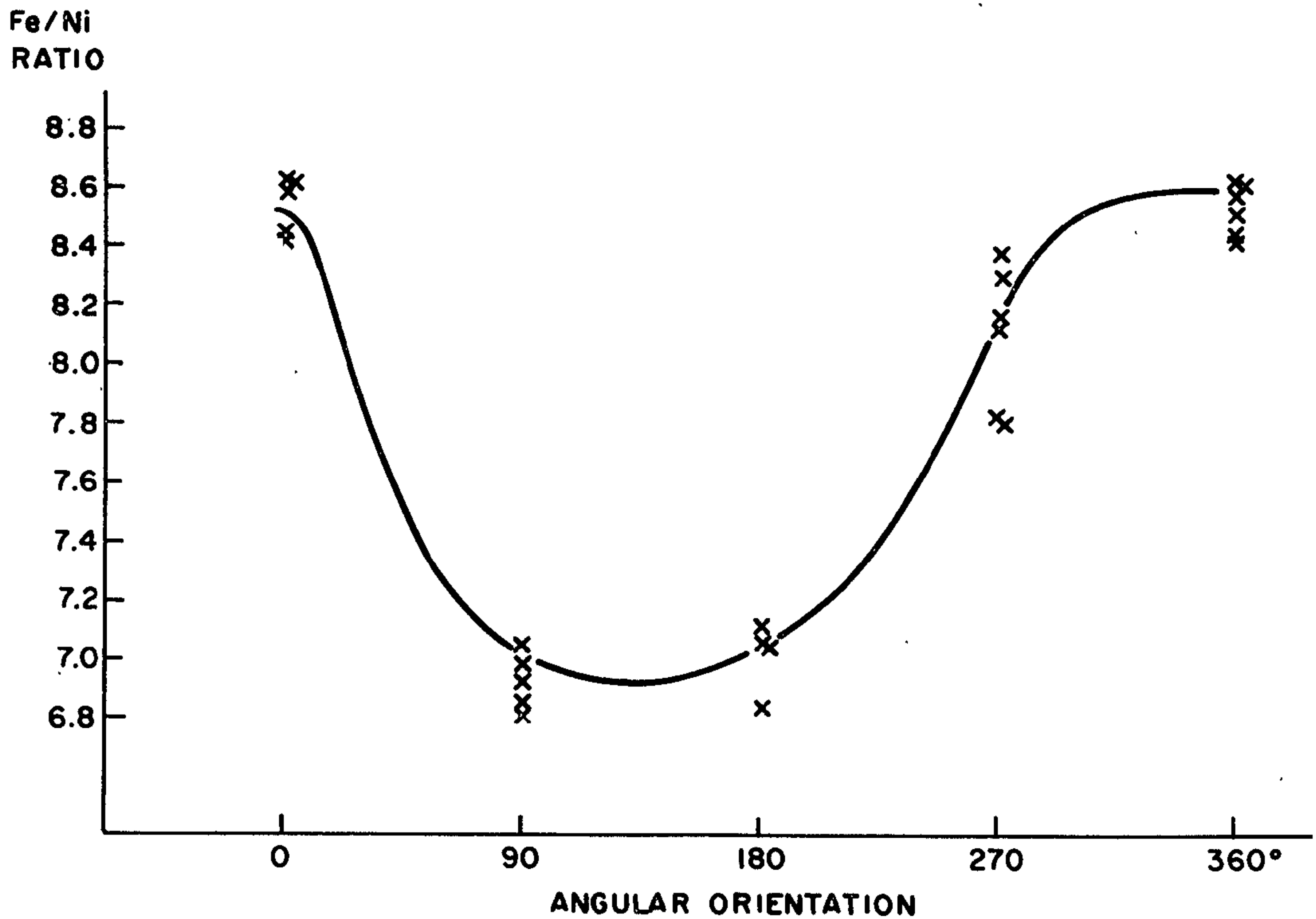

Figure 20. X-ray Intensity Ratios Observed in Iron-rich Wire, Unaged

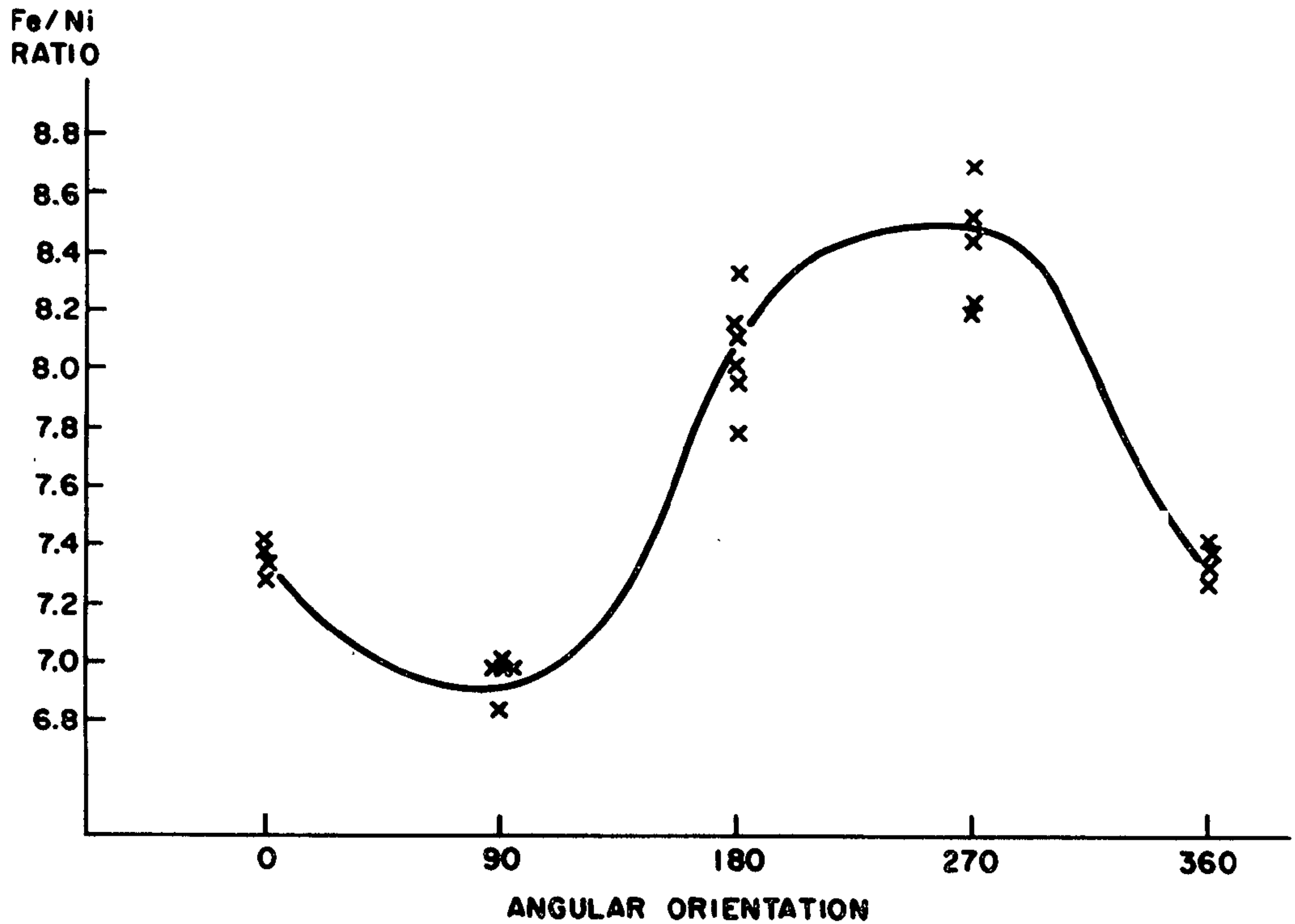

Figure 21. X-ray Intensity Ratios Observed in Iron-rich Wire, Age

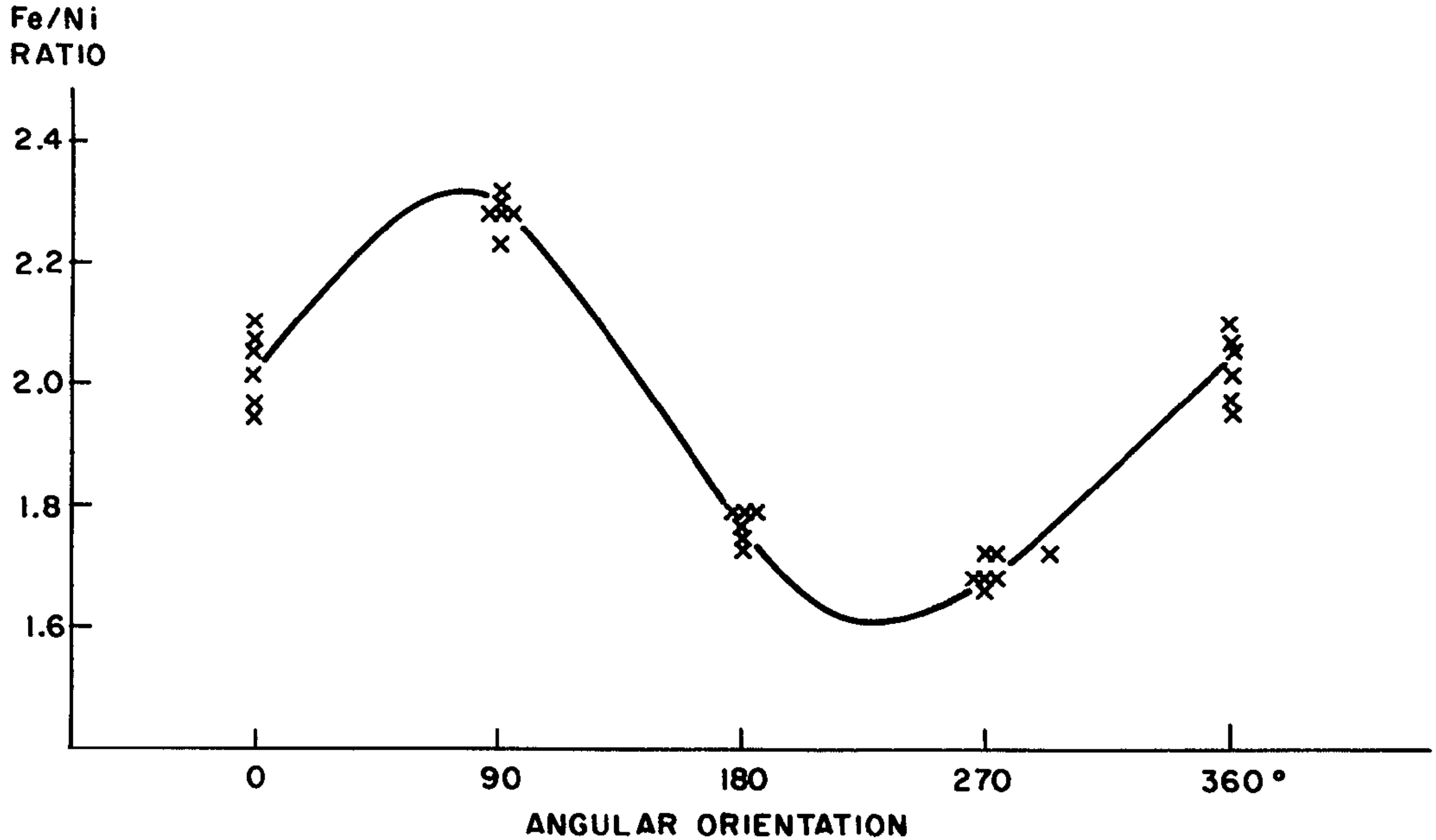

Figure 22. X-ray Intensity Ratios Observed in Nickel-rich Wire, Unaged

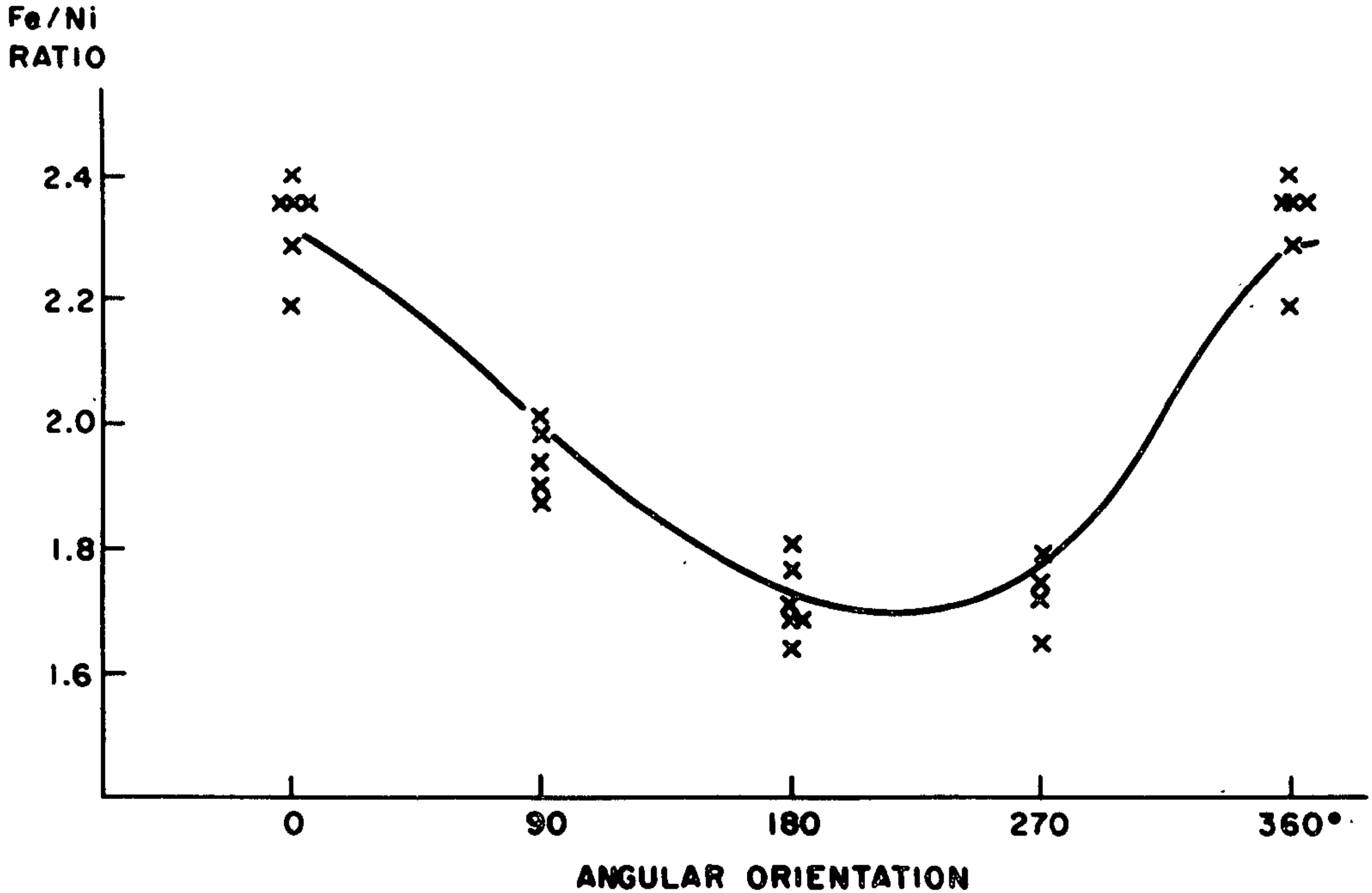

Figure 23. X-ray Intensity Ratios Observed in Nickel-rich Wire, Aged

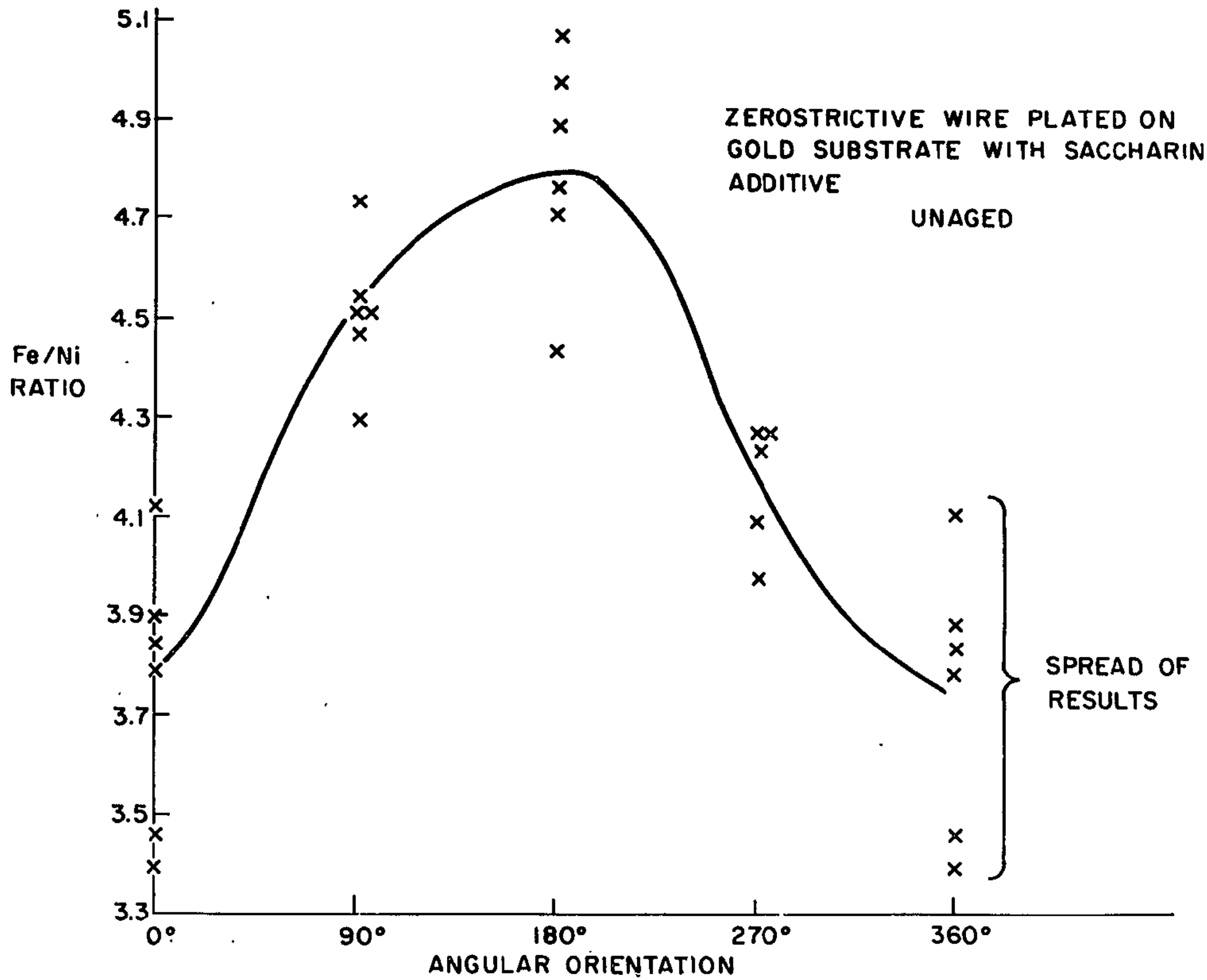

Figure 24. X-ray Intensity Ratios Observed in Zerostrictive Wire on Gold Substrate, Unaged

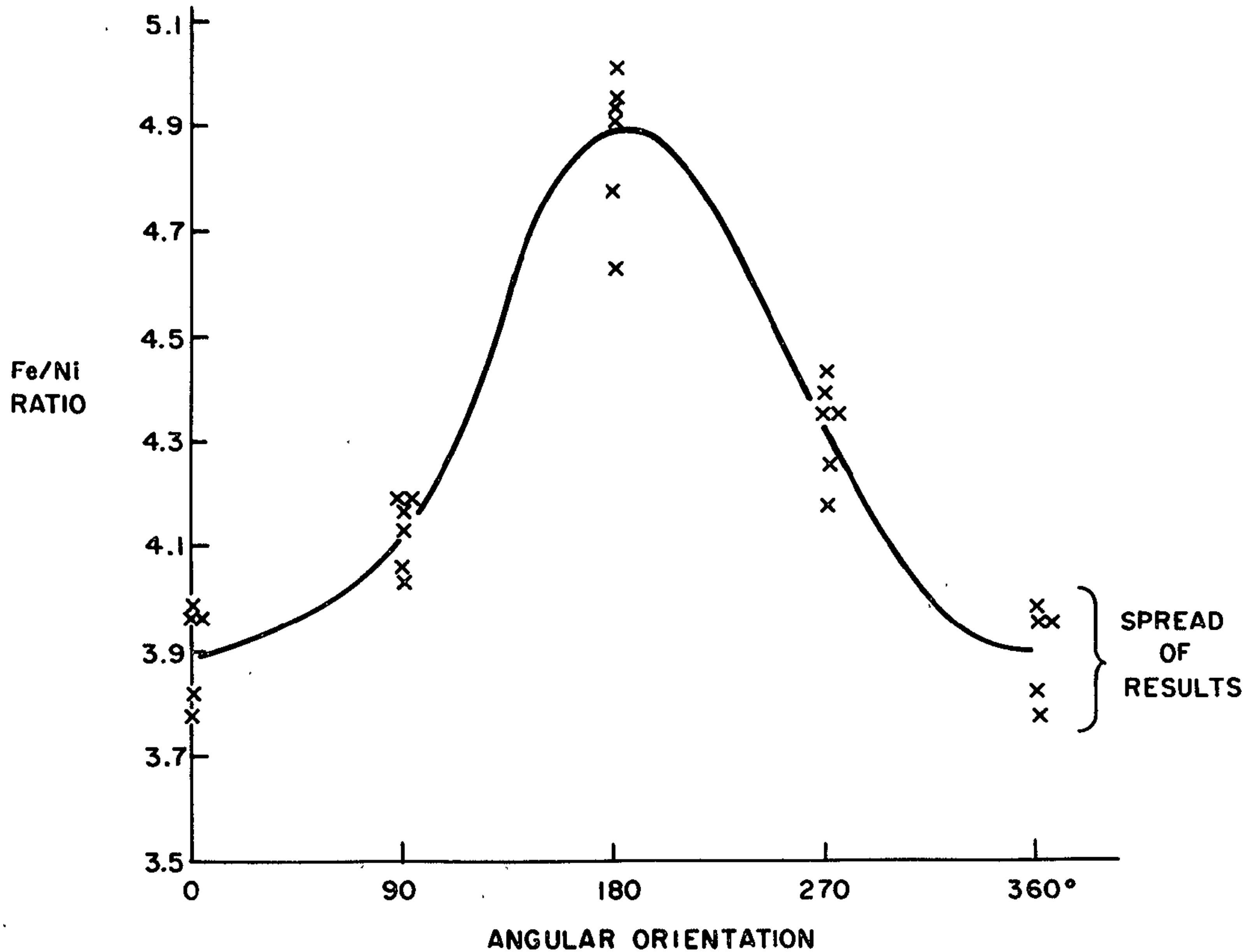

Figure 25. X-ray Intensity Ratios Observed in Zerostrictive Wire on Gold Substrate, Aged

5. Effect of Corrosive Atmospheres –Preliminary experiments were carried out to survey the effect of environment on aging characteristics of wire. Two types of corrosive environment were chosen: distilled water and sea water (that is, water containing the major ingredients of sea water, 1 gm NaCl + 100 mg $MgSO_4$ per liter). In both cases, the wires were immersed in the liquid at 230°C at a pressure equal to the saturated vapor pressure at that temperature (about 25 atmospheres). Control samples were aged in an air environment as previously. The apparatus for the corrosion experiments is shown in Figure 26. A 1/2 inch stainless steel tube 11 inches long was fitted with removable stainless steel end caps equipped with stainless steel ferrules. This provides a sealed container with a working pressure of 2500 psi. The tube has a volume of 27 mil and during the corrosion experiments 15 ml of water were used.

Both atmospheres described above are potentially corrosive. Since the water is sealed off in the presence of air, the requirements of both moisture and air are satisfied.[23]

The effect of the above corrosive aging was determined by photomicrographs, NDRO output profiles, and, in the case of distilled water treatment, by dispersion measurements. It was found that salt water was much more effective than distilled water in its effect on the appearance and output of the wire. A comparison of the control sample, distilled water sample and salt water sample following 16 hours of aging is shown in Figures 27, 28 and 29. These show photomicrographs at 40X and output profiles. The distorted appearance of the surface and the erratic electrical output of the salt water sample are evident. The distilled water sample and control sample do not differ greatly from one another in either respect. An additional comparison of these two samples is made in Figure 30, which shows the dispersion as a function of time. (This figure may also be compared with Figure 12.) Since again there is little difference between the two results, it may be concluded that the corrosive action of moisture and air does not greatly influence the aging process at 230°. In contrast the salt water corrosion is dominant.

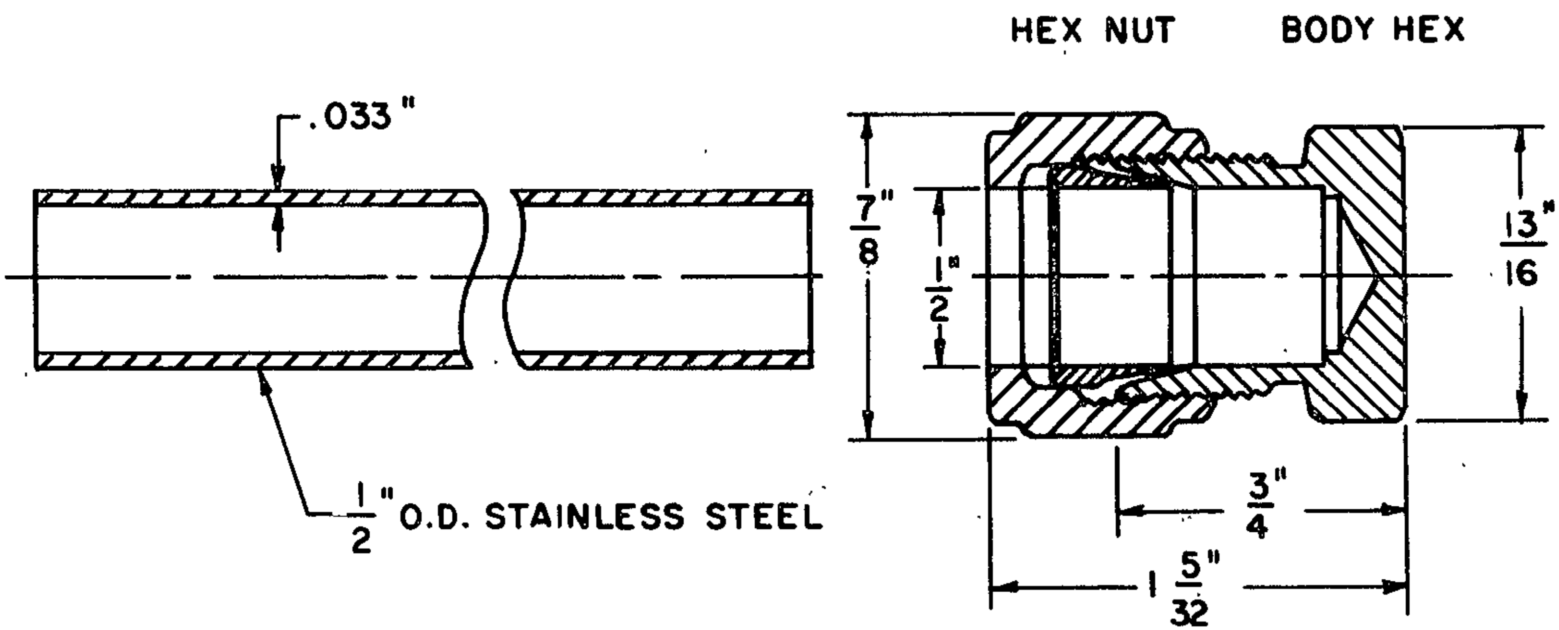

Figure 26. Apparatus for Corrosion Measurements

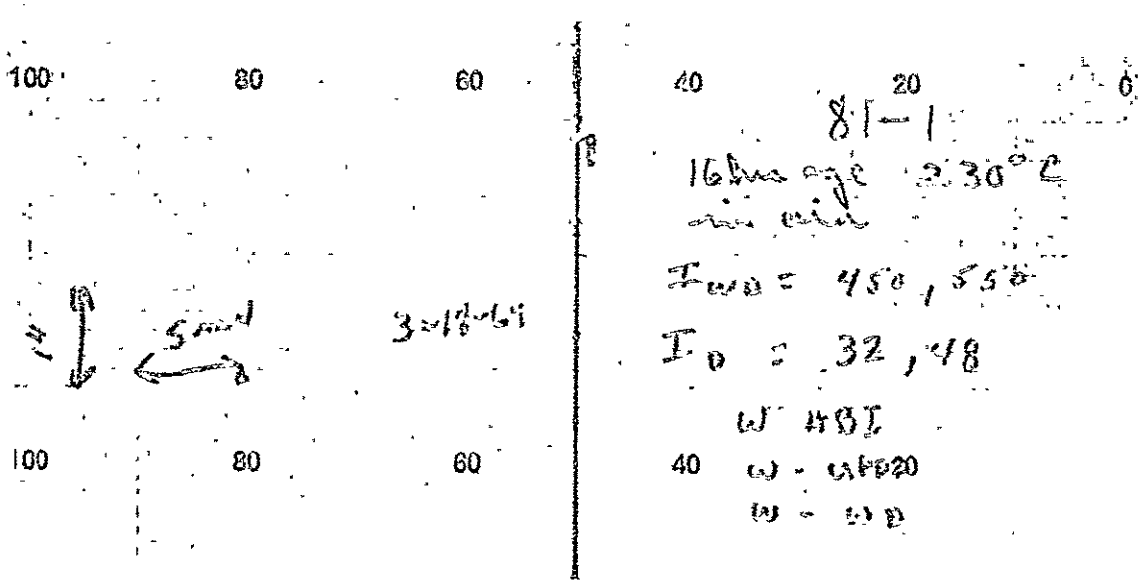

Figure 27. Micrograph and Output Chart, Aging in Air

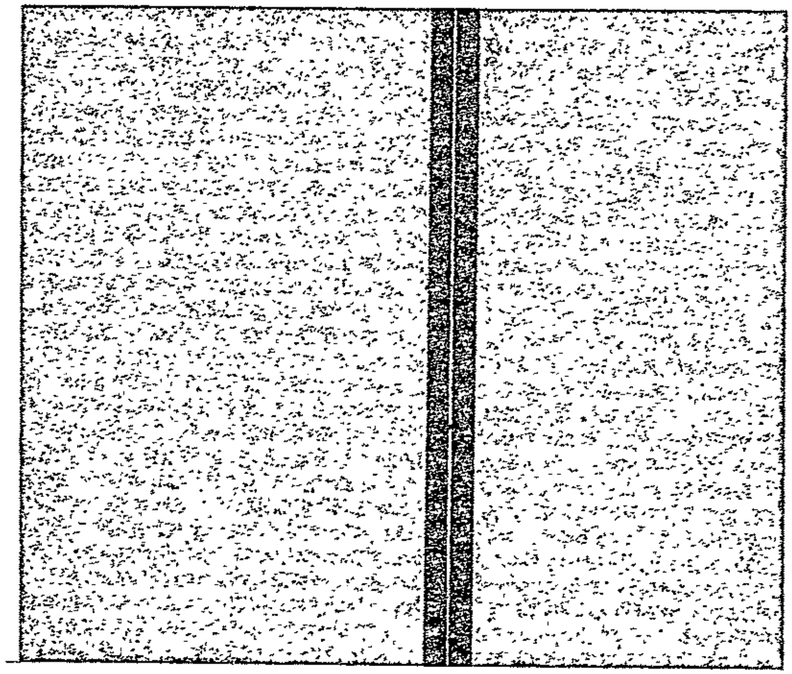

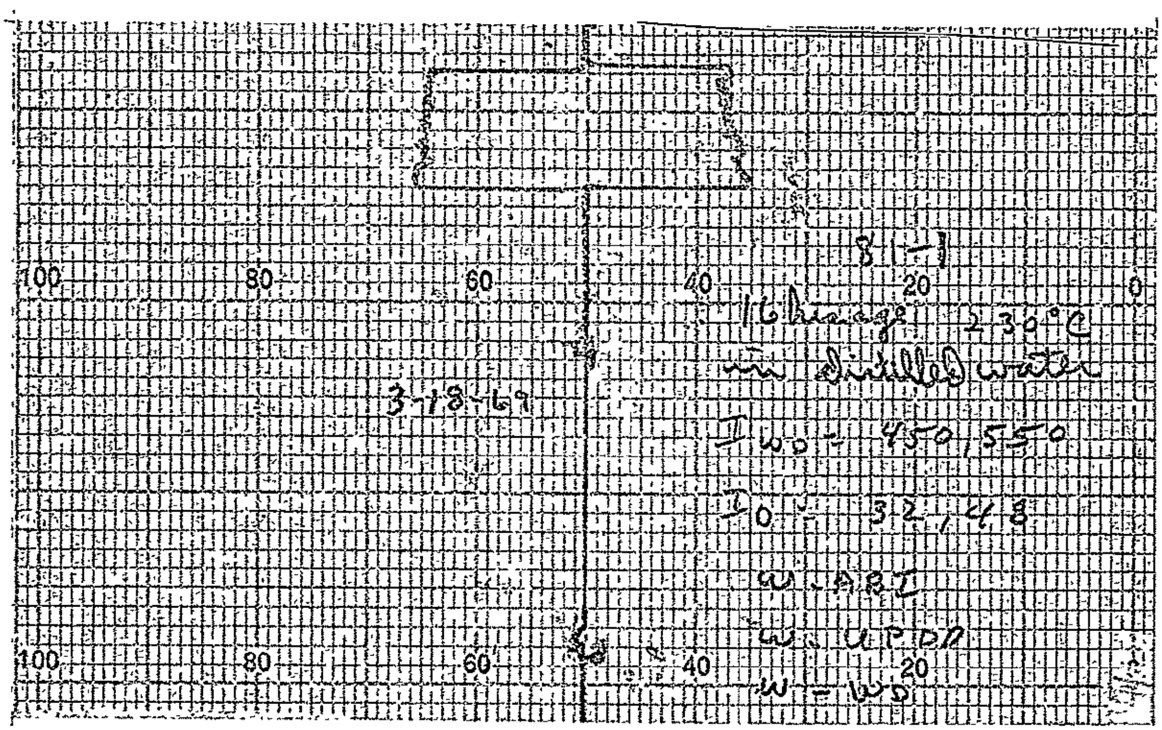

Figure 28. Micrograph and Output Chart, Aging in Distilled Water

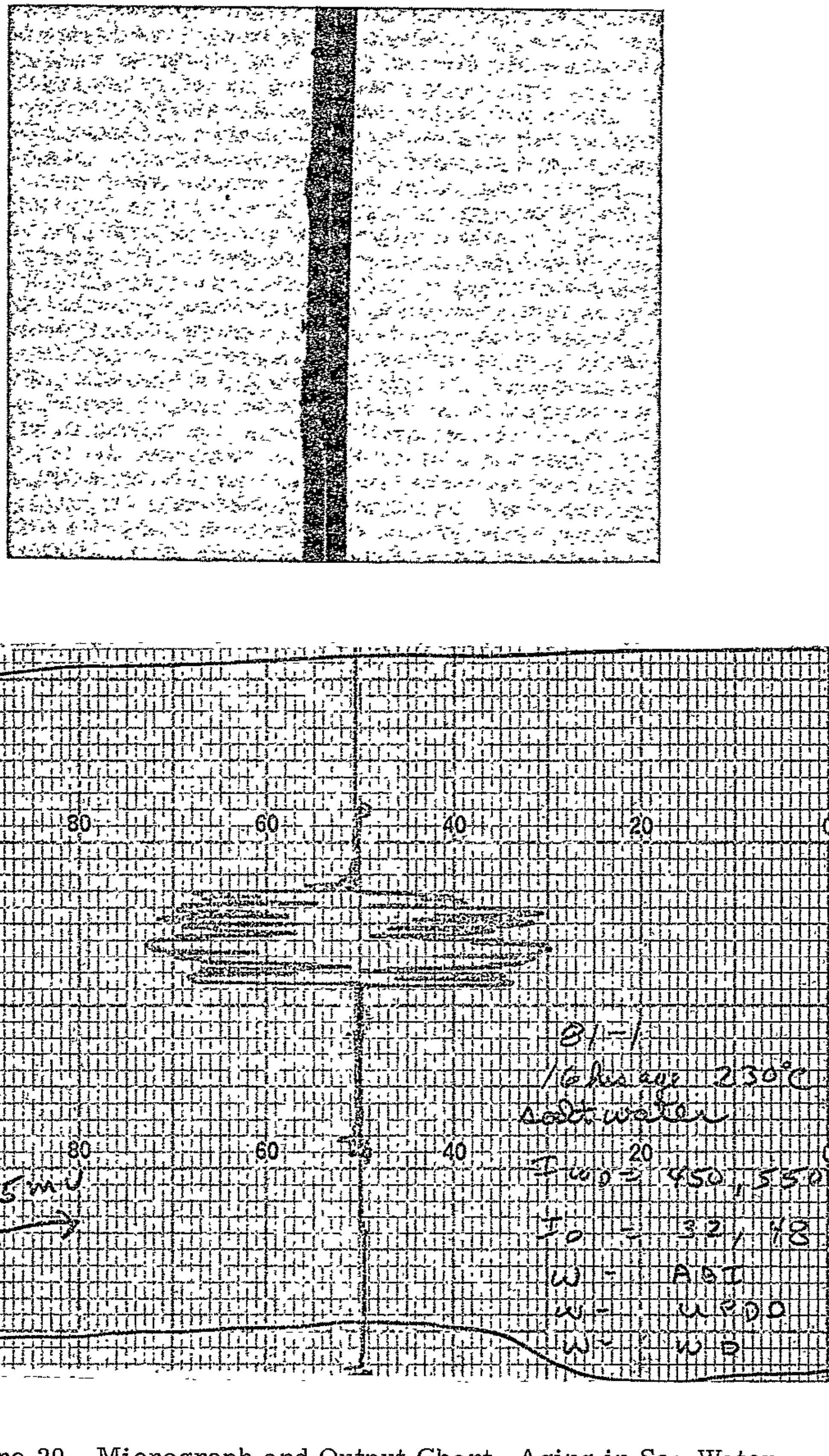

Figure 29. Micrograph and Output Chart, Aging in Sea Water

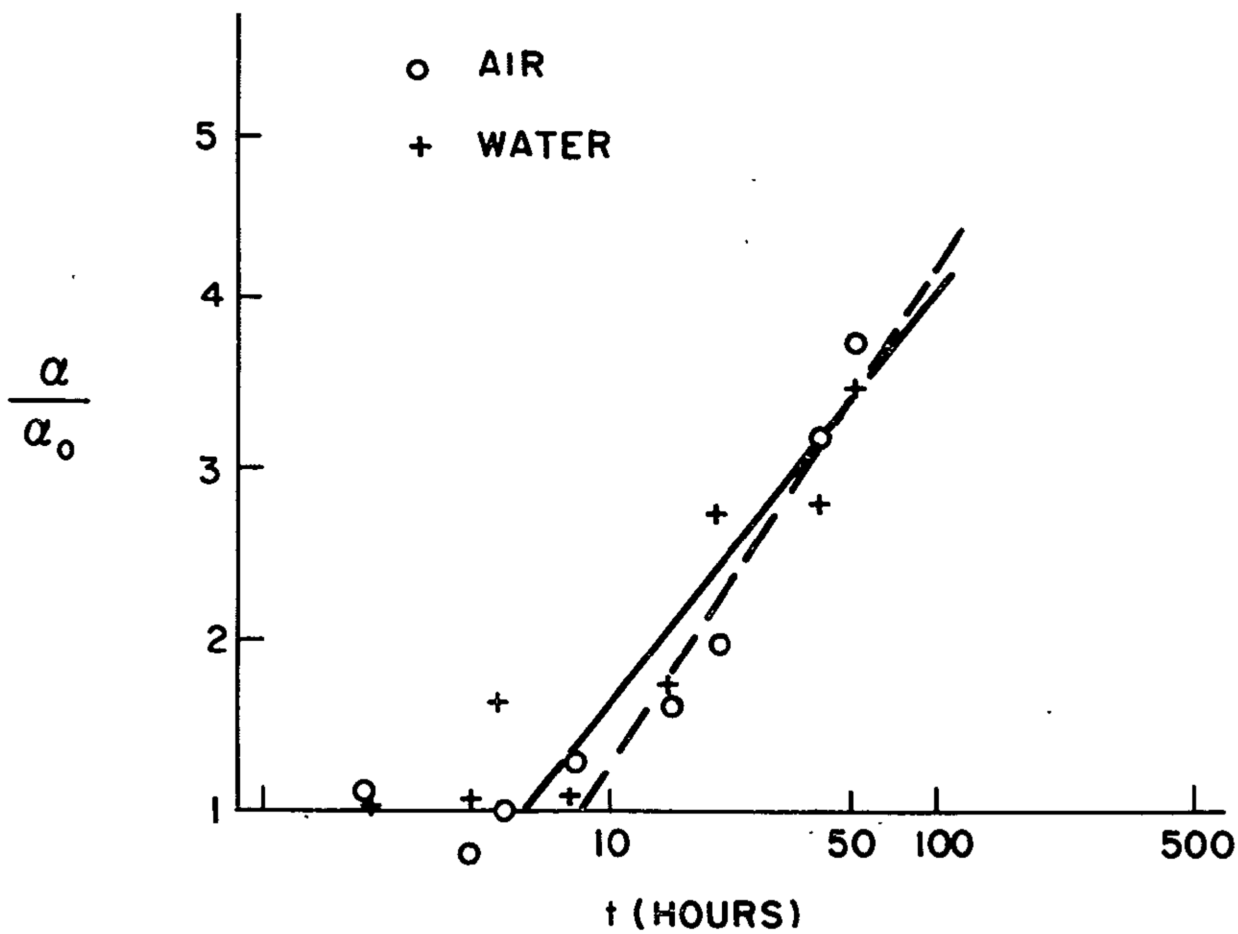

Figure 30. Dispersion Increase in Air and Distilled Water

In the latter type of environment it would be advisable to operate with a hermetically sealed memory or with suitably coated memory wire.

A further remark may be made concerning the effects of oxidation. In general the main aging phenomena discussed in this report occurs irrespective of the presence or absence of air for pressures down to about 2×10^{-6} mm Hg. A comparison of Figures 12 (shielded aging in air) and 20 (shielded aging in vacuum) shows that the time required for the initiation of dispersion increase is about the same for Cu-substrate elements aged in air or vacuum, but the subsequent rate of change is greater in air

6. Effect of Magnetostriction -In order to exaggerate any strain mechanism of aging, extensive experiments were carried out on the effect of deviations from the zeromagnetostrictive composition. The magnetostriction was controlled during deposition by control of the Ni^{++}/Fe^{++} ratio of the bath, as described in Section II. Both Au and Cu substrates were used. Because of its wide acceptance, torsion strain sensitivity(3) was used to determine magnetostriction of the unaged samples. The magnetic properties used as a measure of aging were dispersion, measured by both Belson and field-rotation techniques, anisotropy field, and the torsion sensitivity itself. The aging was carried out under vacuum at pressures less than 10^{-5} mm Hg, and magnetic fields less than 0.2 Oe. The temperature was 230°C unless otherwise specified, and the wire was in a demagnetized state. Measurements were made following removal from the furnace.

The essential results pertaining to influence of magnetostriction on aging characteristics are given in Figures 31 and 32. Figure 31 shows the change with time of dispersion, α, and anisotropy field, H_k, for both Cu and Au substrates. Figure 32 shows the change in torsion strain sensitivity. The parameters of these curves are the composition as measured by the torsion sensitivity test for magnetostriction. Figure 31 shows a pronounced difference in the aging behavior of Fe-rich (positive magnetostriction) and

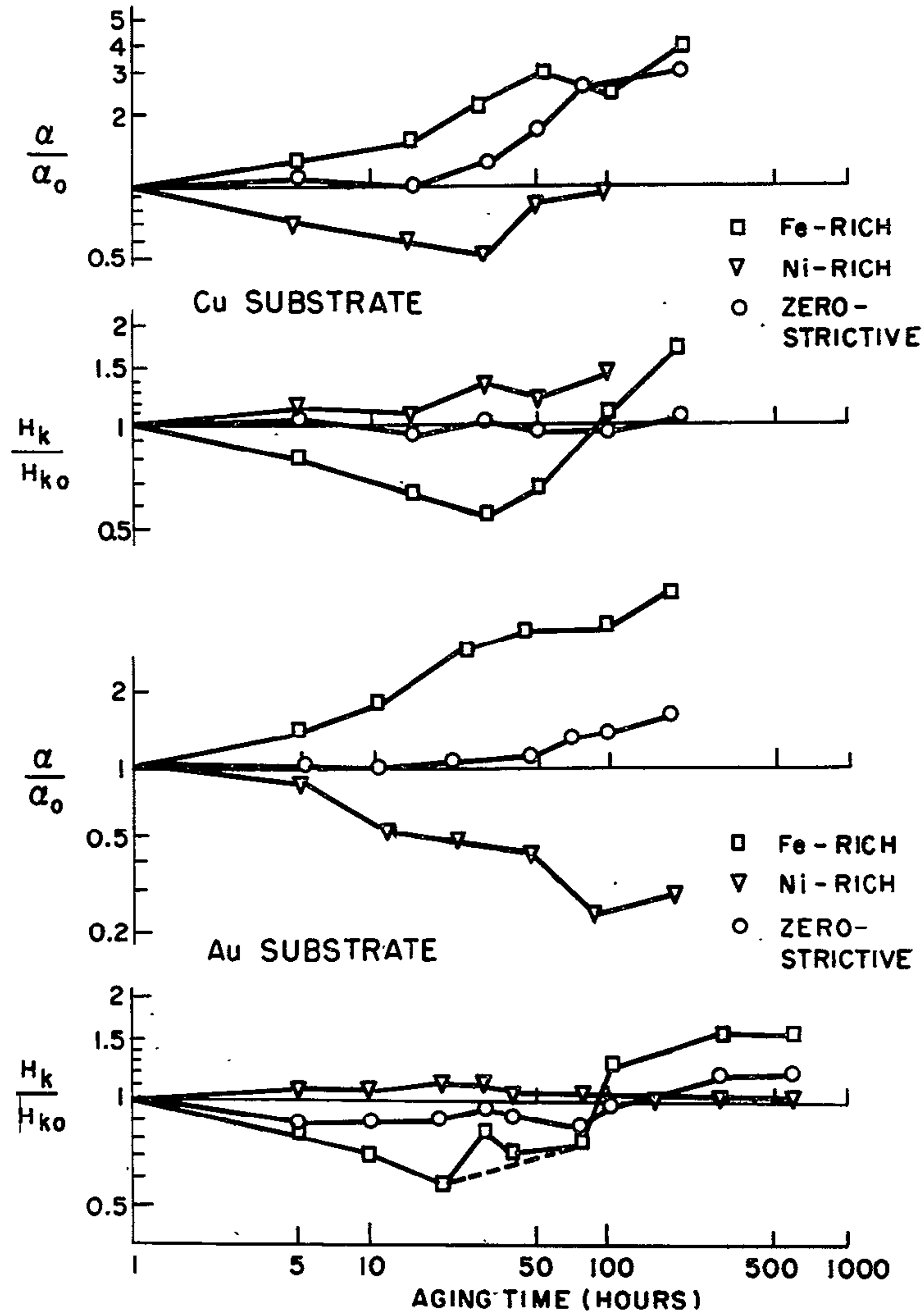

Figure 31. Effect of Magnetostriction and Substrate on Aging Characteristics (vacuum)

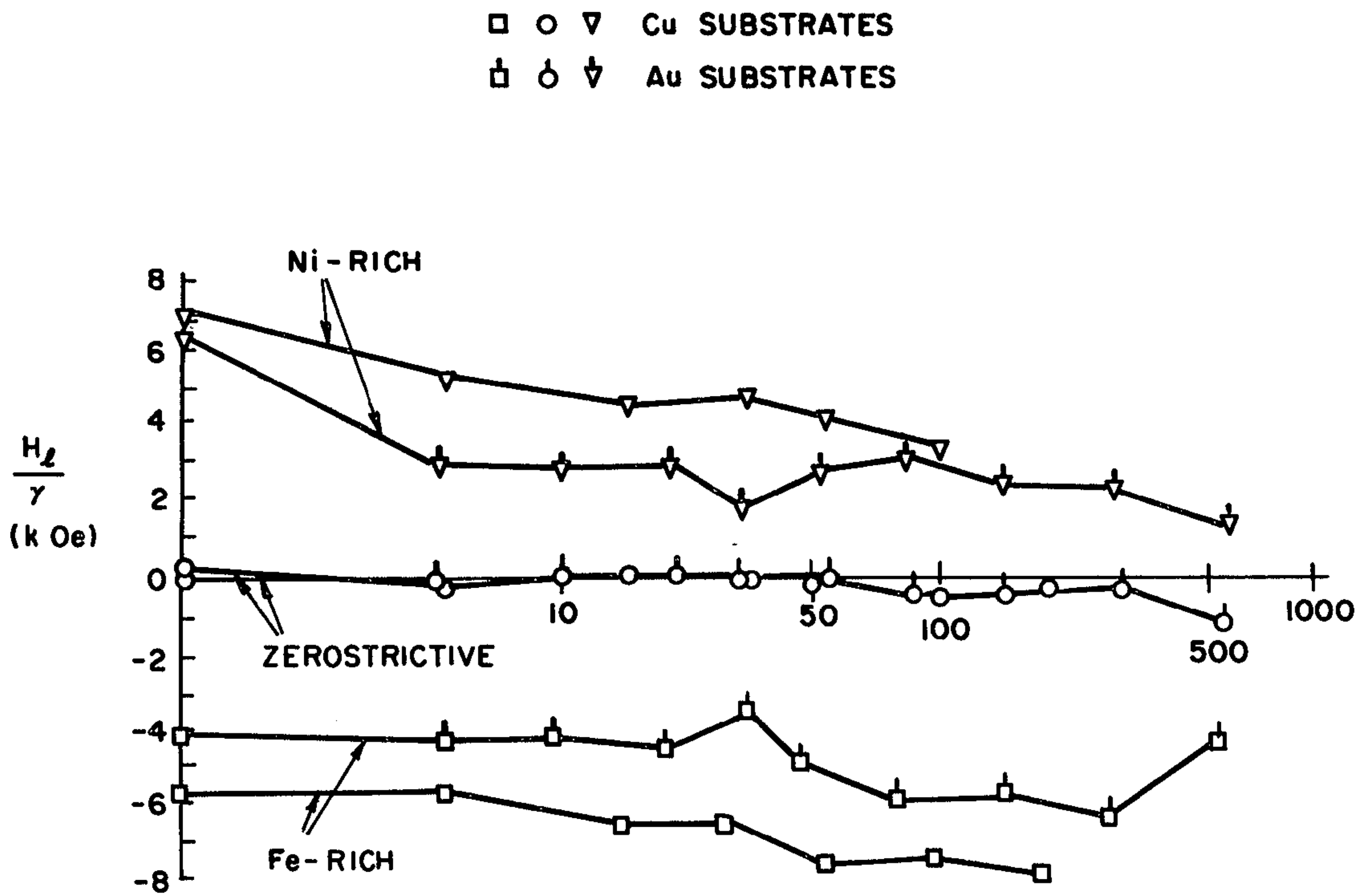

Figure 32. Effect of Aging on Magnetostriction for Different Compositions

Ni-rich (negative magnetostriction) wires. Fe-rich wires show an initial increase in α and an initial decrease in H_k, while Ni-rich wires show opposite behavior. Zerostrictive samples tend to behave as if slightly Fe-rich. After a certain period of time both α and H_k increase with time for all compositions. For purposes of reference we may label the initial period as Stage I, and the later period Stage II. No such composition dependence is found in the magnetostriction (Figure 32). Instead, all compositions show a change toward increasing Fe-richness. This appears similar to other results.[24]

The strongly magnetostriction-dependent aging behavior of α and Hk can logically be explained only as due to a change in strain of the film. Furthermore, it is not hard to show that the strain must have an anisotropic component in order to explain the change in H_k. The existence of tensile strain in electrodeposits is well-known.[25] Normally, such as in the case of flat films, such strain is isotropic. As shown in Appendix II, however, in the case of a cylindrical film there is a slightly greater residual film strain in the circumferential than in the axial direction of the film, due to the different degrees of distortion of the core wire in the two corresponding directions. As shown in Appendix II this effect is described by the following equation:

$$T_c/T_a \cong 1 - (t/R)\,(E_f/E)\,(1 + \sigma)\,(1 + \sigma_f) \qquad \text{(IV-3)}$$

where T_c/T_a is the ratio of circumferential to axial stress, t/R is the ratio of film thickness to wire radius, E_f and E are Young's Modulus for film and wire, respectively, and σ_f and σ are Poisson's ratio for film and wire. Because of the anisotropic stress depicted by Eq. IV-3, there exists a uniaxial stress anisotropy field in the film. It can be shown from the inverse magnetostrictive effect[26] and Eq. IV-3 that the anistropy field resulting from this stress differential is given by:

$$H_{ks} = (3\lambda/M_s)\,T_o\,(E_f/E)\,(1 + \sigma)/(1 + \sigma_f)\,(t/R) \qquad \text{(IV-4)}$$

where λ is the saturation magnetostriction, M_s the saturation magnetization and T_o the average stress, i.e., $(t_c + T_a)/2$. The sign of H_{ks} is seen to depend on the sign of λT_o. For tensile strain and positive magnetostriction, i.e. Fe-rich films, H_{ks} is positive and the induced strain gives an easy-axis component in the circumferential direction. For Ni-rich films, tensile strain gives an easy axis component in the axial direction. We now hypothesize that the initial H_k changes shown in Figure 31 are due to relief of tensile strain in the electrodeposit. Because of the anisotropy this tensile strain relief in plated wire should give a decrease in H_k for Fe-rich and an increase in H_k for Ni-rich films. Denoting such changes by ΔH_k, we should have $\Delta H_k = -H_{ks}$ in each case. We now proceed to a comparison of experimentally observed ΔH_k values with H_{ks} values predicted from auxiliary strain experiments and Eq. IV-4.

Since Figure 31 shows H_k and α in terms of the reduced quantities H_k/H_{ko} and α/α_o, it is supplemented by Table III which gives the magnitudes of H_k and α_{50} as well as of η_o, the magnetostrictive coefficient, prior to aging. The difference in composition, ΔC, from that for zeromagnetostriction, as measured by the torsion sensitivity apparatus, is given approximately by

$$\Delta C(= \text{per cent Ni}) = 0.12\, \eta_o\, (\text{kOe}) \tag{IV-5}$$

From Figure 31, the predicted increase and decrease of H_k with aging for Fe- and Ni-rich wires are seen to occur for both substrates. H_k for Fe-rich reaches a minimum at a time between 20 and 30 hours in each case. It is assumed for the purposes of comparison that this time represents the termination of strain relief. We therefore wish to compare the corresponding ΔH_k to the calculated anisotropy field, H_{ks}. To calculate H_{ks} we need to know λ and T_o. λ is obtained from the data of Bozorth and Walker.[27] T_o has been estimated from a separate experiment as follows: The spiral coil of a contractometer[9] was plated with 0.4μ Au. The coil was then annealed for 32 hours to relieve any stress present in the Au. The coil was then plated at room temperature with $1\,\mu$ permalloy using a non-additive bath. During plating the contraction of the spiral corresponded

TABLE III. MAGNETIC PARAMETERS OF UNAGED SAMPLES

SAMPLE	DESCRIPTION	α_{50} * (DEGREES)	H_k (Oe)	η_o ‡ kOe
AS DEPOSITED BEFORE STABILIZATION				
39-7	UNSTABILIZED, CU, FE-RICH	2.0	5.7	- 19
44-1	UNSTABILIZED, CU, NI-RICH	15.2	6.6	+ 16
36-2	UNSABILIZED, CU, ZEROSTRIC.	6.2	6.9	0.0
67-7	UNSTABILIZED,AU, FE-RICH	1.2	5.5	-13.5
68-2	UNSTABILIZED, AU, NI-RICH	15.0	6.6	+ 7.3
67-5	UNSTABILIZED, SU, ZEROSTRIC.	8.6	5.8	+ 1.8
AFTER STABILIZATION				
39-6	STABILIZED, CU-BASE, FE-RICH	8.2	4.4	- 18
44-2	STABILIZED, CU-BASE, NI-RICH	4.3	6.0	+ 22
57-1	STABILIZED, CU-BASE, ZEROSTRIC.	5.3	5.6	+ 0.4
67-6	STABILIZED, AU-BASE, FE-RICH	4.0	4.5	-13.5
68-1	STABILIZED, AU-BASE, NI-RICH	11.5	5.8	+ 20
67-4	STABILIZED, AU-BASE, ZEROSTRIC.	5.0	5.4	0.0

* FROM FIELD ROTATION TEST

‡ USING SIGN CONVENTION WHEREBY η IS NEGATIVE FOR POSITIVE MAGNETOSTRICTIVE MATERIAL.

to the development of a tensile stress in the film of 74,000 psi. The contractometer was now annealed in air at 215°C for selected time intervals and the resulting change in stress following cooling was observed to be in the opposite direction to that observed during plating. The stress relief appeared nearly complete after about 5 hours, as shown in Figure 33. The total change was about 69,500 psi. Hence the stress relief is only a few percent less than the plating stress and contributions from extraneous sources such as differential thermal expansion are relatively small. From this experiment, therefore, we estimate $T_o \cong 70,000$ psi for Au-substrate permalloy films. (It is assumed that the stress is not relieved during stabilization.)

We may now tabulate the quantities appearing in Eq. IV-4 together with their sources. These are given in Table IV. The only quantities not directly available from handbooks were σ and σ_f, but for a wide range of metals and alloys Poisson's ratio does not differ greatly from 0.35, so that the error in the ratio σ/σ_f resultant from using values for Cu and Ni probably does not exceed 10%. Upon substitution of these quantities into Eq. IV-4, we find for the calculated stress anisotrophy:

CALCULATED STRESS ANISOTROPY FIELDS (Au-Substrate)

Fe-rich:	$H_{ks} = 1.0$ Oe
Ni-rich:	$H_{ks} = 1.6$ Oe

We now derive the experimental results for ΔH_k from Figure 17 and Table III, using observed H_k/H_{ko} for Au-substrate samples at 20 hours, together with the relation $\Delta H_k = H_{ko}$

$$1\left[- \frac{H_k}{H_{ko}}\right]$$

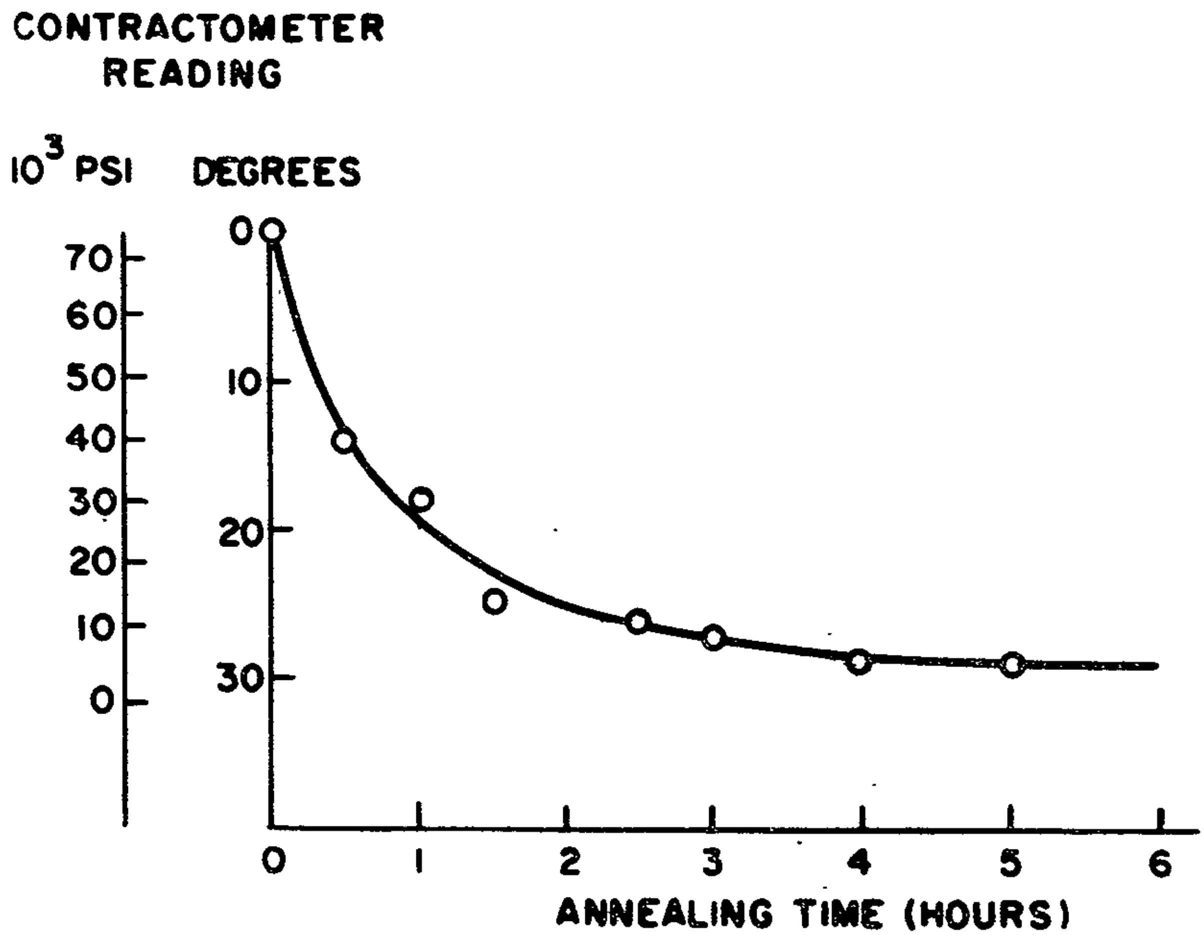

Figure 33. Relief of Film Stress by Contractometer Annealing

TABLE IV. PHYSICAL PROPERTIES FOR CALCULATING STRESS ANISOTROPY

SAMPLE	DESCRIP-TION	η_o * k(Oe)	Δ%Ni	M_s (a) emu	λ	T_o	E**	E_f**	σ ‡	σ_f ‡	t/R
							10^6psi	10^6psi			
67-6	FE-RICH	-13.5	-1.6	880	2.2×10^{-6}	70,000	17	28	0.37	0.34	1.6×10^{-2}
68-1	NI-RICH	+20	+2.4	820	-3.3×10^{-6}	70,000	17	28	0.37	0.34	1.6×10^{-2}
						$\approx 4,9 \times 10^9$ dynes/cm^2					

* USING CONVENTION WHEREBY η_o IS NEGATIVE FOR POSITIVE MAGNETOSTRICTION.
(a) AIP HANDBOOK, FROM TABLE 5h-3.
** METALS HANDBOOK, AMERICAN SOCIETY FOR METALS, 1948 EDITION.
‡ σ, σ_f ASSUMED TO BE THAT FOR Cu AND Ni, RESPECTIVELY.
AIP HANDBOOK, 1st EDITION, TABLE 3f-2.

This gives:

OBSERVED ANISOTROPY FIELD CHANGE (Au Substrate)

Fe-rich	$-\Delta H_k = 1.0$ Oe
Ni-rich	$-\Delta H_k = -0.7$ Oe

In general, the agreement between H_{ks} and ΔH_k is considered a satisfactory confirmation of the stress relief hypothesis. The unbalance between observed Fe- and Ni-rich ΔH_k and H_{ks} values is possibly a result of the effective zeromagnetostrictive point (ZMP) for aging being more Ni-rich than indicated by torsion measurements. Further evidence for this conclusion is contained below. It should be mentioned in passing that further support for the anisotropic strain relief hypothesis is supplied by flat film annealing experiments reported earlier.[28] In these experiments no significant divergence of α and H_k was found during annealing. This is consistent with the present prediction that such effects occur uniquely in the cylindrical geometry.

The calculations and experiments reported in the previous section provide strong evidence that the initial shielded aging stage is due to stress relief in the permalloy film. The stress relieved is due to a small excess tension in the circumferential direction. To verify the equivalence of circumferential tension relief and aging, we carried out auxiliary experiments in which tension was applied in the axial direction, and the resulting change in magnetic parameters observed. Magnetically, tension in the axial direction should be equivalent to tension relief in the circumferential direction. The results for Au-substrate wire are shown in Figure 34. These results confirm in a striking way the equivalence of aging and tension in bringing about dispersion changes. The dispersion aging characteristics "track" with the dispersion-loading characteristics in both sign and magnitude. The positive slopes for nominally zerostrictive elements suggest that the commonly accepted torsion sensitivity test for zeromagnetostrictive point (ZMP) does not provide minimum aging rates. Instead it appears that zero tension sensitivity might

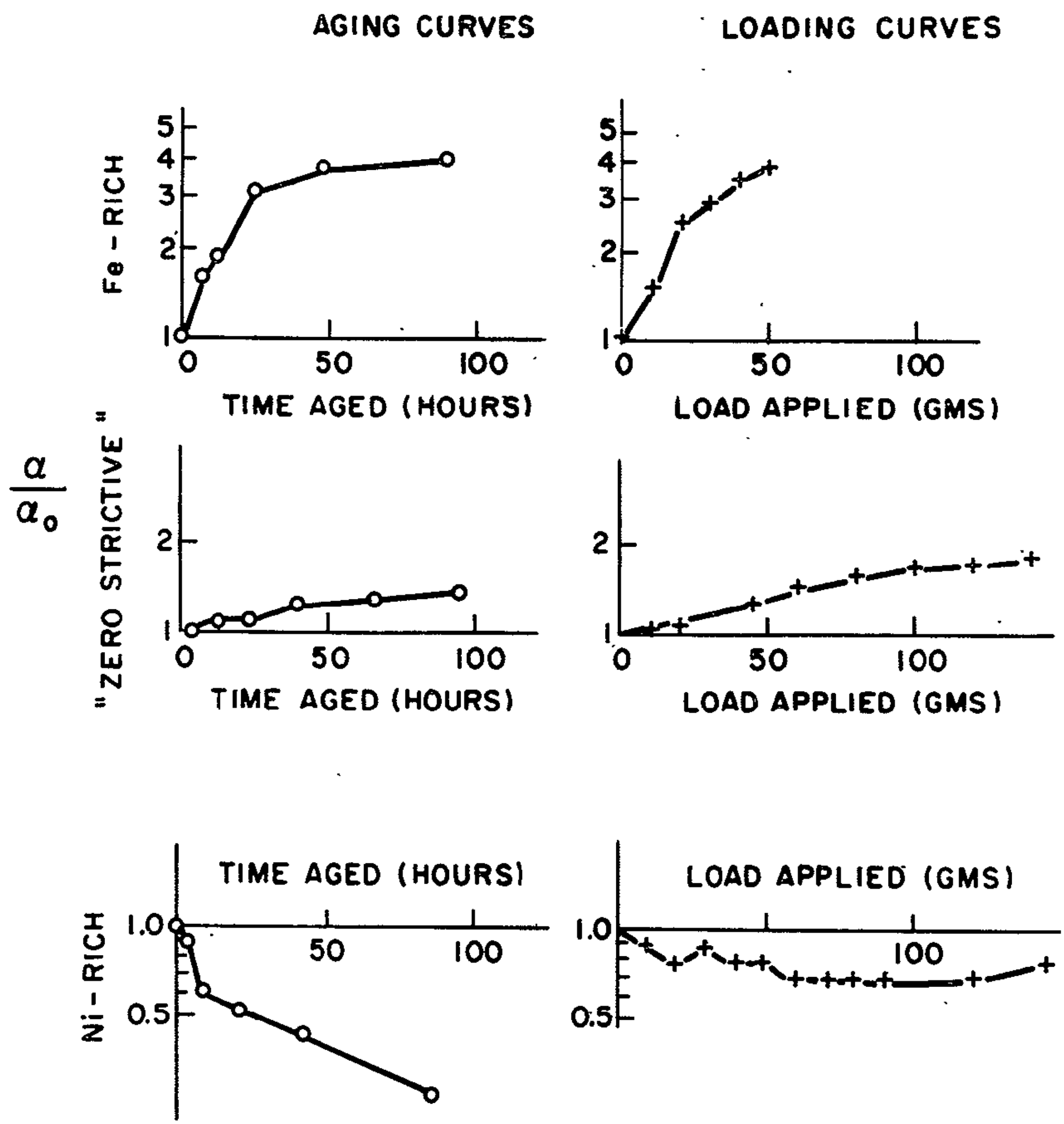

Figure 34. Equivalence of Tension and Aging of Plated Wire

be a better criterion. The relation between aging and tension sentitivity was further examined for a variety of wires having near-zero torsion sensitivity. The results are shown in Figure 35. The samples show wide differences one from the other in aging characteristics (upper part of figure), but again corresponding differences are observed in the strain sensitivities (lower part of figure). Of particular interest is the extremely large aging rate and strain sensitivity of the plated wire made with saccharin bath additive. Figure 35 also shows that stabilization brings about a change in sign in both torsion and tension sensitivities.

Because of the apparent difference between torsion and tension strain sensitivities implied by the aging results, a direct comparison of these quantities was made and is shown in Figure 36. In this figure the tension strain sensitivity is given as the change, ΔH_k, in anisotropy field, divided by the strain, ε, in the permalloy film. ε is calculated from the applied load and Young's Modulus for CuBe (Table IV). The torsion strain sensitivity is given by the quotient H_ℓ / γ, where H_ℓ is the skew-equivalent field of the Belson test, and γ the torsion strain. The samples used for Figure 36 were of Cu substrate and made with non-additive bath. The two different symbols correspond to different plating runs. The torsion strain sensitivity was adjusted by change of flow rate and Ni^{++}/Fe^{++} bath ratio. These results confirm the discrepancy between the two strain sensitivities. The ZMP composition on the tension scale corresponds to 1.4% Ni-rich composition on the torsion scale.

In order to establish the relationship between aging, torsion strain sensitivity and tension strain sensitivity, aging experiments were carried out on the wires used in the strain measurements of Figure 36. These consisted of the usual vacuum-shielded aging at 230°C followed by measurements of dispersion and anisotropy field. The aging time was 60 hours. The degree of aging is measured by the changes brought about in these quantities. The results are shown in Figure 37. The fractional changes in α_{90} (measured by the Belson test) and in H_k are shown as a function of torsion strain

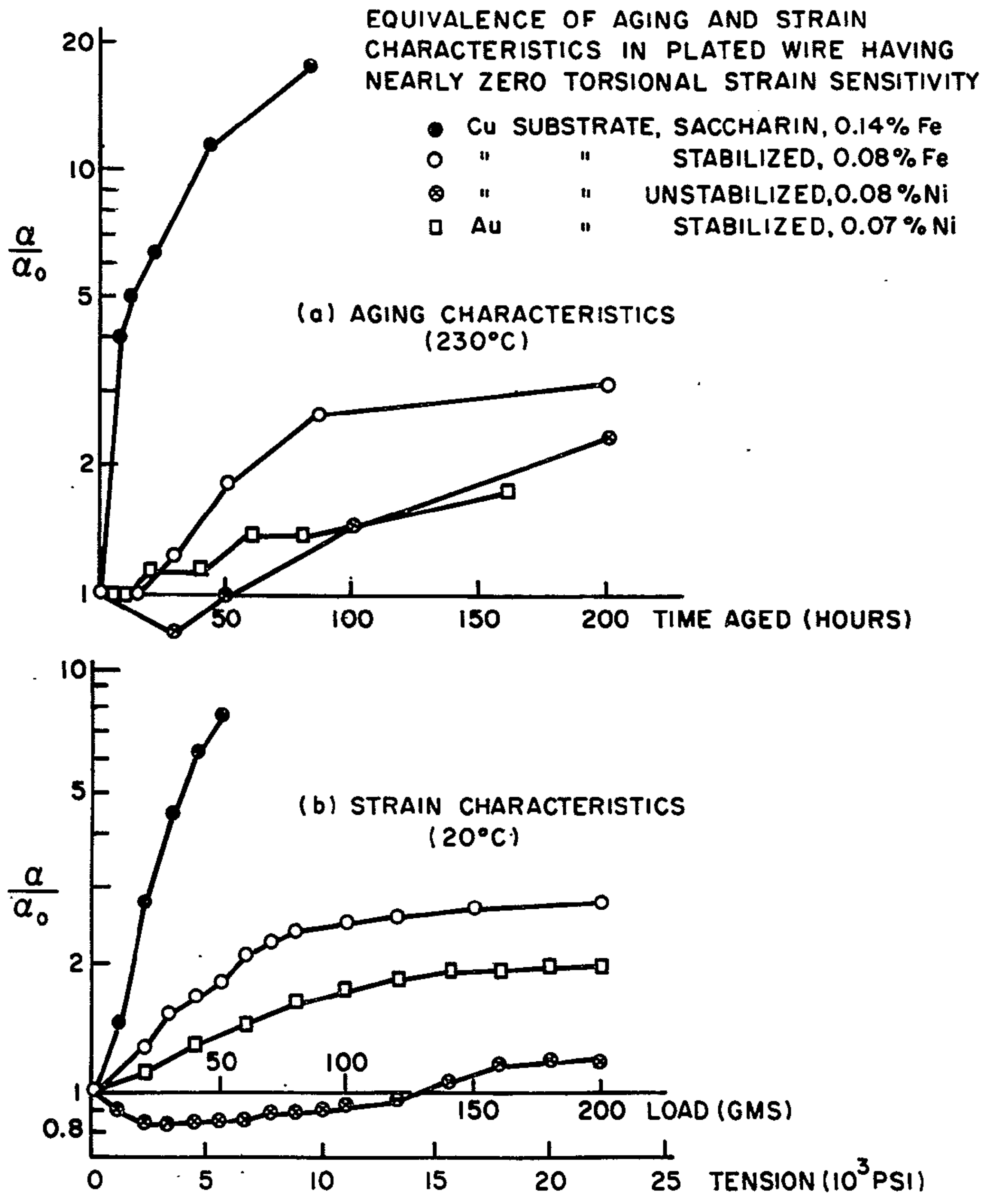

Figure 35. Equivalence of Tension and Aging of Wires Having Near Zero Torsion Strain Sensitivity

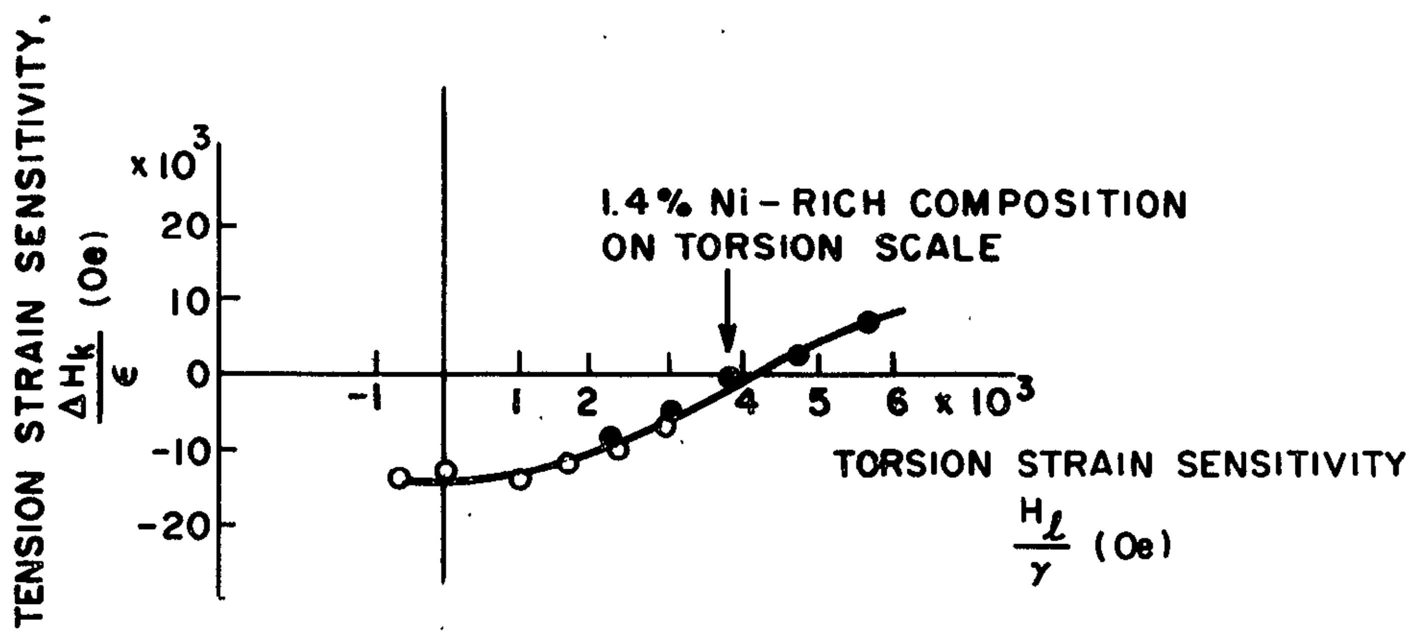

Figure 36. Relation Between Tension and Torsion Strain Sensitivities

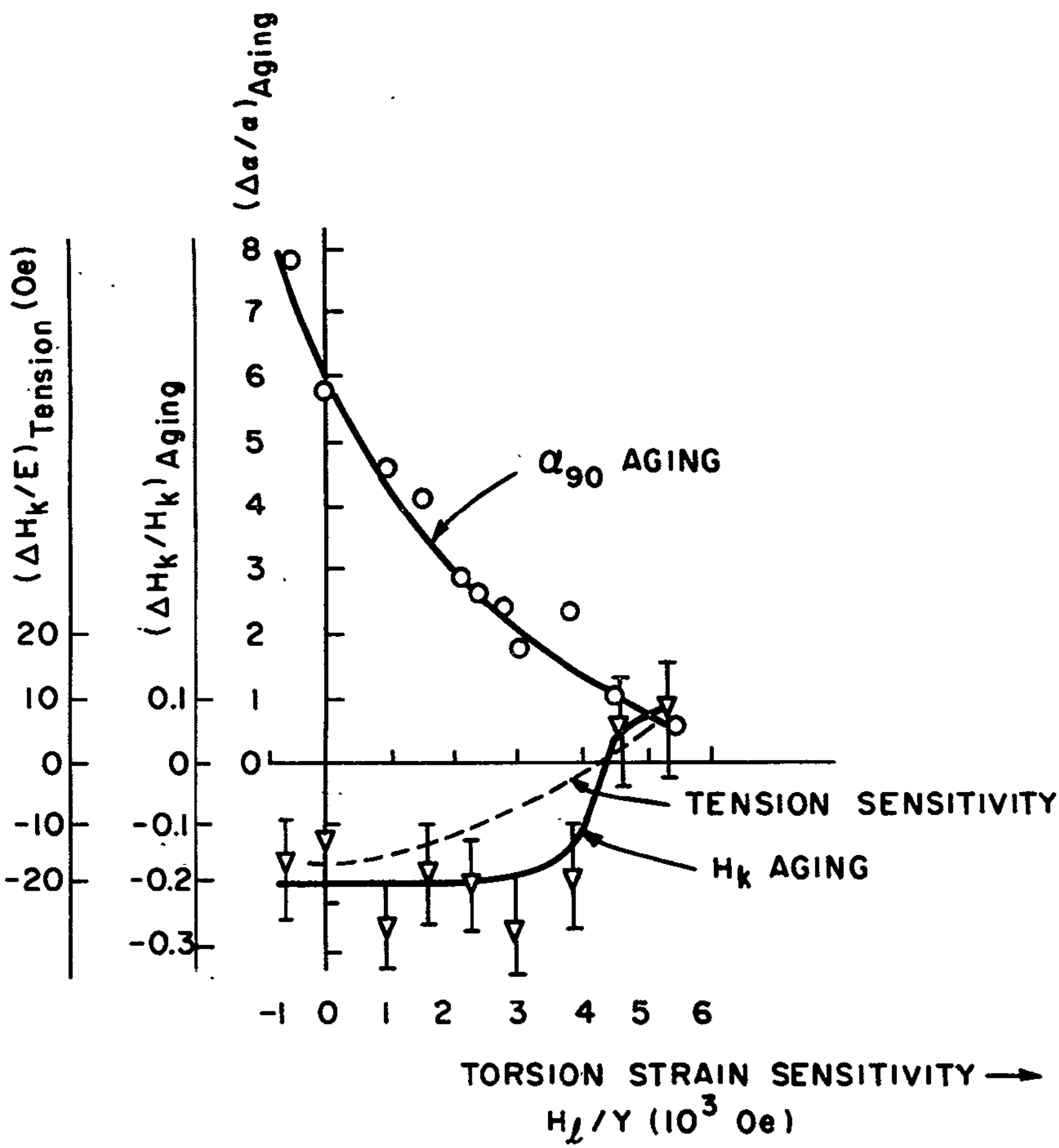

Figure 37. Relation Between Aging Rates and Torsion Sensitivity

sensitivity. In addition the tension strain dependence from Figure 36 is shown as a dashed curve. The torsion strain sensitivity giving null H_k aging is seen to coincide closely with that for null tension sensitivity, i.e., it is at a composition of about 1.4% Ni-rich on the torsion scale. Although the α_{90} aging curve does not reach a null at this composition it has been reduced by a factor of 6 below its value at the torsion ZMP. It is likely that other contributions to dispersion change are entering the picture at 60 hours and preventing the occurrence of a null. Figure 37 represents the simplest demonstration of the relation between aging and magnetostriction and the discrepancy between the ZMP's for torsion and tension.

7. Summary and Discussion of Shielded Aging—The main results of the shielded aging studies are summarized here.

Kinetics studies show similar temperature dependence for dispersion increase and electrical output degradation, with an observed activation energy of about 1.7 eV in the 200°C temperature region. The estimated temperature for 10 year lifetime based on doubling the dispersion was about 150°C.

X-ray diffraction results on grain size showed no pronounced correlation with aging time in the 200°C temperature region. Substrate diffusion into the permalloy was observed by electron microprobe for Cu – but not for Au – substrates. No significant change in composition gradient in the permalloy film was detected by the electron microprobe technique.

An environment of distilled water under its saturated vapor pressure was found to have about the same effect as air in aging studies at 230°C. A similar environment with sea water proved much more corrosive and destructive of memory properties.

The initial stage of shielded aging under vacuum is strongly composition dependent for both Au – and Cu – substrates. Changes in the anisotropy field of stabilized Fe- and Ni-rich samples are in approximate agreement with calculations of stress relief in the permalloy film. The observed changes in dispersion brought about by aging have also been shown similar to changes brought about by application of increasing axial stress to the wire, the latter being equivalent to relief of a small excess circumferential tension. A discrepancy was found between the zeromagnetostrictive compositions (ZMP) for torsion and tension. The latter is Ni-rich relative to the former. Aging rates are significantly smaller at the tension ZMP. The source of the discrepancy between the two ZMP is not presently known, but the observed effect appears to be opposite to that predicted in the case of (111) axial texture in the permalloy.[29] The latter effect would give a tension ZMP on the Fe-rich side of the torsion ZMP.

C. FIELD AGING

1. Analytical Basis of Field Aging – Field aging of plated wire may be defined as the changes of magnetic properties which take place in the presence of an external magnetic field. It is natural to assume that such changes are due to the well-known phenomenon of magnetic annealing.[30, 31, 32] The main feature of this phenomenon is the induced uniaxial anisotropy brought about by heating a magnetic alloy in the presence of a magnetic field. The resultant easy-axis corresponding to the induced anisotropy is in the same direction as that of the magnetization vector during the anneal. Since magnetic thin film memories function as a result of an easy axis of magnetization which originates during deposition, it is important to know how the induced easy axis adds to the original easy axis to bring about aging. In order to illustrate this vector addition, we consider the anisotropy field vector $\overline{H}_k$. For a given component of uniaxial anisotropy this vector has the magnitude of the anisotropy field and the direction of the easy axis for that component. We now consider the addition of two such anisotropy fields, $\overline{H}_k$, the deposition anisotropy field lying along the circumferential wire direction and assumed constant, and $\overline{H}_{k1}$, the aging anisotropy field, the

direction of which is determined by the aging conditions. The vector algebra governing this addition is the same as for ordinary vectors, except that it is carried out in double angle space.[32] The method is illustrated in Figure 38. $\bar{H}_k$ is assumed to lie in the easy (up) direction. $\bar{H}_{kl}$ is taken to lie at an angle φ with $\bar{H}_k$. For addition of the two fields, however, the required angle is 2φ. The resultant anisotropy field $\bar{H}_{k'}$ is at an angle 2β from $\bar{H}_k$ indicating an actual easy axis rotation, or skew, equal to β. Stray induced anisotropy therefore provides a natural explanation of skew occurring during aging. Let us further examine the possibilities of skew aging inherent in the operation of a plated wire memory element. As explained previously, the application of a hard direction read pulse causes rotation of the magnetization vector from its stable easy axis direction to an angle less than 90°. Frequent reading of the memory bit thus means an average angle φ of the magnetization vector somewhere between 0° and 90°. Because of magnetic annealing, an induced uniaxial anisotropy develops in this average direction and is calculable by the procedure illustrated in Figure 38. Since the read pulses are applied only part of the time, we can anticipate a worst case aging condition as the <u>constant</u> hard direction field of magnitude giving maximum skew. This worst case condition is calculable in principle from our previous discussion. First we express the skew angle β in terms of the angle of the induced anisotropy, φ. We may refer to φ also as the annealing angle. Straightforward interpretation of Figure 38 leads to the following equation:

$$2\beta = \tan^{-1}\left\{\left(\frac{H_{kl}}{H_k}\right) \sin 2\varphi \Big/ 1 + \left(\frac{H_{kl}}{H_k}\right) \cos 2\varphi\right\} \qquad \text{(IV-6)}$$

Where H_{kl}/H_k is the ratio of the magnitude of the induced anisotropy field to that of the deposition anisotropy field. It remains to specify the annealing angle in terms of the magnitude of the hard direction field. This relation is given by Eq. IV-6, so that we are now able to relate induced skew to field magnitude $H_\perp$ during hard direction field aging by substituting $\varphi = \sin^{-1} (H_\perp / H_k)$ in Eq. IV-6. Under this condition calculations show

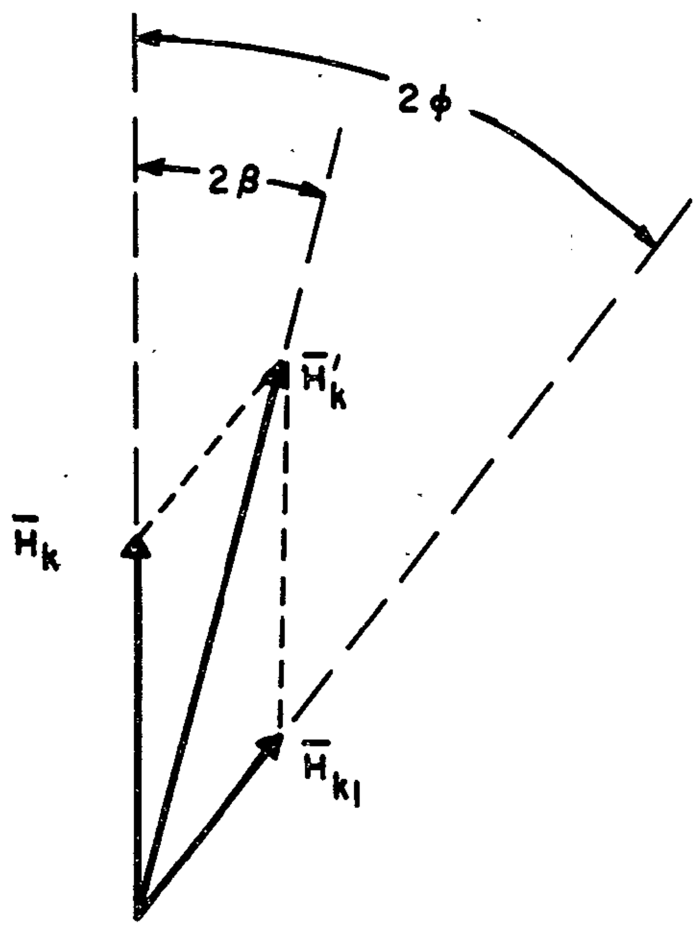

Figure 38. Relation of Easy Axis Skew to Induced Anisotropy

that maximum β should occur at $\varphi \cong 45°$ or $H\perp/H_k \cong 0.7$. Furthermore, the induced skew should be zero for $H\perp/H_k = 0$ and $H\perp/H_k = 1$. In order to compare these predictions with experiment and to determine the actual worst case hard-direction field condition, aging experiments were carried out at different field magnitudes and for different wire types. These are discussed below.

2. Effect of Field Magnitude—Experiments were carried out to compare with Eq. IV-6. Wires characterized by high and low values of dispersion were used. The wire properties are summarized below:

SUMMARY OF MAGNETIC PROPERTIES PRIOR TO FIELD AGING

Sample Number	H_k (Oe)	α_{90} (By Belson) (Degrees)	α_{50} (By Field Rotation) (Degrees)
60-1	2.5	1.2	0.7
49-1	5.7	1.6	5.6

Sample 60-1, which had a low dispersion and anisotropy field, was made using a high additive electroplating bath, while 49-1 was made with small additive content. Both series were on-line stabilized prior to aging (see later section). The wires were magnetized during aging.

The effect of aging field magnitude on the resultant skew is shown in Figure 39. The aging condition was 198°C for one hour with the field along the axial direction. The graph shows skew (relative to maximum observed) as a function of field (relative to anisotropy field). Also shown, for comparison, is the theoretical field dependence from Eq. IV-6. The experimental results agree with the prediction of a maximum skew occurring at small fields. The location of the maximum is at a smaller field for both samples, however, than predicted from the theory. This location is at $H\perp/H_k \cong 0.4$ for the high dispersion sample and at $H\perp/H_k \cong 0.5$ for the low dispersion

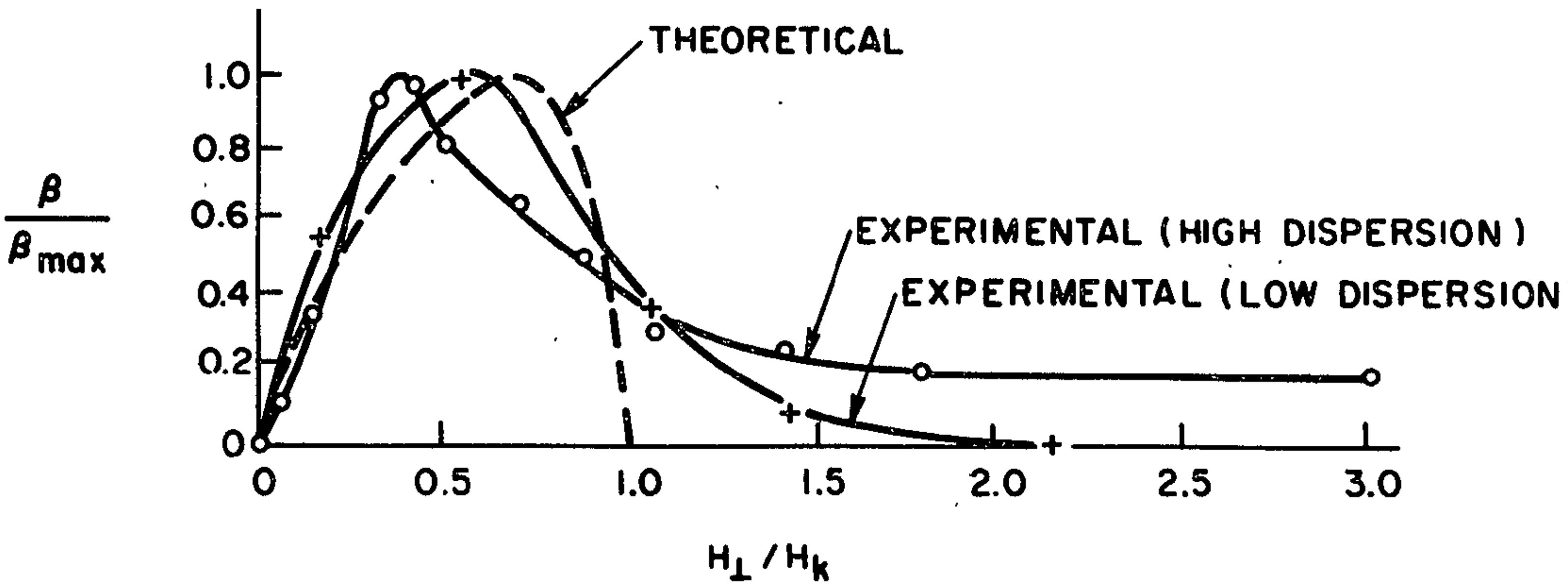

Figure 39. Field Dependence of Induced Skew

sample. It is also clear that an intercept on the field axis is more clearly defined for the low dispersion case. The open end on the field axis for high dispersion wire is similar to the switching threshold curve for such wire.[19] In general this suggests high H_k components not reflected in the determination of the average H_k of the wire. This property is of importance in NDRO applications.

From the standpoint of aging and memory failure the importance of the field dependence lies in establishing a worst case hard direction field for aging. This field is evidently in the vicinity of 0.5 H_k. In actual operation of an NDRO plated wire memory the hard direction field used for interrogation is equal to or greater than H_k and the worst case condition is satisfied only during the relatively short rise and fall times of the pulse. Furthermore, a particular memory bit is subjected to pulses only a fraction of the time. A d.c. field equal to 0.5 H_k is, therefore, a stringent aging condition, at most only approached in practice. Lifetimes calculated from accelerated aging tests using this field condition, therefore, tend to be lower limits.

3. Effect of Stabilization Temperature – The preceding discussion suggests a natural test for the effectiveness of wire stabilization procedures. Wires stabilized under different conditions are compared by aging at an arbitrary temperature in the presence of a hard direction field equal to 0.5 H_k. The wire showing the smallest skew development will be judged as having had the best stabilization treatment. Such a comparison is shown by Figure 40a. The curves show skew vs aging time at 180°C with stabilization temperature as parameter. Stabilization time was 20 seconds. It is seen that increasing the stabilization temperature reduces the effect of field aging. The curves of Figure 40b obtained with the aging field equal to H_k, confirm that this condition results in a smaller skew and are thus consistent with Eq. IV-1 and Figure 39. These curves prove the important role of stabilization in reducing field-induced skew.

The effect of stabilization was further established by comparison of output profiles of wires stabilized at different temperatures. The techniques for such measurements have been referenced in Section III. Results are shown in Figures 41 and 42. In these figures the "1" and "0" output are shown for aged samples at two different digit currents for stabilization temperatures of 400°C (Figure 41) and 350°C (Figure 42).

The aging field was $H_\perp = 0.5\, H_k$ and the aging temperature was 180°C. The chart distance corresponds to about two inches of wire. The 350°C stabilized sample shows output failure for the "1" polarity at 32 hours aging time. The 400°C stabilized sample still shows satisfactory output at aging times up to 158 hours. In both samples the occurrence of output skew is evident, as expected from the above discussion of easy-axis skew. The weak polarity output is improved by increasing the digit current, as also is to be expected in general.[19] It should be noted that the pulse profiles of the 350°C stabilized sample appear irregular even before aging. This probably indicates domain wall creep effects in under-stabilized wire. It is concluded from the results that the stabilization temperature is highly critical to the stability of the memory element from the standpoint of both skew failure and output uniformity.

The results reported above show a monotonic decrease in skew susceptibilities for stabilization temperatures up to 400°C. For temperatures above 350°C, grain growth and dispersion increase are known to occur.[33] It is likely that such processes limit the practical attainment of complete stabilization against field-aging, as suggested by Doyle, et. al.[34] The present experimental results serve to define stabilization conditions giving adequate lifetime.

4. Kinetics Studies and Lifetime Evaluation – Figure 40 shows that at least two aging rates are operative in field aging. At 180°C most of the easy axis skew occurs in the first half hour. This is followed by a slower skew increase. The amount of initial fast skew, as well as the subsequent rates, depends on the stabilization temperature. Since the time scale of Figure 40

A

B

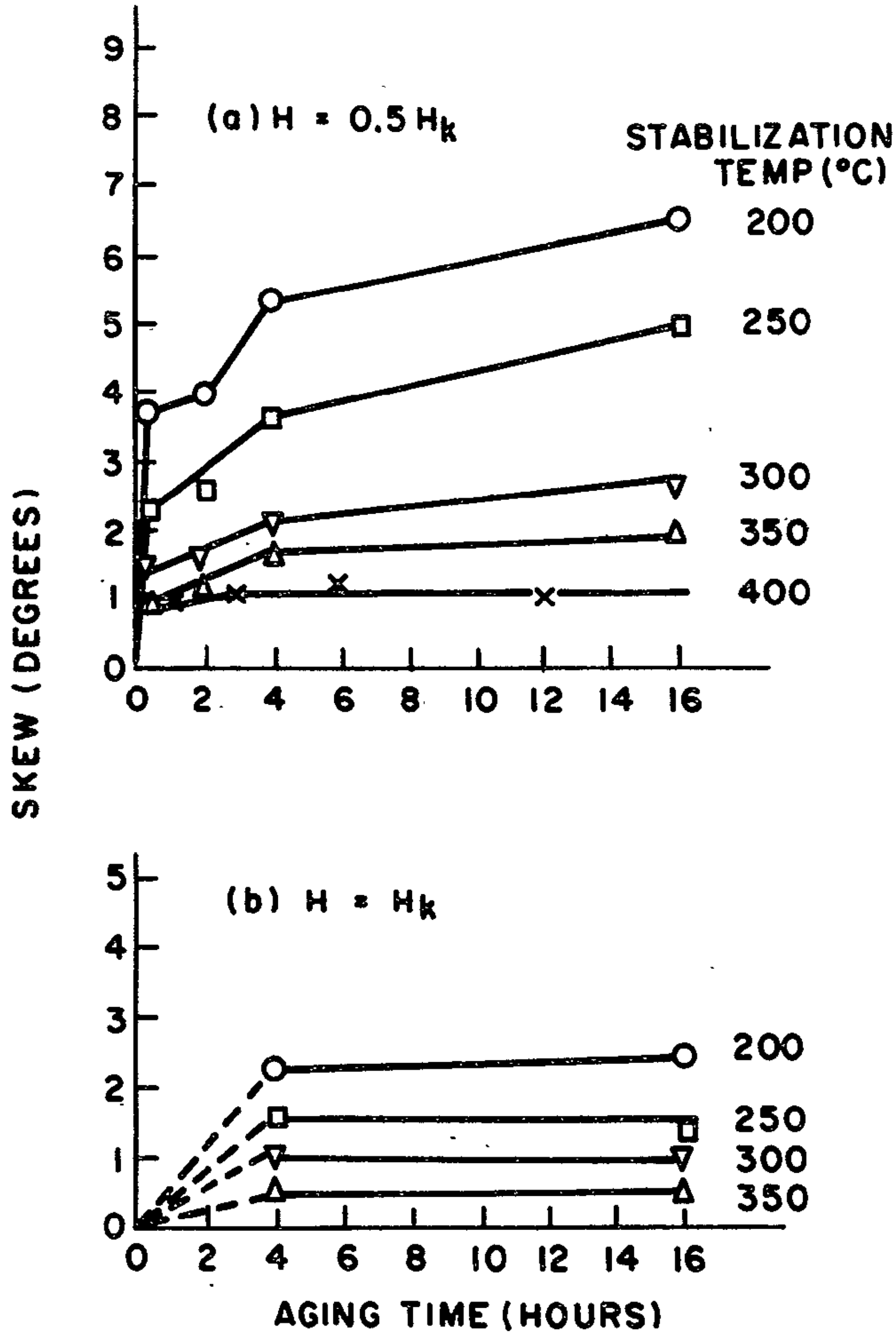

Figure 40. Effect of Stabilization Temperature on Field Aging

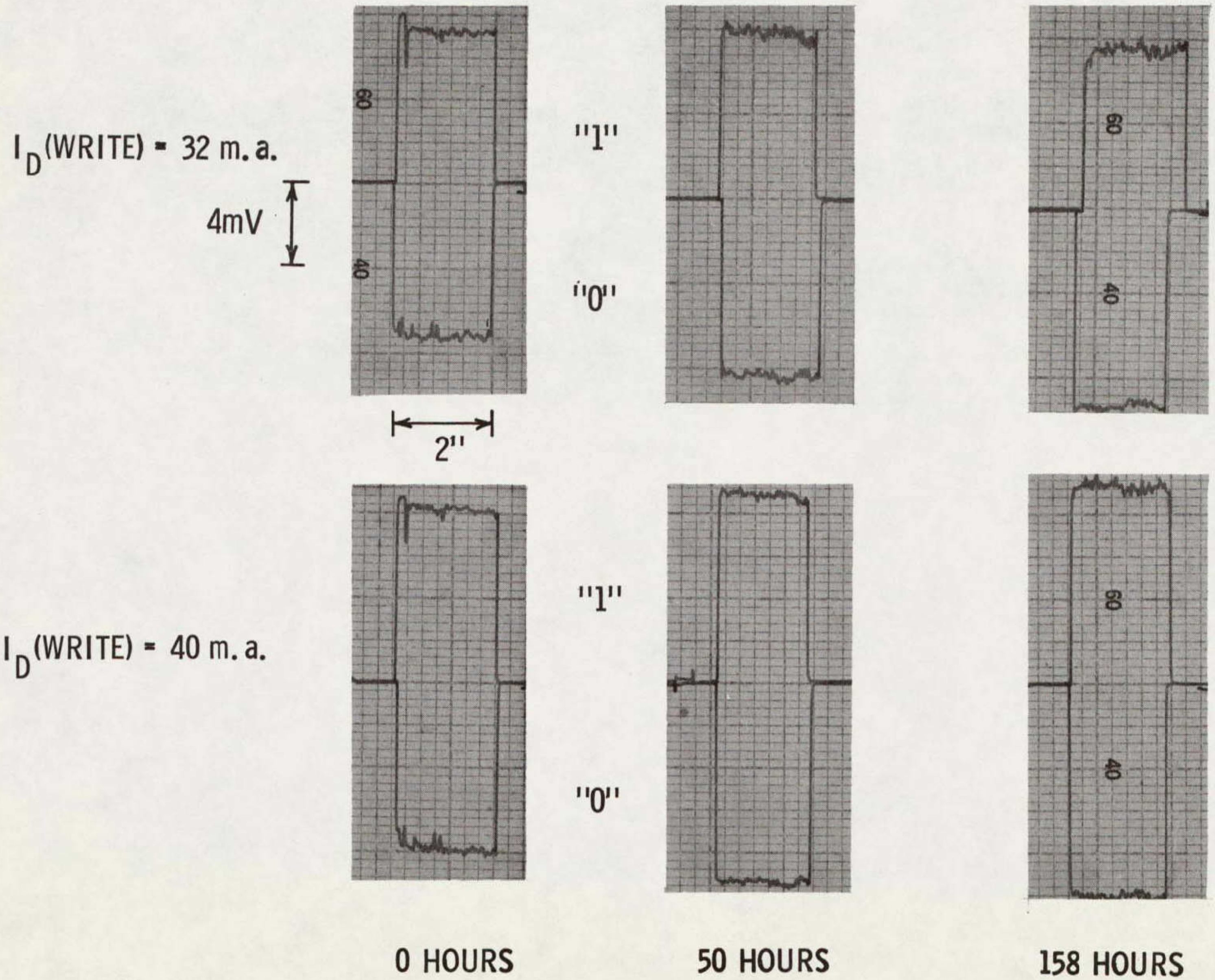

Figure 41. Pulsed Output Profiles Before and After Field Aging, 400°C-Stabilized Wire

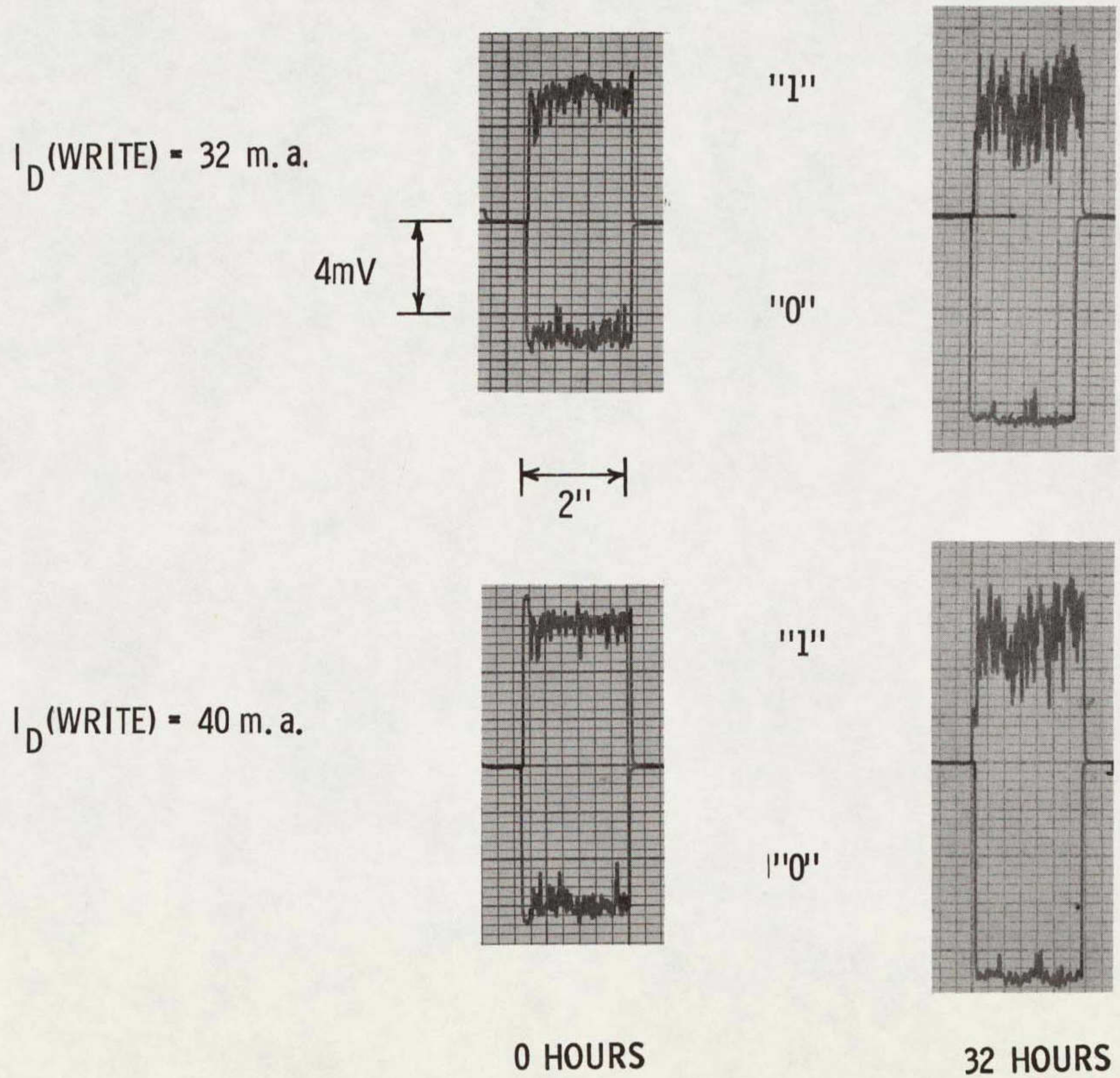

Figure 42. Pulsed Output Profiles Before and After Field Aging, 350°C-Stabilized Wire

is inappropriate to observe details of the fast skew process, studies of skewing were also made at lower temperatures. These results are given in Figure 43, which shows the dependence of skew on aging time for temperatures between 60° and 120°C. The hard direction field, as usual, was $0.5\ H_k$. The time dependence may be interpreted as a combination of fast and slow processes given by:

$$\beta_\infty - (\beta - At) = \beta_\infty \exp - (t/t_o) \qquad \text{(IV-7)}$$

in which β is equal to the observed skew at time t, β_∞ is the saturated fast component, A is the rate constant for the slower process, and t_o the time constant for the fast process. (t_o is the time required for the fast component to reach 0.63 of its ultimate value, i.e. $0.63\ \beta_\infty$.) Analysis of these results gives the following time constants for Eq. IV-7:

T (°C)	t_o (minutes)	
120	9	
100	23	
80	98	
60	330	
(20)	(9800)	(By extrapolation)

These results show that the fast skew would be expected to reach 0.6 of its saturation value after only 150 hours at room temperature. Since this is well below acceptable lifetime, we arrive at the important requirement that the saturation value of fast skew must be sufficiently small to not impair the worst case output below an operable value. Furthermore, we require that other, slower, skew processes will not result in memory failure within required lifetimes. The first condition is satisfied by our previous data on plated wire stabilized at 400°C (Figure 41), since after 180°C and 158 hours of field aging the fast component is certainly saturated and the wire still has

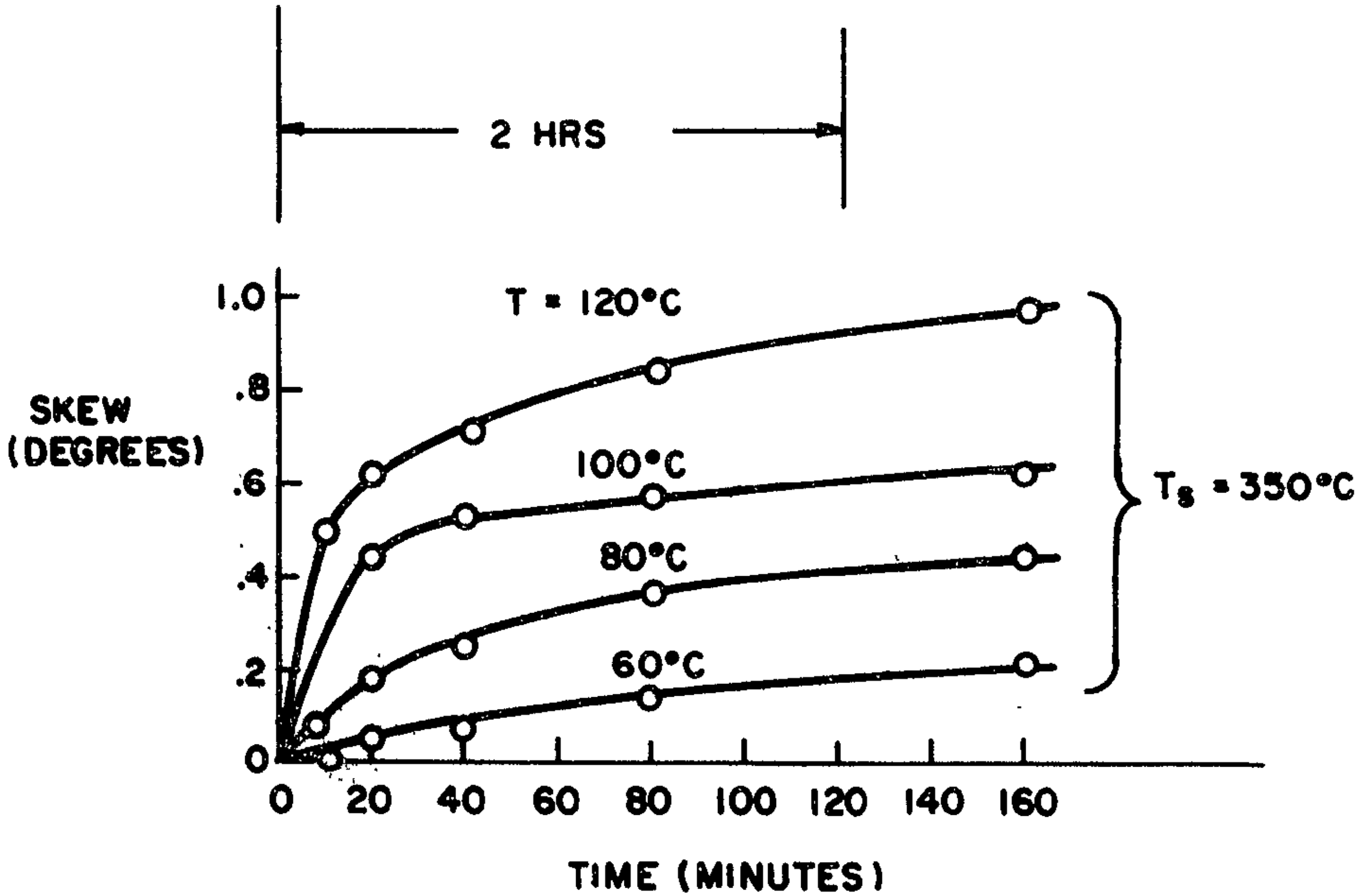

Figure 43. Field Aging Rates Near 100° C, 350°C-Stabilized Wire

satisfactory output. In order to satisfy the second condition we must insure that worst case extrapolation procedure gives satisfactory lifetime at operating temperatures. We discuss this requirement through Figure 44. This shows the usual semi-log plots of lifetime vs. reciprocal temperatures. In the case of worst-case field aging at 180°C $\left[T^{-1} = 2.21 \times 10^{-3} \ (°K)^{-1}\right]$ we have established a minimum lifetime of 158 hours. This point is plotted on the graph. We may now assume a lifetime extrapolation from this point by means of an assumed activation energy. It is, of course, understood that more than one process, hence more than one activation energy, may be operative. It has been pointed out that lower activation energy processes may be unobservable at higher temperatures but important at lower temperatures.[21] All such extrapolation must, therefore, be done with this in mind.

For purposes of illustration we have included in Figure 44, activation energies of 0.70 and 0.46 eV in order to extrapolate from the minimum observed 180°C lifetime. The 0.7 eV curve predicts 10 year lifetime at about 60°C while the 0.46 eV curve predicts the same lifetime at 20°C. If we inquire what minimum aging lifetime is required at 180°C to insure 10 year life at 20°C, assuming 0.70 eV, we find a requirement of 5 hours, as indicated in Figure 44. The choice of 0.7 eV represents a lower limit for previously observed activation energies for output degradation.[19, 21]

5. Outgassing and Solubility Studies—The systematic reduction of skew susceptibility with increasing stabilization temperature has been discussed in Section IV C-3. One possibility for explaining this phenomenon is an outgassing of volatile impurities from the film, brought about by diffusion and desorption processes. In particular it is known that hydrogen is a common impurity in electrodeposited films [35] and that it may enter indirectly into magnetic ordering (induced anisotropy) processes. [36]

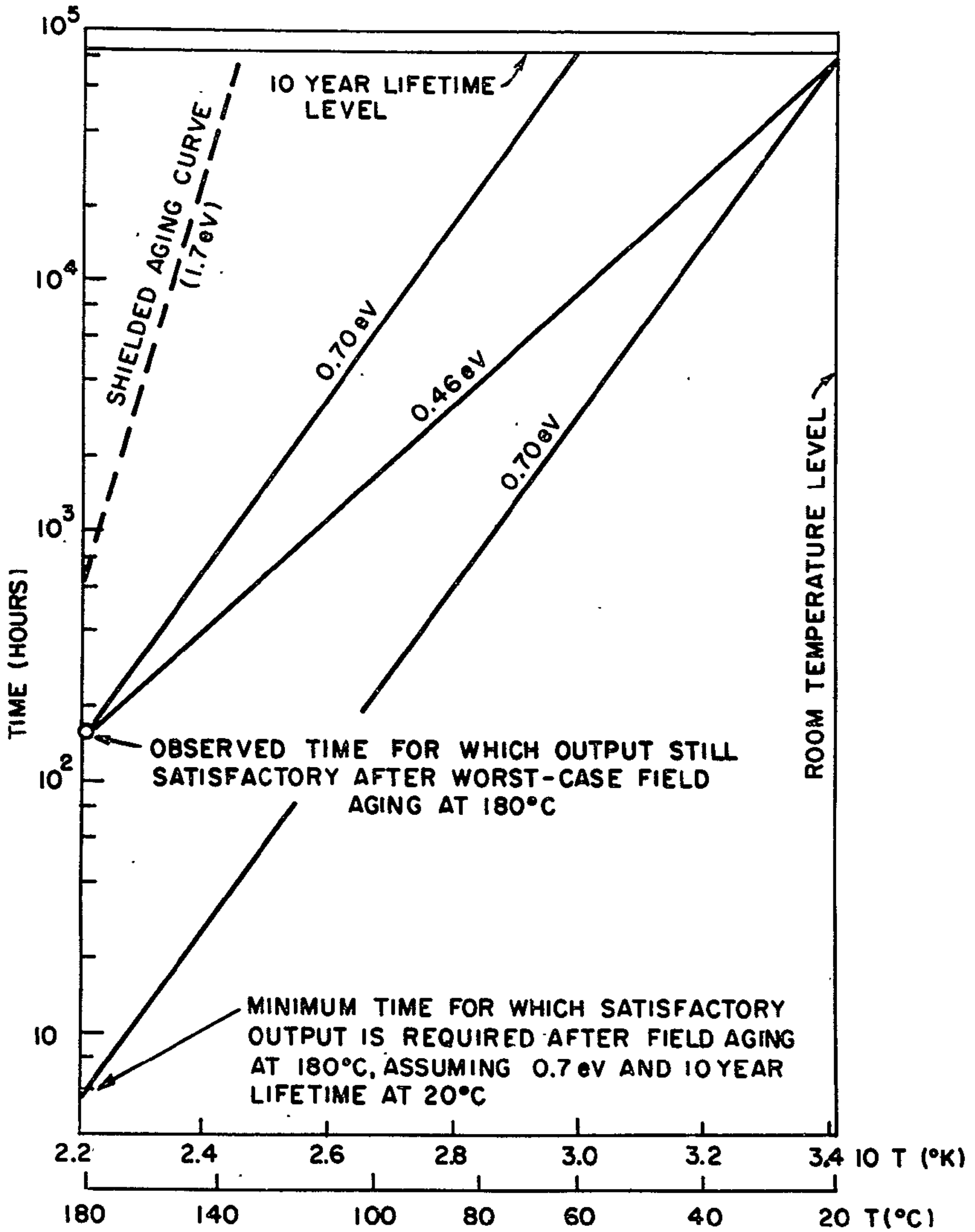

Figure 44. Field Aging Lifetime Extrapolations

Accordingly, we undertook mass spectrometer analytical studies to ascertain whether or not a correlation exists between hydrogen content and magnetic skew-aging susceptibility. The procedure consisted of making measurements of both skew-aging susceptibility and hydrogen content on a series of samples having different stabilization temperatures, hence varying degrees of stabilization. The on-line stabilization was carried out in 20 seconds, with stabilization temperatures of 20° (unstabilized), 200°, 250°, 300°, 350°, 375° and 400°C. The skew susceptibility measurements were made by the method described in a previous section. The hydrogen content determination was made by heating the plated wire to a standard temperature, about 520°C, inside the ionization chamber of a mass spectrometer. The mass spectrometer was set at mass 1. During the heating the pumping speed of the vacuum pump was sufficiently high that the recorded chart signal was proportional to the rate of evolution of hydrogen from the heated sample. The total hydrogen evolved was then proportional to the integrated area under the curve of rate vs. time. It was assumed in turn that this quantity was proportional to the total content of gas in the film following its stabilization treatment (and prior to its mass spectrometer outgassing).

Figure 45 shows both skew susceptibility and hydrogen content as functions of prior stabilization temperature, T_s. Both quantities are shown relative to their maximum observed value over the range of stabilization temperature. Most of the hydrogen points are the result of two separate determinations and such points are shown with the range of observed values. The two types of data are seen to have similar dependences on stabilization temperature. (It is concluded that the stabilization process reduces skew susceptibility and hydrogen content simultaneously.)

According to the diffusion theory of gas desorption [37] the residual average gas content, $\overline{C}$, of a wire following annealing at temperature, T, is given by

$$\overline{C} = \text{constant} \times \sum \frac{1}{\alpha_n^2} e^{-D\alpha_n^2 t} \qquad \text{(IV-8)}$$

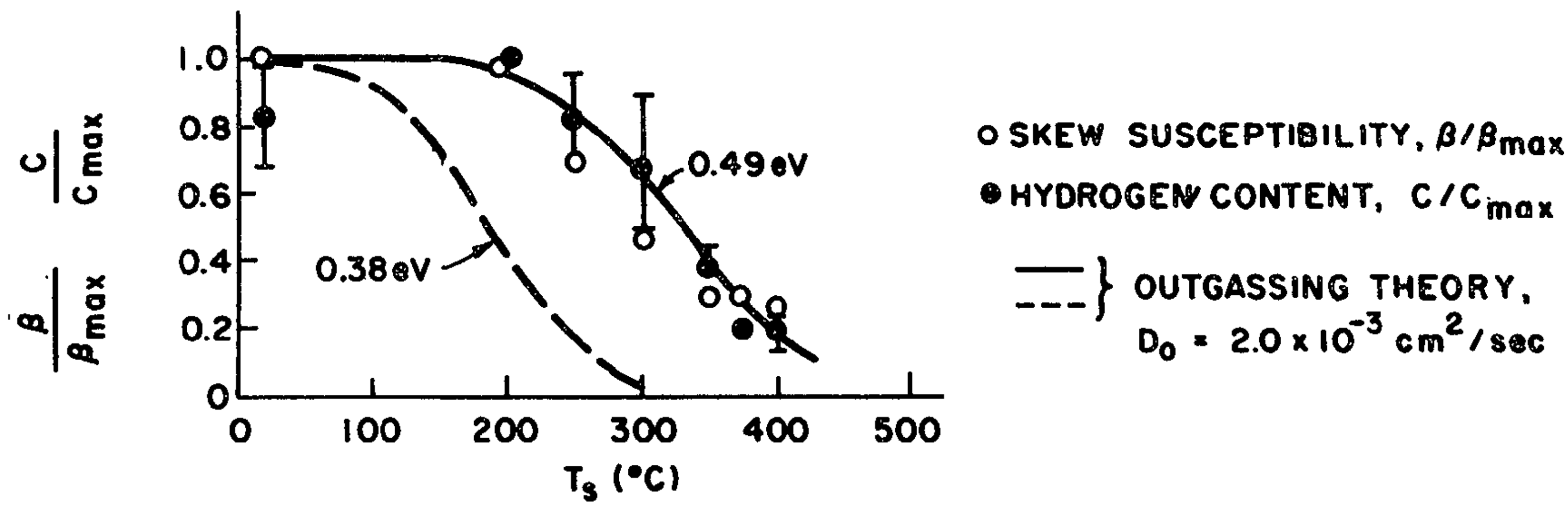

Figure 45. Effect of Stabilization Temperature on Skew Susceptibility and Hydrogen Content

Where D is the diffusion constant for the gas, t is the annealing time, and the α_n are inversely proportional to the wire radius. Eq. C-3 has been calculated using published diffisuon constant results for hydrogen in nickel.[38] According to these results D is given by

$$D = D_o e^{-E_D/RT} \tag{IV-9}$$

with $D_o = 2 \times 10^{-3}$ cm^2/sec, and E_D = 8700 cal/gm-atom, or 0.38 electron-volts/atom. The calculated outgassing curve using Eq. (IV-8) and Eq. (IV-9) is shown as a dashed curve in Figure 45. This calculated curve is seen to predict outgassing at lower temperatures than observed experimentally. For comparison a second curve using the same D_o but an E_D of 0.49 eV is shown to fit the data. An obvious possibility for the higher observed activation energy is the fact that the film is not pure nickel but rather permalloy. Another possibility would be the existence of a surface barrier such as an oxide, which would tend to increase the required outgas energy. Gas trapping in non-interstitial locations would also tend to modify the observed temperature dependence.

The possibility that the hydrogen in the film is not dissolved in interstitial locations is suggested by calculations of the absolute hydrogen content from the mass spectrometer data. Such calculations show that the amount of outgassed hydrogen is at least an order of magnitude larger than predicted from previous solubility data. Attempts were made to re-introduce skew susceptibility by annealing outgassed wires in hydrogen at temperatures up to 400°C and hydrogen pressures up to 2300 psi. These experiments were negative. In fact, stabilization in the presence of hydrogen was found equally satisfactory to stabilization in nitrogen with respect to skew susceptibility. It appears that the hydrogen content resulting from electrodeposition is much greater than the ordinary solubility and that the film is thus initially supersaturated with hydrogen. The results of Figure 45 indicate a relationship between field aging and hydrogen content but the solubility and hydrogen anneal results indicate that the mechanism is other than interstitial orientation of dissolved hydrogen atoms.

6. Summary of Field Aging — Studies were made of skew susceptibility (the amount of rotation of the easy axis brought about by annealing in a hard direction field, $H_{\perp}$). The susceptibility was found to be a maximum for $H_{\perp}/H_k \cong 0.5$.

Kinetics studies showed that time constants for skew development are too short to be acceptable as memory lifetime. It is, therefore, crucial that the saturated skew be insufficient in magnitude to cause memory failure. An investigation was made of the reduction in skew susceptibility obtained by stabilization anneals in an easy direction field. Wire stability determinations based on observations of electrical output degradation were found satisfactory for elements stabilized at 400°C.

The dependence of skew susceptibility on stabilization temperature was correlated with a similar dependence of residual hydrogen content, as determined from mass spectrometer techniques. The hydrogen content of unstabilized wires appears higher than is to be expected from solubility estimates. Attempts to induce skew susceptibility increases by dissolving hydrogen at elevated pressures during annealing were unsuccessful.

V. EFFECT OF AGING ON MEMORY OPERATION

A. FAILURE MODES

In operation a memory element is subjected to combinations of easy and hard direction magnetic fields which serve both to store information (write) and to interrogate (read). In addition, a stored bit is subjected to disturbing fields due to reading and writing in adjacent bits. A memory element may fail to function properly if either it is not capable of successful storage, or if the stored information is destroyed by either reading (destructive read) or by adjacent bit interference. It is convenient to discuss aging failure modes by referring to distortion of the switching threshold. This is illustrated in Figure 46, where for simplicity the threshold curve is shown as an astroid. In the general case the switching threshold curve has a more complicated shape and departs from a sharply defined curve because of the effects of dispersion and domain wall creep. Figure 46a shows the main features of NDRO operation. The film is assumed initially switched in the down, "O", direction. Writing is achieved by coincident hard and easy direction magnetic field pulses. Since the resultant write field lies above the threshold in the upper quadrant, it switches the film to a "1" direction. Disturb pulses are experienced due to easy direction fields, analogous to half-select currents, of such direction as to re-switch the film to the "O" direction. Read pulses are applied in the hard direction with the same magnetic field previously used for the coincident write.

Aging failure may now be conveniently discussed as distortion of the switching threshold due to physical and chemical changes such as those discussed in previous sections of this report. Possible idealized failure modes are depicted in Figure 46. In general, failure occurs if the write field lies inside, or if either disturb or read fields lie outside, the threshold. Insufficient write failure will occur when the threshold distortion is such

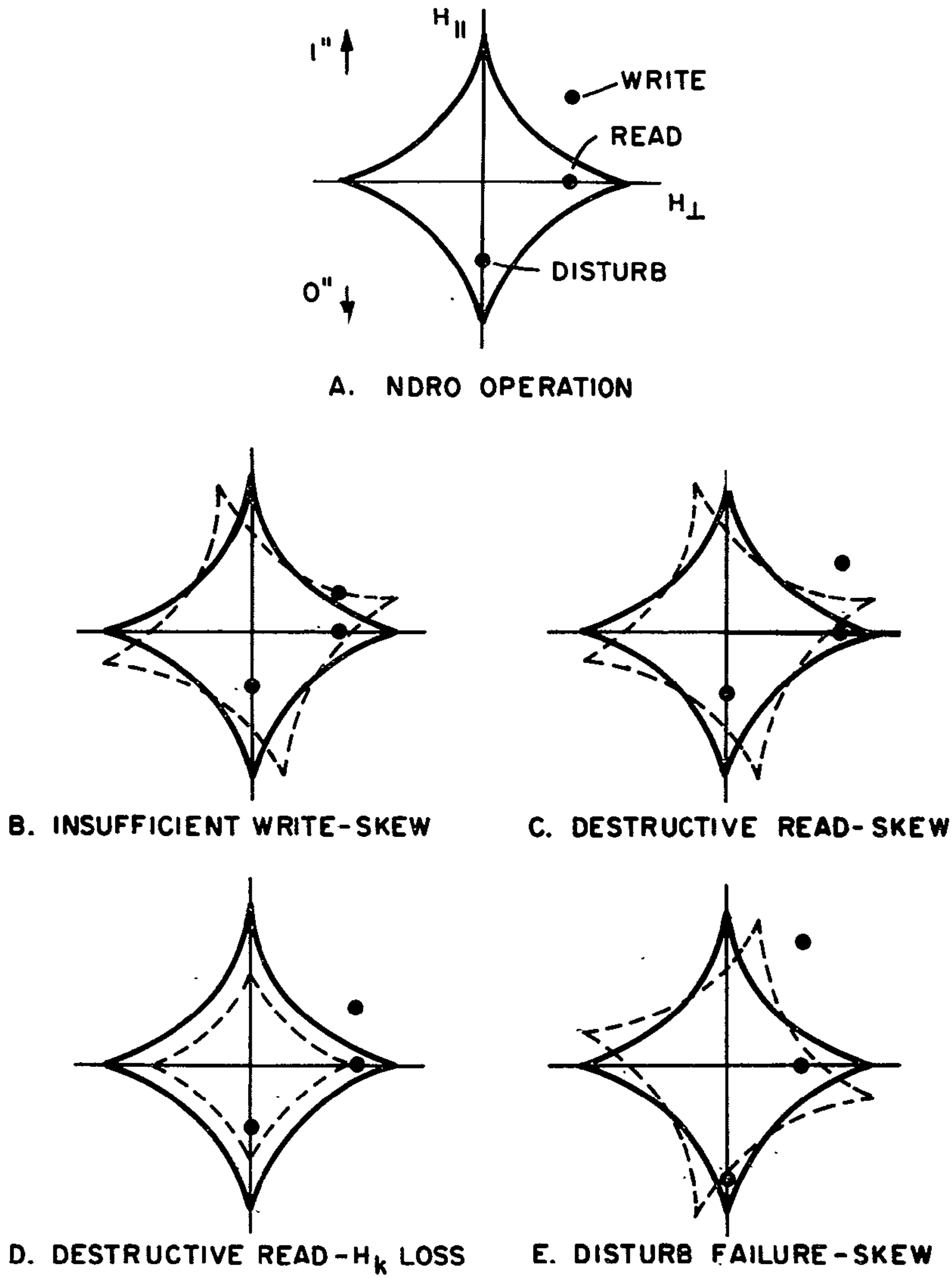

Figure 46. NDRO Failure Modes

as to move the threshold outside the write field. This mode is depicted in Figure 46b as due to a skewing of the threshold. Such skewing can occur due to external field conditions or internal film changes. Similarly Figures 46c and 46d show two failure modes in which the threshold moves to a location inside the read field. The first of these read failure modes is taken to be a reduction of the H_k of the film. The second read failure mode shown is that of skew failure in which the threshold is rotated outside the read field. Note that in this case the read field does not demagnetize the film but instead always restores the magnetization to the "O" direction. Hence, it is destructive for the "1" store. Finally, failure by disturb is depicted in Figure 46e. Here the threshold is skewed outside the disturb field. An important point illustrated by Figure 46 is that the choice of operating fields can determine the failure mode. We note, also, that insufficient write due to dispersion[19] is represented by the skew mode (Figure 46b) since dispersion is due to local skew throughout the film.

B. PLATED WIRE PULSE TESTING

We now relate the previous discussion of aging failure modes to actual pulse testing of plated wire elements. A typical pulse program designed to simulate worst case (consistent with memory operation) conditions is shown in Figure 47. The program is divided into four sections, History, Write, Disturb and Read. Pulse patterns are shown for a fixture incorporating a central and two adjacent word straps, designated left and right. The wire current (digit current) pulses are applied in bipolar units to minimize creep effects, while the word current pulses are always supplied with a single polarity. The magnitudes of the pulses are designated by the index numbers below while number of pulses is shown above. An explanation of the pattern is now given:

> <u>HISTORY</u>: The center and both adjacent bits are written with a "O" with maximum digit and word currents (index 2). This presets the element with maximum magnetization in the direction opposite to that to be used for the test write.

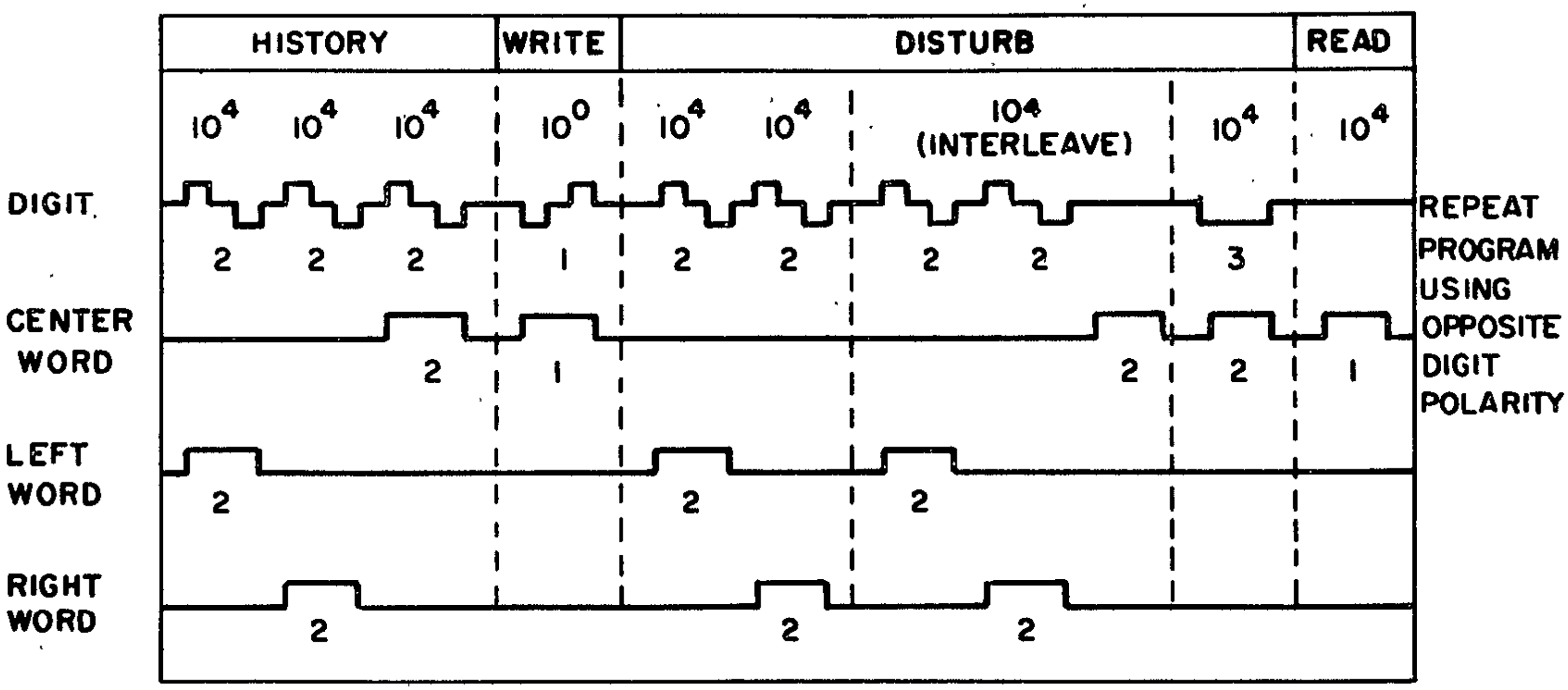

NOTE: (a) NUMBER OF PATTERN REPETITIONS IS SHOWN ABOVE PATTERN.
(b) PULSE HEIGHT INDEX IS SHOWN BENEATH THE PULSE SYMBOL.

Figure 47. Pulse Test Program

WRITE: The center bit is written into with a "1" with minimum digit and word currents (index 1). This switches the element with minimum magnetization; in other words the store is as weak as possible (insufficient write).

DISTURB: This is divided into three parts: (a) Adjacent bits are further strengthened by hard writes in the "O" direction (disturb-creep). (b) Word read pulses of maximum amplitude are alternated with further adjacent bit disturbs (destructive read). (c) Word read pulses of maximum amplitude are combined with small amplitude digit pulses (index 3) simulating stray currents in the wire (destructive read-"crawl").

READ: The center bit is interrogated with minimum level word current.

It should be noted that the adjacent bit word currents correspond to relatively small fields at the center bit and therefore are correctly represented as DISTURB in Figure 46.

Since the magnitude of the read voltage following a realistic pulse program reflects the success of the store as well as the resistance to destructive read and adjacent bit interference, it is the most representative quantity for evaluating the progress of aging failure, and should be incorporated in reliability specifications.

VI. SUMMARY AND DISCUSSION

Structural investigations of permalloy films deposited on BeCu wires showed inhomogenities in composition, surface topography and grain size. In addition, twins and faults were detected by electron diffraction, which also revealed evidence for the presence of an α (Fe-rich) phase in the film.

Aging studies were made mainly in the 200°C region where the memory properties were known to degrade significantly in convenient measurement times. Electron transmission and diffraction studies did not reveal corresponding consistent changes in microstructure. Likewise, changes in composition were not detected on a one micron scale. The diffusion of substrate atoms into the permalloy film was found to occur in the case of Cu substrate but not for Au-substrate wires. Since the main magnetic aging characteristics were similar for both types of substrates, these characteristics are probably not explained by the Cu diffusion.

Controlled atmosphere aging experiments showed that sea water has a drastic corrosive effect on the magnetic and physical properties in comparison to distilled water or air atmospheres. Little difference was found between the latter two aging environments.

A major source of aging was found to exist in the relief of film stress. Such stress is inherent in the electrodeposition process and appears to be present even after stabilization. The apparent existence of this magnetostrictive aging mode in elements showing zero torsion strain sensitivity has led to the discovery of a pronounced discrepancy between the zero-magnetostriction composition (ZMP) determined from tension and torsion. The source of this discrepancy is not presently known. A comparison of aging rates for compositions on the Ni-rich side of the torsion ZMP showed a significant reduction in rates at the tension ZMP. The latter corresponds to about 1.4% Ni-rich composition on the torsion scale.

The susceptibility of plated wire to field-aging, i.e., the amount of rotation of the magnetic easy-axis during annealing in a magnetic field, was correlated with the amount of residual hydrogen in the film following various degrees of stabilization. It appears, however, that the action of hydrogen in aging cannot be due simply to its presence in solid solution, since annealing in hydrogen at high pressure does not re-introduce the field-aging susceptibility.

Kinetics studies of the field aging phenomenon showed that the easy-axis skew approaches saturation in times which are short compared to desired memory lifetime. This means that the magnitude of the saturated skew must be kept sufficiently small so as not to degrade the output below acceptable standards. Pulse tests under simulated memory conditions showed this to be true for plated wire stabilized at 400°C.

REFERENCES

1. A. Brenner, Electrodeposition of Alloys, Vol. 1, p. 77. Academic Press (1963).

2. H. Dahms and I. M. Croll, J. Electrochem. Soc. 112, 771 (1965).

3. T. R. Long, J. Appl. Phys. 37, 1470 (1966).

4. M. N. Sagal, J. Electrochem. Soc. 112, 174 (1965).

5. A. Brenner, op. cit., chapters 6 and 11.

6. R. J. Prosen, B. E. Gran, J. Kivel, C. W. Searle and A. H. Morrish, J. Appl. Phys. 34, 1147 (1963).

7. C. J. Owen, H. Jackson and E. R. York, Plating Magazine, 821 (July 1967).

8. A. Brenner, op. cit., p. 219.

9. A. Brenner and S. Senderoff, J. Res. Nat. Bur. Stds. Research paper RP 1953, 42, Feb. 1949.

10. R. Weil, W. W. Jaubus, Jr., and S. J. DeMay, J. Electrochem. Soc. 111, 1046 (1964).

11. R. Fisher, J. Electrochem Soc. 109, 479 (1962).

12. R. S. Smith, L. E. Godycki and J. C. Lloyd, J. Electrochem Soc. 108, 996 (1961).

13. O. S. Lutes, R. B. Fryer, J. O. Holmen, and J. R. Kench, Quarterly Technical Report No. 2, Contract NAS 12-2003, NASA Electronics Research Center, Jan. 15, 1969; S. J. Strobl, IEEE. Transactions on Magnetics, MAG 5, 139, June 1969.

14. H. W. Katz, et al, IEEE Trans. on Magnetics, MAG-1, 218 (1965).

15. T. S. Crowther, J. Appl. Phys. 34, 580 (1963).

16. H. S. Belson, Proc. Intermag Conf. 1963, p. 12.4.

17. O. S. Lutes, R. B. Fryer, J. O. Holmen and J. R. Kench, Quarterly Report No. 1, Contract NAS 12-2003, NASA Electronics Research Center, Oct. 15, 1968.

18. R. F. Soohoo, Magnetic Thin Films, (Harper and Row, 1965); M. Prutton, Thin Ferromagnetic Films, (Butterworths, London, 1964).

19. O. S. Lutes and T. J. Cebulla, IEEE Trans. on Magnetics, MAG-4, 171 (1968).

20. See, for example, Lange's Handbook of Chemistry, Ninth Edition, Handbook Publishers, Inc., Sandusky, Ohio. 1956, p. 1718.

21. R. G. Brown, R. T. Richard, and Y. Narahara, J. Appl. Phys. 40, 984 (1969).

22. I. Danylchuk, V. F. Gianola, and J. T. Sibilia, Bell Syst. Tech. J. 47, 1539 (1968).

23. See, for example, Metals Handbook, 1948 Edition, American Soc. for Metals, Cleveland, Ohio (1948), p. 443.

24. H. B. Shukovsky and T. P. Turnbull, IEEE Trans. on Magnetics, MAG 4, 59 (1968).

25. A. G. Gray, Modern Electroplating, John Wiley and Sons, Inc., New York, 1953, p. 348.

26. S. Chikazumi, Physics of Magnetism John Wiley and Sons, Inc., New York, 1964, p. 182.

27. R. M. Bozorth and J. G. Walker, Phys. Rev. 89, 624, (1953).

28. O. S. Lutes, J. O. Holmen, and J. R. Kench, Quarterly Tech. Report No. 4, Contract NAS 12-2003, NASA Electronics Research Center, July 15, 1969.

29. J. P. Jadot, J. Appl. Phys. 40, 3186 (1969).

30. C. D. Graham, Jr., in Magnetic Properties of Metals and Alloys, R. Bozorth, Ed. (American Society for Metals, Cleveland, Ohio, 1959).

31. J. C. Slonczewski in Magnetism, F. T. Rado and H. Suhl, Eds. (Academic Press, Inc., New York, 1963), Vol. 1, Chap. 5.

32. J. C. Slonczewski, N. G. Ainslie, and W. R. Beam, J. Appl. Phys. 38, 2667 (1967).

33. J. T. Chang, A. R. Von Neida, and C. J. Calbick, J. Appl. Phys. 37, 1472 (1966).

34. W. D. Doyle, R. M. Josephs, and A. Baltz, J. Appl. Phys. 40, 1172 (1969).

35. A. G. Gray, Op. Cit., p. 57.

36. B. F. Rothenstein and J. D. Artzner, J. Appl. Physics 39, 4476 (1968).

37. R. M. Barrer, Diffusion in and Through Solids, Cambridge Univ. Press, 1951, p. 34.

38. C. J. Smithells, Metals Reference Book, Butterworth, 1962, p. 580.

VII. ACKNOWLEDGEMENTS

The experimental studies on aging were carried out by R. P. Ulmer, S. Marquardt and C. Knudson. Valuable advice regarding electroplating and contractometer studies was given by Dr. H. V. Venkatasetty. Mr. G. Rork designed and carried out the mass spectrometer experiments. Useful discussions were held with Dr. J. A. Sartell, F. N. Simon, W. L. Walters, and Dr. J. H. Chaffin of the Corporate Research Center, as well as with N. Patt, P. Poirier, and Dr. T. Altshuler, all of the NASA Electronics Research Center.

APPENDIX I

TENSION SENSITIVITY FIXTURE

An apparatus was designed to place a magnetic wire under tensile strain while being tested for its magnetic properties. (See Figure I-1.) The device attaches to fixtures for measuring dispersion, skew and anisotropy field.

The wire is clamped at one end with a rotatable clamp designed to eliminate torsion on the wire after clamping. The second clamp is attached to a copper cable which passes over a ball bearing pulley to a pan which is loaded with weights. The second clamp slides on a flat surface eliminating any possible twisting of the wire during test.

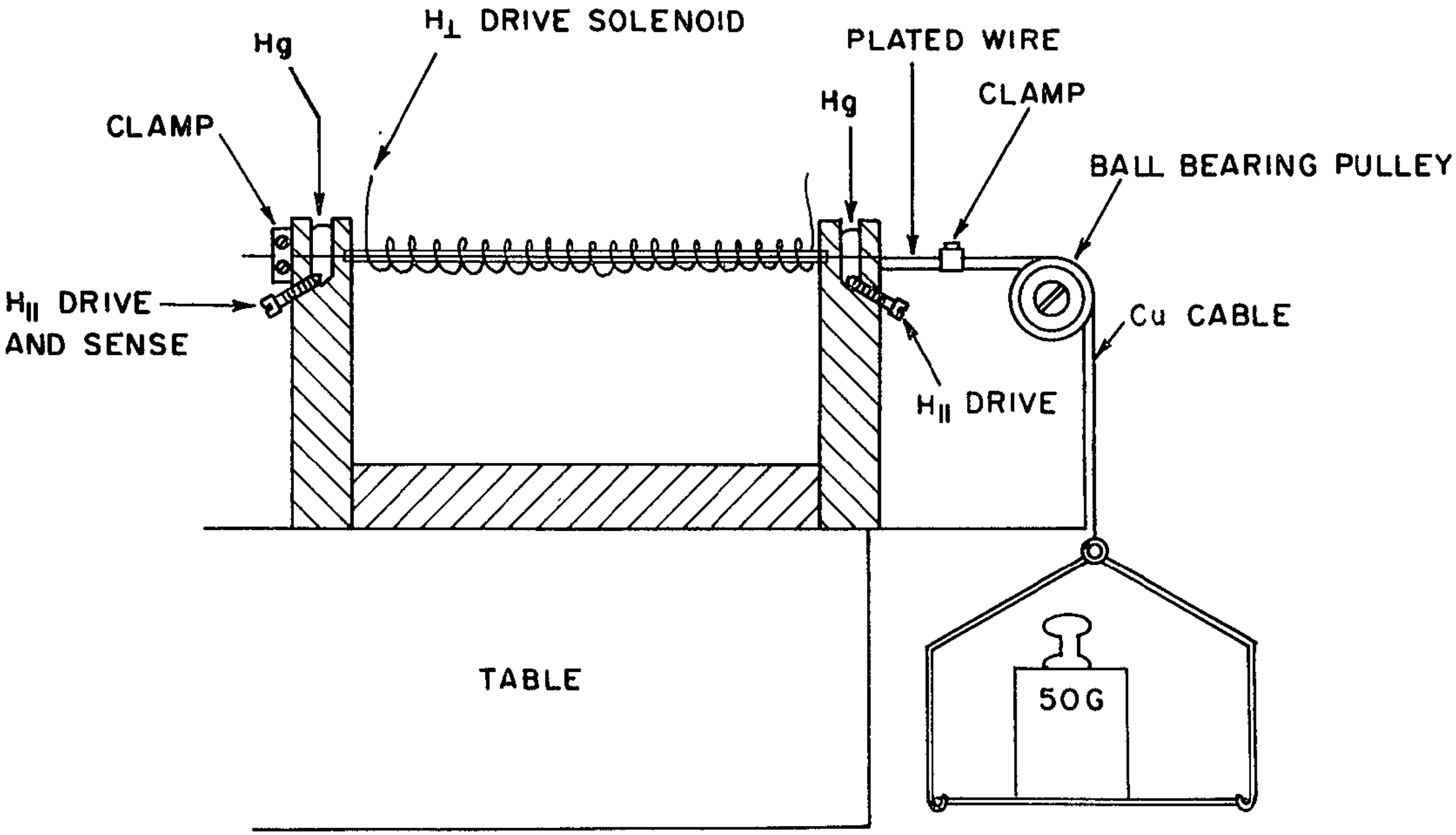

Figure I-1. Tension Sensitivity Fixture

APPENDIX II

ANISOTROPIC STRESS IN PLATED WIRE

Because of cylindrical geometry the circumferential strain in a permalloy film electrodeposited on wire is greater than the axial strain. This difference comes about through anisotropic distortion of the wire caused by the film stress resulting from the electrodeposition process. Conditions are presented for strain equilibrium between film and wire, and expressions for the anisotropic film strain and stress are derived in terms of elastic constants and geometry.

A. STRESS-STRAIN EQUATIONS FOR WIRE

Let e_1 be the axial strain and e_2, e_3 the mutually perpendicular radial strains. Let T_1, T_2, T_3 be the corresponding applied stresses, and λ, μ the elastic constants of the wire material. The stress-strain relations are as follows[1]

$$T_1 = (\lambda + 2\mu)\, e_1 + \lambda\, e_2 + \lambda\, e_3 \tag{1}$$

$$T_2 = \lambda\, e_1 + (\lambda + 2\mu)\, e_2 + \lambda\, e_3 \tag{2}$$

$$T_3 = \lambda\, e_1 + \lambda\, e_2 + (\lambda + 2\mu)\, e_3 \tag{3}$$

By symmetry, $e_2 = e_3$ and $T_2 = T_3$. The equations then become:

$$T_1 = (\lambda + 2\mu)\, e_1 + 2\lambda\, e_2 \tag{4}$$

$$T_2 = \lambda\, e_1 + (2\lambda + 2\mu)\, e_2 \tag{5}$$

(1) See, for example, J. C. Slater and N. H. Frank, Mechanics, McGraw Hill Book Company, Inc. (1947), Chap. 12.

B. STRESS-STRAIN EQUATIONS FOR FILM

Let e_a, e_c and e_r be the axial, circumferential, and radial strains, respectively, for the film. Let T_a, T_c and T_r be the corresponding stresses, and λ_f, μ_f the elastic constants of the film material. The stress-strain relations are as follows:

$$T_a = (\lambda_f + 2\mu_f)\, e_a + \lambda_f\, e_c + \lambda_f\, e_r \tag{6}$$

$$T_c = \lambda_f\, e_a + (\lambda_f + 2\mu_f)\, e_c + \lambda_f\, e_r \tag{7}$$

$$T_r = \lambda_f\, e_a + \lambda_f\, e_c + (\lambda_f + 2\mu_f)\, e_r \tag{8}$$

C. CONDITIONS FOR FILM-WIRE EQUILIBRIUM

Equations (1), (5), (6), (7) and (8) constitute the separate stress-strain relations for the wire and for the deposited film. Consideration of equilibrium between film and wire yields further equations relating the stresses and strains of the film to those of the wire.

1. Stress Relations

We assume for purposes of analysis that the film is under tension and correspondingly the wire is under compression. First we consider the equilibrium between forces in a plane transverse to the wire axis acting on a thin shell of wire shown shaded in Figure II-1a. The relevant forces are those due to the radial components of film stress, T_r, and wire stress, T_2. Since the shell may be taken arbitrarily thin, equilibrium requires that the two stresses be equal, i.e.,

$$T_2 = T_r \tag{9}$$

We next consider equilibrium of forces acting on a composite section of film and wire, shown shaded in Figure II-1b. These forces are the tensile force, F_c, exerted by the remainder of the film, and the compressive force, F_2, in the wire. The equilibrium condition is given by:

$$F_2 = 2 F_c \tag{10}$$

In terms of the stresses, assuming unit length of wire,

$$2 T_2 R = -2 T_c t \tag{11}$$

or,

$$T_2 = -(t/R) T_c \tag{12}$$

where the negative sign is used to indicate that the wire is under compression.

We finally consider equilibrium in the axial direction. Referring to Figure II-1c and equating the tensile film force to the wire compressive force, we find

$$T_1 = -2 (t/R) T_a \tag{13}$$

where the negative sign, as before, indicates that the wire is under compression, and the relations $F_1 = \pi R^2 T_1$, $F_a = 2\pi Rt$ have been used.

2. Strain Relations

We now derive the relations between wire and film strain. Assume, as before, that the film in under tension, i. e., elastically stretched to fit over the wire. Let ℓ_o and r_o be the unstrained length and radius of the film, i. e., the dimensions which the film would have if it could contract to its unstrained condition. Similarly let L_o and R_o be the unstrained length and radius of the wire. Let L and R be the length and radius of both film and wire after plating. The wire strain is then given by the following expressions:

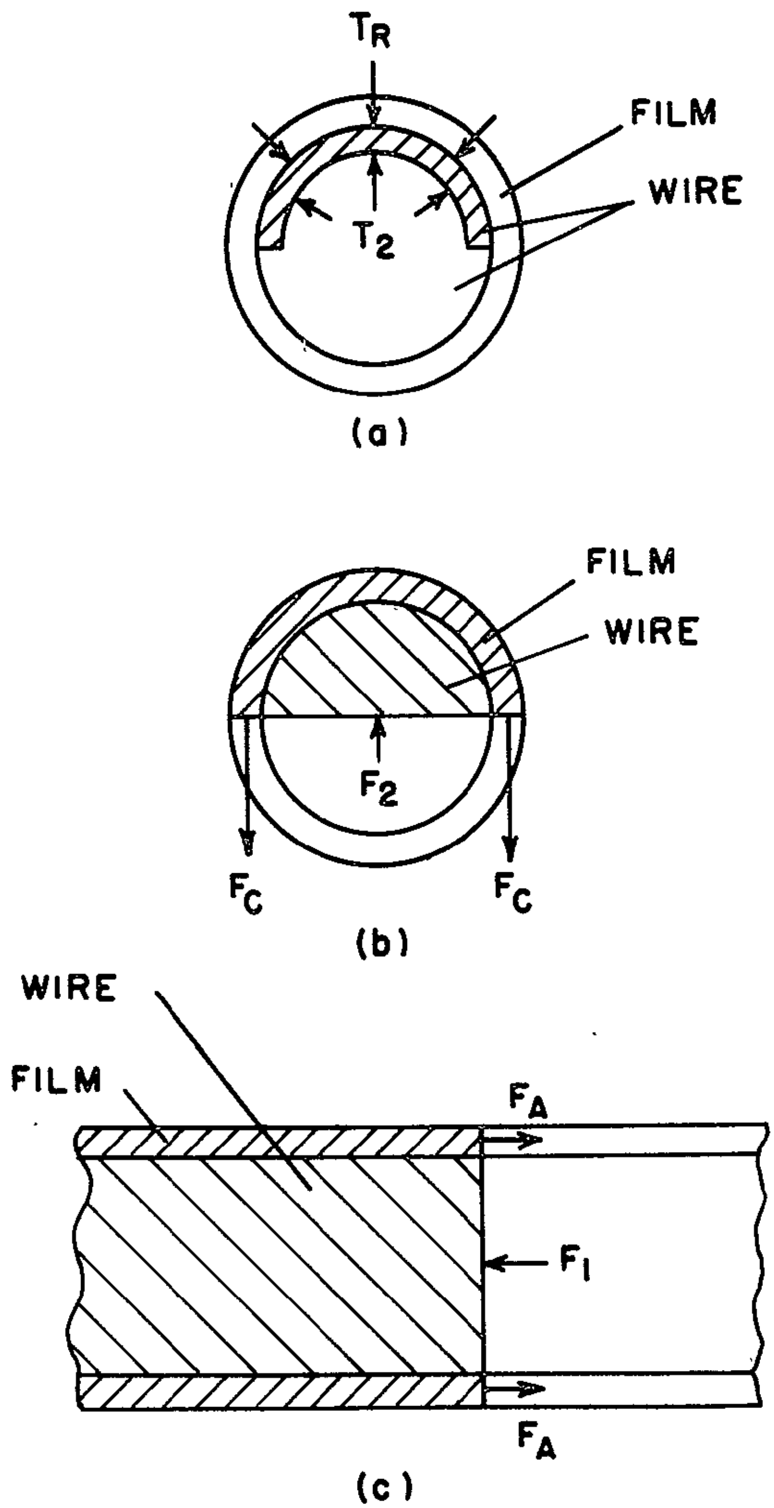

Figure II-1. Conditions of Equilibrium in Plated Wire

$$e_1 = (L - L_o)\,L_o \tag{14}$$

$$e_2 = e_3 = (R - R_o)\,/R_o \tag{15}$$

Similarly the film strain is as follows:

$$e_a = (L - \ell_o)\,/\ell_o \tag{16}$$

$$e_c = (R - r_o)\,/r_o \tag{17}$$

Combining Equations (14), (15), (16), and (17) yields the relation between film and wire strain:

$$e_c - e_2 = R\,(R_o - r_o)\,/\,R_o r_o \tag{18}$$

$$e_a - e_1 = L\,(L_o - \ell_o)\,/L_o \ell_o \tag{19}$$

D. APPROXIMATE EQUATIONS FOR FILM

1. Approximate Stress-Strain Relations

The radial components of stress and strain in the film may be neglected by consideration of wire geometry. Since t/R is of order 10^{-2}, it follows from Equations (9), (12), (7), and (8) that $e_r << e_c$ to good approximation. Thus Equations (6) and (7) may be approximated as follows:

$$T_a \cong (\lambda_f + 2\,\mu_f)\,e_a + \lambda_f\,e_c \tag{6'}$$

$$T_c \cong \lambda_f\,e_a + (\lambda_f + 2\,\mu_f)\,e_c \tag{7'}$$

2. Approximate Strain Relations

Since within the elastic limit R and L will differ from R_o and L_o by only a fraction of one per cent, Equations (18) and (19) may be approximated by

$$e_c - e_2 \cong e_o \tag{18'}$$

$$e_a - e_1 \cong e_o \tag{19'}$$

where $e_o \equiv (R_o - r_o)/r_o = (L_o - \ell_o)/\ell_o$, i.e., e_o is the fractional difference between a dimension of the unstrained wire and the corresponding dimension of the unstrained film. e_o may also be interpreted as the isotropic film strain observed in experiments where the substrate is relatively thick and therefore not strained appreciably by the stretched film.

E. DERIVATION OF ANISOTROPIC STRAIN

Equations (4), (5), (12), (13), (18'), (19'), (6') and (7') may now be combined and restated as follows:

$$-2\,(t/R)\,T_a = (\lambda + 2\mu)\,(e_a - e_o) + 2\lambda\,(e_c - e_o) \tag{4'}$$

$$-(t/R)\,T_c = \lambda\,(e_a - e_o) + (2\lambda + 2\mu)\,(e_c - e_o) \tag{5'}$$

$$T_a = (\lambda_f + 2\mu_f)\,e_a + \lambda_f\,e_c \tag{6'}$$

$$T_c = \lambda_f\,e_a + (\lambda_f + 2\mu_f)\,e_c \tag{7'}$$

These four equations contain five unknowns, T_a, T_c, e_a, e_c, and e_o, as well as the elastic constants of film and wire. We may therefore solve for the ratio e_c/e_a in terms of the elastic constants. Assuming $t/R << 1$, the ratio is found to be as follows:

$$e_c/e_a \cong 1 + (t/R)\left[(\lambda_f + \mu_f)/\mu\right] \quad (20)$$

Hence the circumferential film strain is greater than the axial strain in all cases. The ratio e_c/e_a increases with increasing t/R and with increasing ratio of film to wire modulus, as expected. Utilizing Equations (6'), (7') and (20) we find also:

$$T_c/T_a \cong 1 + (t/R)(\mu_f/\mu) \quad (21)$$

or alternatively:

$$T_c/T_a \cong 1 + (t/R)(E_f/E)(1 + \sigma)/(1 + \sigma_f) \quad (22)$$

where

E_f = Young's Modulus for film.

E = Young's Modulus for wire.

σ_f = Poisson's Ratio for film.

σ = Poisson's Ratio for wire.

APPENDIX III

NEW TECHNOLOGY

The major purpose of this study was to determine causes of aging in plated wire computer components and to recommend directions for improvement. In this section on new technology it is appropriate to state briefly the most important findings of the research and the corresponding recommendations.

A. AGING DUE TO STRESS RELIEF

The magnetic properties were found to change spontaneously in magnetostrictive samples as a result of the relief of film tension. The problem is aggravated by the further discovery that the zeromagnetostrictive composition cannot be achieved simultaneously for both torsion and tension.

Two possibilities exist for the solution to this problem. They are (a) to reduce the film stress and/or stress anisotropy and (b) to reduce the magnetostriction. Approaches to reduction of film stress include lowering the plating bath temperature and use of various combinations of additives. The analysis in Appendix II indicates that the stress anisotropy would be reduced in thinner films, thicker wires, and for larger wire elastic modulus. Reduction of tension magnetostriction can be achieved, as shown in the body of the report, with non-zero torsion magnetostriction. Hence a tradeoff is possible between aging and torsion sensitivity. A more fundamental approach is equalization of torsion and tension zerostrictive compositions through alterations of the process.

B. AGING DUE TO MOBILE DEFECTS

It was found that the tendency of the magnetic easy axis to skew rapidly in the presence of a magnetic field is systematically reduced by increasing the temperature of the on-line stabilization anneal. This dependence on stabilization temperature is similar to that for reduction in hydrogen content of the film. As shown in the body of the report, satisfactory stability is achievable at an on-line stabilization temperature of 400°C. At the present time the stabilization temperature is critical, since at appreciably lower temperatures the skew susceptibility becomes unacceptable, while at higher temperatures the easy-axis dispersion following stabilization increases, lowering the electrical output. It is, therefore, important to seek methods of reducing the impurity and defect content by process innovations other than stabilization anneal.

C. CORROSION

It was found that salt solutions simulating sea water had a corrosive action on the film surface and the memory output characteristics, which was drastic compared to that of distilled water or air. In general the main findings of this report concerning aging causes are unrelated to oxidation. Nevertheless, the possibility of corrosion in unusual environments should be precluded by protective coatings on the wire.